INVESTIGATIONS OF AZINOMYCIN BIOSYNTHESIS AND MACULAR DEGENERATIVE DISEASES

A Dissertation

By

BRENDAN FOLEY

Submitted to the office of Graduate and Professional Studies
Texas A&M University
in partial fulfillment of the requirements for the degree of

DOCTOR OF PHILOSOPHY

Chair of Committee,	Coran M.H. Watanabe
Committee Members,	David P. Barondeau
	Tadgh P. Begley
	Margaret E. Glasner
Department Head,	Simon North

December 2020

Major Subject: Chemistry

ABSTRACT

The discovery of natural products has been a beneficial tool that provides a window into the bioorganic chemistry of organisms and offers a template for drug discovery and development. Natural products can be utilized to positively impact the deleterious effects of diseases or they can incur toxicity in certain biological systems. The aim of this work is to elucidate the biosynthetic pathway of the natural product Azinomycin and to evaluate the effects and treatments for macular degenerative diseases.

Azinomycin A and B are antitumor natural products that are isolated from *Streptomyces sahachiroi*. Azinomycin A and B form interstrand crosslinks with DNA through their electrophilic epoxide and aziridine [1,2-α] pyrrolidine ring moiety. The biosynthetic pathway for aziridine ring formation was investigated. AziC5 and AziC6, enzymes with a high similarity with transketolase enzymes, are shown to catalyze a thiamin mediated two-carbon extension of N-acetyl glutamate semialdehyde into an α,α' dihydroxy intermediate.

The naphthoate ring on Azinomycin forms noncovalent interactions with DNA that are pivotal for successful cross-linking. 5-methyl-Naphthoic acid is created with a multi-domain polyketide synthase enzyme, AziB. The acyl carrier protein (ACP) domain of AziB is post-translationally modified by PPTases. The optimization of the post-translational modification was achieved through the identification of the most effective PPTase. The thioesterase (TE) domain of AziB hydrolyzes the thioester bond between 5-methyl-naphthoic acid and the ACP domain. The rate of hydrolysis was determined for

AziG and a series of AziG mutants to demonstrate which residues are essential for substrate cleavage.

The main contributing factors of macular degenerative diseases are the accumulation of lipofuscin in the retina and the eye's inability to degrade them. Vitamin A can form dimers, A2E and cycloretinal, in enzymatic and non-enzymatic reactions. The negative effects of macular diseases are hypothesized to decrease with the clearance of accumulated lipofuscin. While the toxicity of A2E has been investigated, the toxicity of cycloretinal has not. Cycloretinal liposomes were synthesized and cycloretinal cytotoxicity was evaluated. In addition, MsP1, a heme-based peroxidase enzyme, was shown to degrade the toxic, all-trans retinal dimers. The degradation products of these dimers were evaluated to display MsP1's efficaciousness for gene therapy.

The mechanism of formation for cycloretinal was shown non-enzymatically, with catalytic L-proline, and enzymatically, with the whey protein β-lactoglobulin (BLG). Also, a series of halogenated α, β-unsaturated aldehydes were employed to inhibit cycloterpenal formation. These inhibitors were employed to prevent the dimerization of α, β-unsaturated aldehydes and promote retro-aldol cleavage on a series of aldehydes with hydrophobic side groups.

The experiments in this dissertation seek to further our knowledge of the biosynthesis of Azinomycin. In addition, the contributing factors and inhibitors to macular degenerative diseases were investigated to demonstrate the harmful effects of certain natural products. The investigations into natural product formation could yield beneficial therapeutic agents amongst a wide array of diseases

ACKNOWLEDGEMENTS

I would first like to thank my advisor, Dr. Coran M.H. Watanabe, and all of my fellow and former lab mates for all their support throughout the years. I am grateful for Dr. Watanabe for her guidance and insight while working on these projects. I would've been unable to complete my studies without her help.

I would also like to thank my committee members, Dr. David P. Barondeau, Dr. Tadgh Begley, and Dr. Margaret Glasner, for all of their invaluable advice and creative suggestions. I am thankful to Dr. Yohannes Reznom in the A&M mass spectrometry lab for assistance and guidance with the Cycloretinal projects.

Additionally, I would like to thank my mentor in the earlier years of my studies, Irum Perveen. Irum was incredibly helpful whenever I had instrumentation questions or needed to bounce ideas off of her. She was a critical guide in helping me familiarize myself with the macular degenerative projects. I am extremely thankful for Dr. Keshav Nepali for all the assistance he provided me in the Azinomycin projects. I'd also like to thank my current and former lab mates: Shogo Mori, Brian Young, Lauren Washburn, Brett Johnson, Flor Rodriguez, Jean Kim, and Hieu Nyugen for providing a clean and safe work environment.

Finally, I would like to extend a special gratitude towards my family and close friends. They provided a tremendous amount of support and I couldn't have succeeded without them.

CONTRIBUTORS AND FUNDING SOURCES

Contributors

This work was overseen by the dissertation committee of Professor Coran M. H. Watanabe (advisor) and Professors David Barondeau and Tadhg Begley of the Department of Chemistry and Professor Margaret Glasner of the Department of Biochemistry and Biophysics.

The MS/MS data for Chapter II and II was gathered by Dr. Yohannes Rezenom. The following Undergraduate Researchers contributed to Chapter II and III through cloning and protein expression: Janet Rodriguez, Kenneth Williams, Kendall Pryor, and Emily Rimes. All other work conducted for the dissertation was completed by the student.

Funding Sources

This work was also made possible in part by the National Science Foundation under Grant Number 1904954. Its contents are solely the responsibility of the authors and do not necessarily represent the official views of the National Science Foundation.

NOMENCLATURE

HPA	Hydroxypyruvic Acid
F6P	Fructose-6-phosphate
X5P	Xylulose-5-phosphate
NADPH	Nicotinamide Adenine Dinucleotide Phosphate
NADH	Nicotinamide Adenine Dinucleotide
PPTase	Phosphopantetheinyl Transferase
Ppant	Phosphopantetheine
ACP	Acyl Carrier Protein
PCP	Peptide Carrier Protein
CoA	Coenzyme A
PKS	Polyketide Synthase
PK	Polyketide
TE	Thioesterase
NMR	Nuclear Magnetic Resonance
TLC	Thin Layer Chromatography
DTT	Dithiothreitol
IPTG	Isopropyl β-d-1-thiogalactopyranoside
TCEP	Tris(2-carboxyethyl) phosphine Hydrochloride
ATP	Adenosine Triphosphate
AMP	Adenosine Monophosphate
PPi	Pyrophosphate

LC-MS	Liquid Chromatography – Mass Spectrometry
HPLC	High Performance Liquid Chromatography
EIC	Extracted Ion Chromatogram
BLG	β-Lactoglobulin
ATR	All-Trans Retinal
A2E	N-retinyl-N-retinylidene ethanolamine

TABLE OF CONTENTS

LIST OF FIGURES

LIST OF SCHEMES

LIST OF TABLES

CHAPTER I

INTRODUCTION: NATURAL PRODUCT BIOSYNTHESIS

Introduction

Since the earliest civilizations, mankind has utilized naturally occurring organisms for purposes such as food additives, food preservation, and medicinal usage. The earliest recorded example of the utilization of compounds found in nature to elicit a physiological effect was seen approximately 5000 years ago on ancient Sumerian clay slabs. Twelve drug recipes were discovered that utilized over 250 plants such as mandrake, poppy, and henbane.[1] Plants have continued to serve as an excellent resource for botanical remedies. From ancient Chinese remedies that utilized ginseng and cinnamon bark to modern examples like penicillin mold and willow bark, plants have served as vital resources for the extraction of naturally occurring compounds.[2] Many of these biologically effective molecules are secondary metabolites that are inessential to the growth, development, or reproduction of the host organism. The term natural product was coined to describe secondary metabolites that are biosynthetically produced by organisms to aid in biological systems. Many microorganisms release natural product toxins into an environment to eliminate competitors, such as vancomycin and penicillin, which inhibit bacterial cell wall production in $Gram^{+}$ bacteria.[3] In addition to defending the host organism, certain natural products can be utilized in different biological systems to combat harmful organisms that contribute to certain to diseases. Natural product research has been a vital source for the discovery of chemically complex compounds.

The evolution of the isolation and identification of natural products

The earliest natural products were isolated and extracted from plant species or microorganisms, but their identification and characterization involved a slow and inefficient pathway towards categorization. The discovery of a biologically active natural product involved a drug target or ailment being exposed to a series of crude extracts of natural products. Only when an extract exhibited positive effects would it be purified to isolate and identify the natural product. Although this modality of search has afforded the identification of drugs such as digitoxin, quinine, and penicillin, this is an untenable means of search to meet the problems of the modern era.[4,5,6]

Microorganisms opened a new window to natural product exploration. From whole cell screening methods to low-throughput fermentation, natural product identification occurred with relative ease. [7] However with technological advances, the search for natural products has dwindled because of high throughput screening and combinatorial libraries.[8] Instead of pursuing new compounds in different organisms, existing natural products were used as development tools towards active chemical leads.[9] Combinatorial libraries were created from derivatizing existing compounds, but these molecules lacked the complexity of natural products. When juxtaposed to these large combinatorial libraries, natural products were much more complex with rare organic properties such as polycyclic structures, multiple chiral centers, and unique chemical moieties. [10] Due to the lack of development and creation of innovative, novel bioactive compounds, new strategies were employed to create compounds with structural complexity and biological functions.

Natural product importance

Given the limitations of combinatorial libraries and their lack of chemical complexity, alternative routes were pursued to continue developing novel biologically active compounds. Natural products or natural product derivatives and mimics consist of 52% of the drugs approved by the FDA since 1981.[11] Since this is such a large percentage of drugs that are in clinical trial, the continued study of natural products is vital so that enzymatic or synthetic derivatives and mimics can be made and investigated.

The creation of natural product-based drugs are primarily achieved through three routes. One of these routes include synthetic recreations of products that are difficult to isolate in large quantities. Another approach is a semi-synthetic recreation which involves the reconstruction of the molecule in part through enzymatic pathway and in part through synthetic means. Lastly, enzymatic development towards macromolecules or natural product mimics can be pursued.

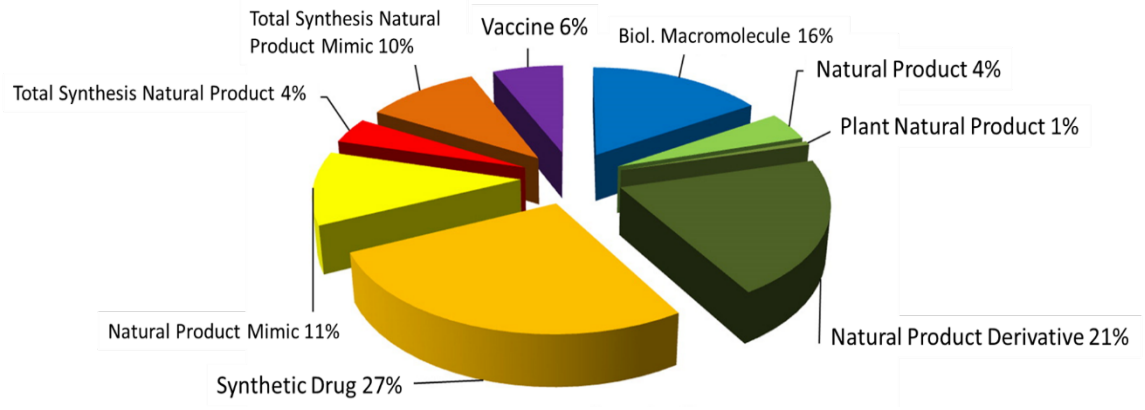

Figure 1 Clinical Drugs Sources by Percentage. Adapted from reference 11.

Metabolic pathways

The life of an organism requires a cascade of reactions that allows for the consumption and renewal of energy, the construction of building blocks necessary for the formation of macromolecules, and the elimination of waste. Primary and secondary metabolic pathways perform these reactions to ensure cell viability. The primary metabolic pathways are directly involved in normal cell activity. Examples of primary metabolic pathways include glycolysis, the pentose phosphate pathway, and the Krebs cycle. The secondary metabolic pathway constitutes the formation of molecules that are not directly involved in the normal function of the cell.

Organisms form secondary metabolites as a resistance to their surroundings.[6] Primary metabolic pathways are generally conserved across a vast array or organisms, but secondary metabolic pathways can be specific organism's response to a particular environment and can produce novel, bioactive compounds. Considering the overwhelming amount of FDA approved drugs that have been directly linked to natural products, the characterization of the biosynthetic pathway for these compounds is valuable. Characterizing these pathways identifies enzymes that are capable of performing synthetically difficult, unique chemical reactions. This characterization of these pathways opens possibilities such as implementing semi-synthetic pathways that enhance production of existing natural products or the utilization of unique enzymes to create new natural products.

The natural products of Streptomyces

A genus of interest with a vast array of natural products is *Streptomyces*. This genus creates a myriad of compounds ranging from immunosuppressants, hormone-like signals, and pigments.[11] *Streptomyces* are a gram-positive genus filamentous actinomycetes that form branching filaments during growth.[12-13]

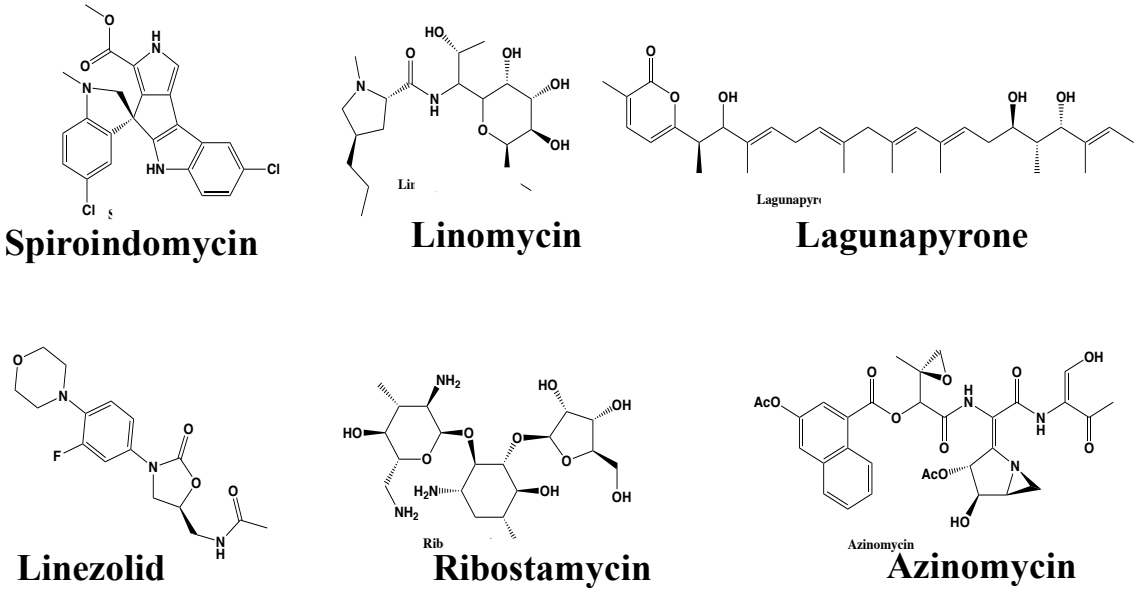

Figure 2 Streptomyces Natural Products

Thus far, *Streptomyces* is the largest antibiotic producing genus in the world with 80% of the antibiotics originated from actinomycetes.[13] Not only are all of the examples in Figure 2 bioactive, they represent a wide array of chemical complexity that represents several types of natural products. Spiroindimicin has a macro-cyclic complex structure, Lagunapyrone consists of terpene subunits, and Azinomycin possesses polyketide synthase (PKS) fragments.

Azinomycin

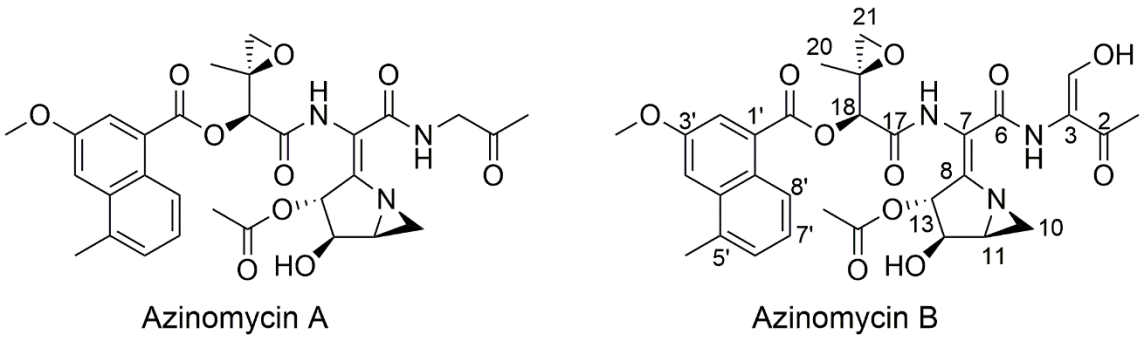

Figure 3 Structure of the Azinomycin A and B

With the vast array of natural products produced by *Streptomyces,* Azinomycin is among the most chemically complex. Azinomycin is produced by the Gram-positive soil dwelling bacteria *Streptomyces sahachiroi.* It was first discovered as carzinophilin A in 1954 and was found to inhibit Yoshida sarcoma and increase life expectancy in murine samples.[14] Further studies with *Streptomyces* revealed that *Streptomyces griseofuscus* produced Azinomycin A, Azinomycin B, and its epoxyamide.[15] With increased spectroscopic advancements, the structures of Azinomycin A and B were elucidated and Azinomycin B was found to be identical to carzinophilin A. [16]

The azinomycin's are structurally identical with the exception of their final fragment. The azinomycin's contain 4 major fragments: the naphthoate ring, the epoxide moiety, the aziridine ring, and a final group. Azinomycin A contains an amino acetone group while Azinomycin B contains an enol fragment. To test its use as a potential therapeutic reagent, the azinomycin's were tested against the National Cancer Institute's

60 cell line.[17] The azinomycins and murine samples were analyzed against P338 leukemia, P815 Mastocytoma, B-16 melanoma, and Ehrlich carcinoma. Azinomycin A and B both increased the life spans of the mice. Each azinomycin exhibited ~150% ILS (Increased Life Span) with Erlich Carcinoma, while Azinomycin B was most effective against P388 leukemia showed a 193% ILS.[18] Azinomycin B also displayed a higher ILS than azinomycin A in P815 Mastocytoma and Erlich carcinoma cell lines. The clinical drug mitomycin C exhibited a 204% ILS against P388 leukemia under the same conditions, but at a 60-fold concentration higher.[18]

Azinomycin mode of action

Azinomycin B displays anti-tumor characteristics through its ability to form covalent linkages between complimentary strands of DNA. These covalent linkages form between the electrophilic C10 aziridine ring and the C21 epoxide moiety.[19] These electrophiles are attacked by the N7 position of purine bases which

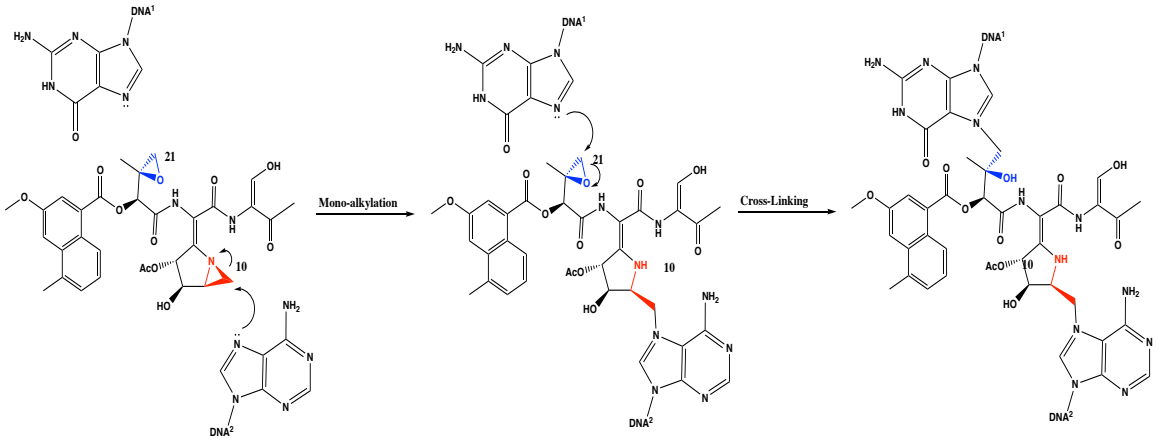

Figure 4 Azinomycin Mediated Covalent Linkage. The initial alkylation occurs at the C10 aziridine ring, shown in red. The dialkylation occurs at the C21 position of the epoxide ring, shown in blue.

break open the aziridine and epoxide rings.[20] This mechanism is enacted sequentially, with the initial mono-alkylation occurring at the C10 position of the aziridine ring. The di-alkylation occurs rapidly as the C21 epoxide ring is attacked by a purine base on a complimentary strand of DNA.[21] While azinomycin forms inter-strand crosslinks with the di-alkylation of the aziridine and epoxide ring, both of these moieties have been shown to form DNA adducts and induce toxicity by themselves.[22-23] The naphthoate-epoxide fragment forms DNA adducts and exhibits toxicity, but the epoxide ring without the naphthoate was unable to form the adduct.[24] This shows that the naphthoate fragment is necessary to form the epoxide-DNA adduct and its non-covalent interactions facilitate adduct formation.

Azinomycin Biosynthesis

Azinomycin is a novel therapeutic because it contains the extremely rare azabicyclo [3.1.0] hexane ring that has only been found in a few natural products. While this aziridine ring has identified in mitomycin C, azicemicin A, azinomycin B, and maduropeptin, the biosynthetic pathway of these unique molecules has yet to be characterized. The enzymes involved or the mechanism of formation for the aziridine ring is still unknown. [25-28]While the enzymatic catalysis of this functional group is still unknown, organic synthesis of aziridine rings has been achieved through several forms of β-carbon activation such as sulfonylation, phosphorylation, halogenation, or adenylation.[29]

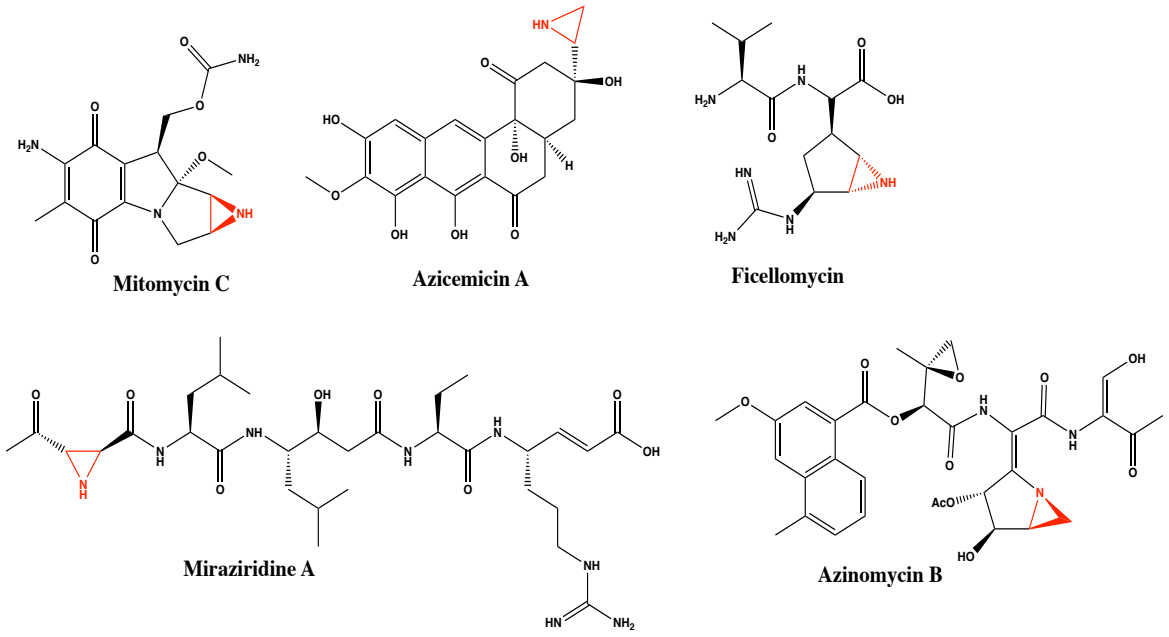

Figure 5 Natural Products with Aziridine Rings

In addition to the novel biosynthetic pathway for the construction of the azabicycle moiety, azinomycin A and B are biosynthesized through a hybrid polyketide synthase (PKS) and non-ribosomal peptide synthase (NRPS). The alternating amide backbone of azinomycin indicates it was assembled through amino-acid like condensation reactions that are NRPS mediated. The remaining components of azinomycin and their predicted starter units are illustrated in Figure 6.

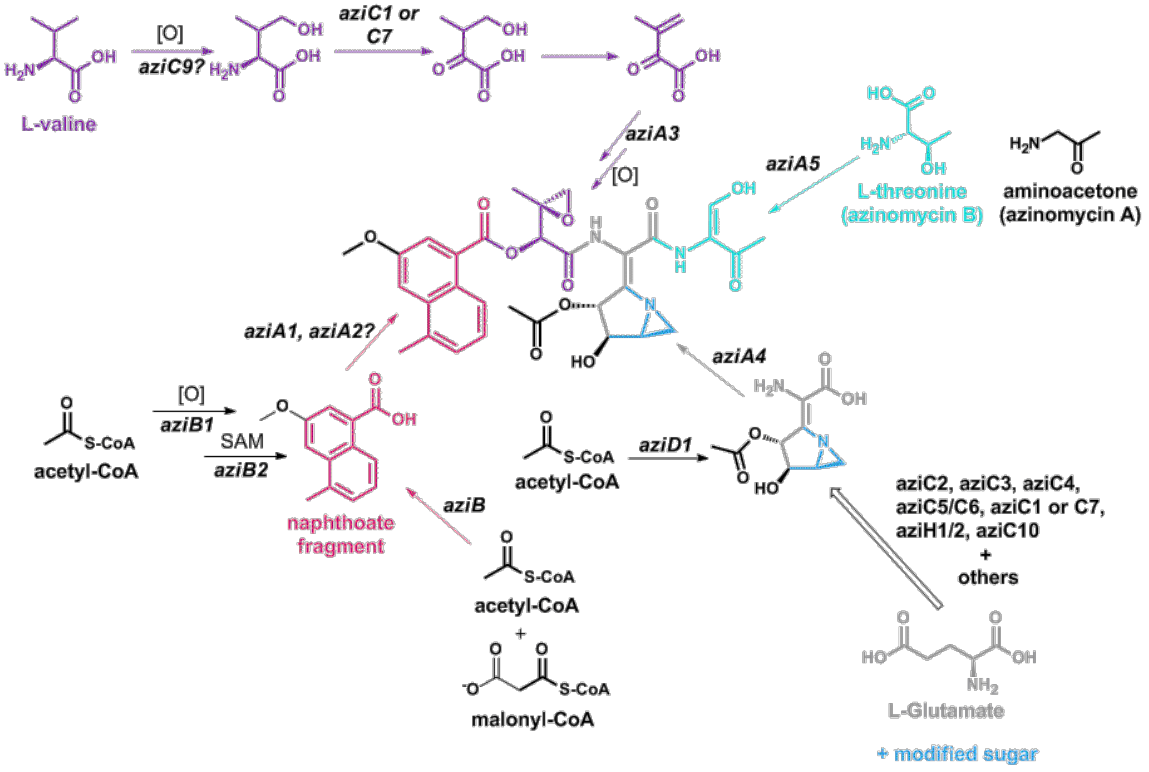

Figure 6 Proposed Azinomycin Biosynthetic Route

Whole cell feeding studies were performed to determine the precursor units of each of these fragments. While ornithine was initially conceived to produce the azabicycle, radiolabeled glutamic acid was shown to incorporate within the backbone of the aziridine ring.[30] When radiolabeled acetate was fed to *Streptomyces Sahachiroi,* it was sequentially incorporated within the naphthoate fragment, indicative of a PKS mediated assembly.[31] In addition to its naphthoate incorporation, radiolabeled acetate also incorporated into the azabicycle ring and the enol fragment of Azinomycin B. The incorporation of labeled acetate is proposed to occur through the cycling of acetate with α-ketoglutarate in the

azabicycle moiety and through threonine in the enol fragment.[32,33]Radiolabeled valine was fed to *Streptomyces sahachiroi* and was discovered to be the precursor to the epoxide moiety.[34]

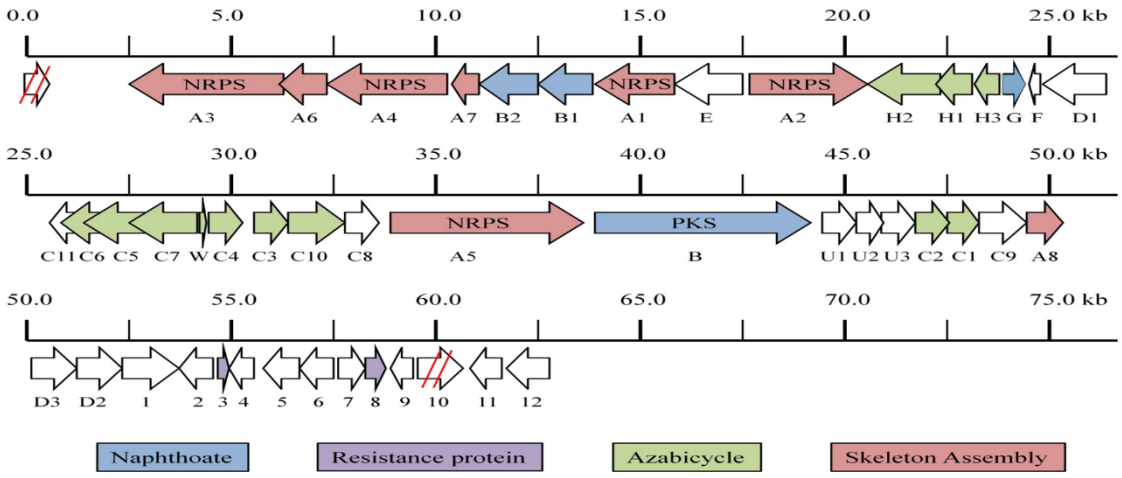

Figure 7 Azinomycin Biosynthetic Gene Cluster

Given azinomycin's unique biological properties and complex chemical structure, annotating the *Streptomyces Sahachiroi* genome allows for the identification of enzymes that perform complicated chemistry. Zhao and colleagues analyzed the azinomycin B biosynthetic gene cluster based on PCR sequencing of the genome for the iterative PKS.[34] Further bioinformatic analysis revealed that in addition to the PKS genes, there were multiple NRPS genes, two acyl ligase genes, and a series of enzymes that could be associated with the assembly of the azabicycle moiety. A biosynthetic pathway for the biosynthesis of the azabicycle was hypothesized with 14 possible enzymatic steps.

Transketolase enzymes

In order to determine the foundational building block of the azabicycle's construction, feeding studies were performed and radiolabeled glutamic acid was found to be incorporated into the azinomycin backbone.[30] The complete azabicycle ring is two carbons larger than glutamic acid, so further modification needed to occur before its completion. An enzyme superfamily capable of mediating a two-carbon extension is the Transketolase family. Transketolase (TK) enzymes are thiamin dependent enzymes that are members of the pentose phosphate pathway and the Calvin cycle.[35] Between the two catalytic sites, Transketolase enzymes are capable of mediating the reversible transfer of a dihydroxyl group from a ketose donor to an aldose accepter.[36] These enzymes reversibly link glycolysis to the pentose phosphate pathway by converting D-xylulose-5-phosphate and D-ribose 5-phosphate to D-glyceraldehyde-3-phosphate and D-sedohep-tulose-7-phosphate.[37] These processes form the products D- fructose 6-phosphate and D-erythrose 4-phosphate, which are precursors to amino acid formation.[38]

Transketolase enzymes are thiamin dependent enzymes that have the highly conserved residues Gly-Asp-Gly followed by 21 residues with less homology.[39-40] A hydrophobic pocket is able to form at the interface of the two subunits and a cofactor Mg^{2+}-ThDP complex forms, which exposes the C2 position of the thiazolium ring in thiamin.[42-44] This enables deprotonation of C2 and triggers the mechanism shown in Figure 8.[45]

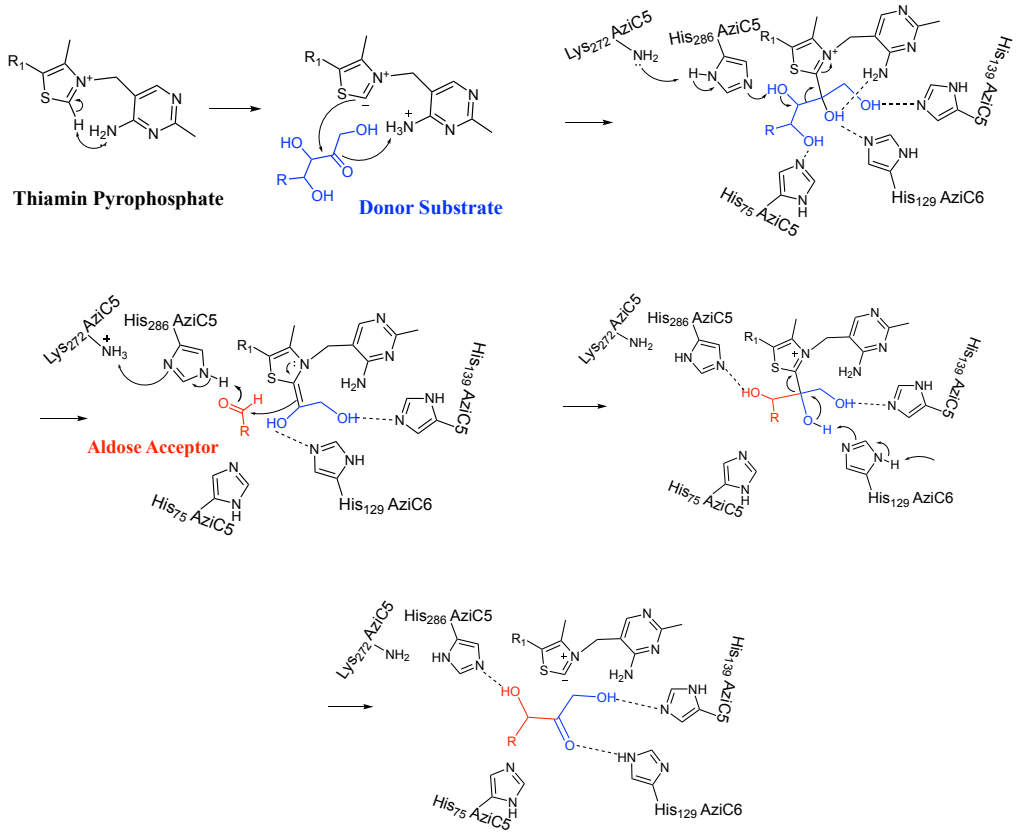

Figure 8 Thiamine-mediated Transketolase Activity. The donor substrate, shown in blue, coordinates with thiamine to create the two-carbon extender unit. The aldose acceptor, shown in red, contains an aldehyde electrophile which forms the carbon-carbon bond.

Diseases caused by thiamin deficiencies, such as beriberi and Alzheimer's, are linked with decreased transketolase activity. Increasing and restoring TK activity has been explored as possible treatment for these afflictions.[46-49] TK enzymes have industrial applications from their ability to produce amino acids, to form stereospecific carbon-carbon bond synthesis, and to create easily activated intermediates.[50-52]

The identification of putative transketolase genes, *aziC5* and *aziC6,* within the azinomycin gene cluster provides an opportunity for discovering enzymes involved in the

biosynthesis of the azabicycle moiety. AziC5 and AziC6 have the ability to perform a difficult carbon-carbon bond in the construction of azabicycle ring.

Polyketide Synthase Enzymes

Polyketide Synthases perform a stepwise biosynthesis of diverse carbon skeletons with acyl-Coenzyme A starter units, such as acetyl Coenzyme A. PKS can be iterative, where the final PKS product can be constructed from one module, or non-iterative, forming from multiple modules. There can be two types of PKS in bacteria, type I and type II. Type I PKS are multi-domain enzymes that are coded by a single gene, while type II function by each domain being coded by a separate gene. At minimum, a PKS module contains a ketoacyl synthase (KS), an acyltransferase (AT), and an acyl carrier protein (ACP) domain, while ketoreductase (KR), dehydratase (DH), and enoyl reductase (ER) domains are frequently present.[53]

Thiolation domains (acyl carrier protein domain) require post-translational modification by phosphopantetheinylation of a serine residue to create an acyl-CoA transthiolation. AT domains can then work to extend the carbon skeleton by nucleophilic attack on malonyl-CoA extender units via serine. This creates an acyl intermediate that can be transferred to the thiolation domain via phosphopantetheine arm. Chain elongation is initiated by the decarboxylation of a malonyl-CoA extender unit by the ketosynthase domain.

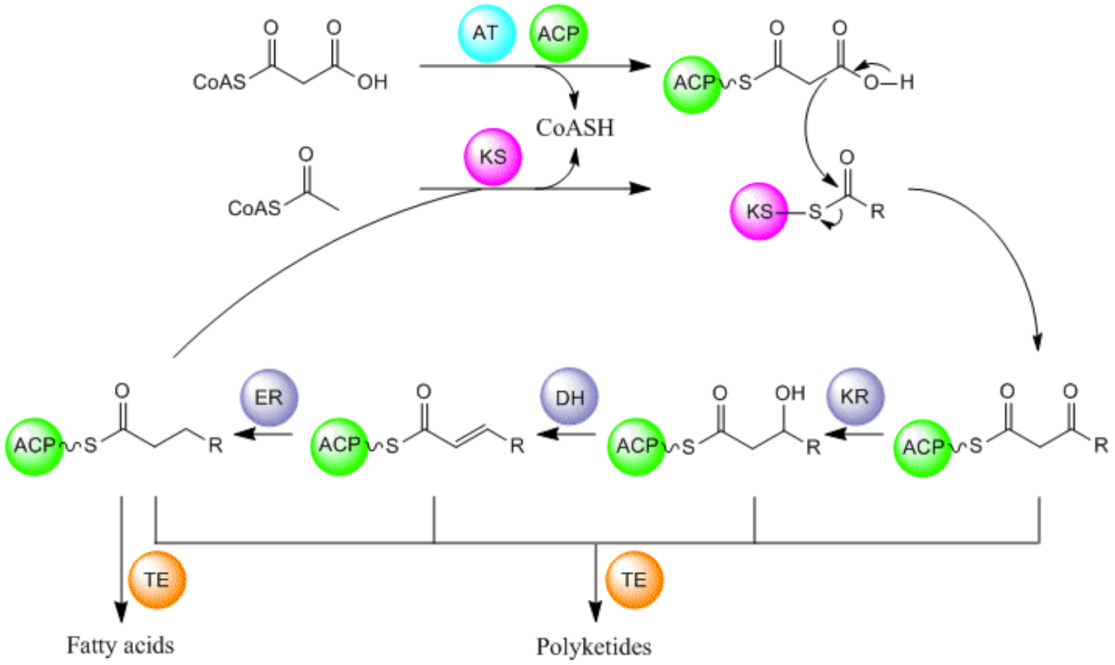

Figure 9 PKS Module Mechanisms. An acetyl-CoA starter unit binds to the ACP domain and is grows through the activity of the AT, KS, and KR domains. The compound is cleaved from the protein by the TE domain.

PPTase enzymes

Phosphopantetheinyl transferases (PPTase) post-translationally modify iterative and modular synthases such as PKS, fatty acid synthases (FAS), or non-ribosomal peptide synthases. These enzymes are capable of tethering 4'-phosphopantetheine onto the carrier protein domain of synthases. PPTases mediate the transfer and covalent attachment of PPant arms from coenzyme A (CoA) to conserved serine residues of the CP domain through phosphoester bonds. These essential post-translation protein modifications convert inactive apo-synthases to active holo-synthases.[54] There are three types of PPTases and they can be separated by amino acid sequence and structure. *Holo*-ACP

synthase (AcpS) acts on FAS, Surfactin phosphopantetheinyl transferase (Sfp) installs the PPant on the PCP of surfactin synthase, and the third family of PPTases post-translationally modifies apo-ACPs prior to assembly of the mega-synthases.[54] The Sfp type has been shown to have the broadest substrate range.[55-57]Identifying the most efficient enzyme and conditions of post-translational modification unlocks better PKS activity.

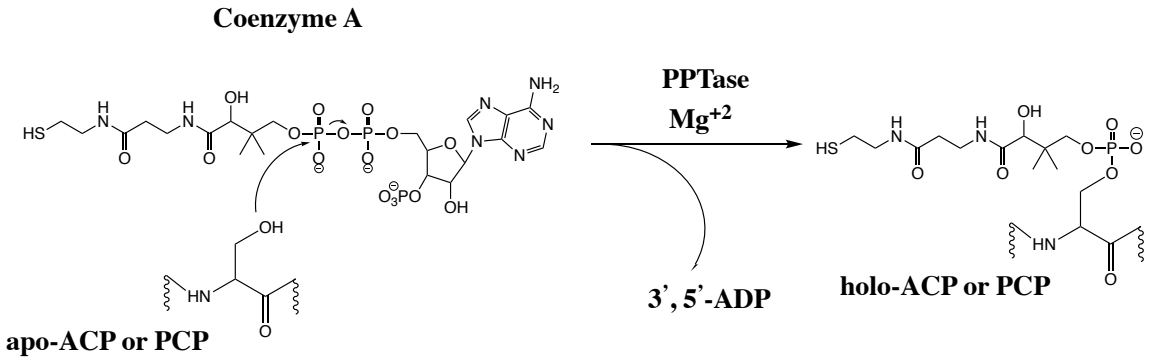

Figure 10 PPTase coordination to ACP through a serine mediated phosphoester bond

Thioesterase enzymes

As the polyketide product grows, it remains covalently attached to the PPant arm on the ACP domain. Once the PKS chain reaches its full length, the cleavage of the thioester bond that keeps it tethered to the ACP domain is achieved by the thioesterase (TE) domain.[58] TE domains are the best understood aspect of PK systems and the structures of multiple TE domains have been identified.[59,60] These enzymes are capable of regio- and stereoselective cyclization of peptides, which is difficult to achieve through organic synthetic means.[61-63]The thioesterase domain is generally located at the C-terminus of PKS and they have a conserved triad of Ser-His-Asp, as seen in Figure 11.[64]

When the PKS chain reaches its complete length, the substrate is brought to the hydroxyl of the TE serine residue. This serine becomes activated from the conserved histidine residue, which is previously activated by the conserved aspartate residue.[58]

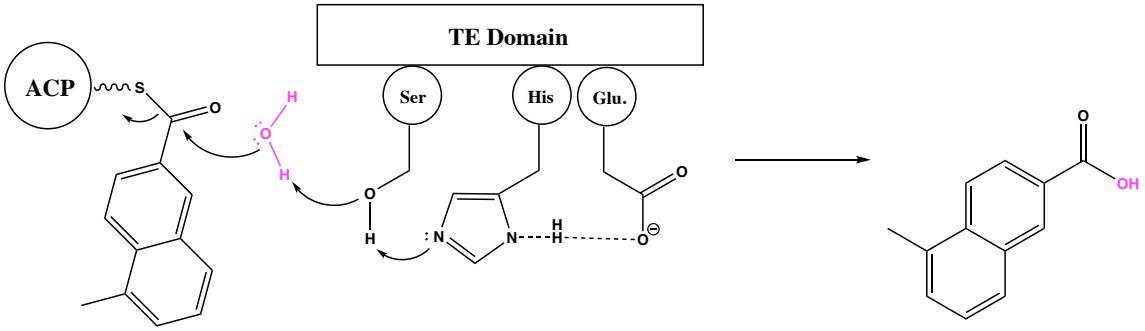

Figure 11 Base catalyzed hydrolysis facilitated by catalytic triad of TE domains

The proposed mechanism of TE activity involves a base mediated catalysis. In the base catalyzed mechanism, the activated serine could deprotonate water, which then acts as the nucleophile. This type of thioester hydrolysis is seen in yersiniabactin, vancomycin, and the ACV 54 tripeptide precursor of b-lactam antibiotics.[65-67]

The TE domains capabilities are not limited to cleaving the thioester bond between substrate and ACP domain. TE domains are also capable of facilitating intramolecular macrocyclization, macrolactonization, macrothiolactonization, and oligomerization.[68-72] The catalytic triad of TE domains can impact the formation and release of PKS mediated products. The TE domain of azinomycin, AziG, is essential for both the creation of the naphthoate moiety and for the hydrolysis from AziB. Without the TE domain, the PKS enzyme produces a truncated product, 2-methyl-benzoic acid.

Macular degenerative disorders

Although there are an innumerable number of instances where natural products exhibit a positive effect in certain biological systems, natural products can also exhibit deleterious effects. The macula is the central area of the retina and facilitates central vision and high-resolution visual activity.[73] Macular degenerative diseases involve the deterioration of the retina and includes partial or complete vision loss. Macular degenerative diseases are defined by the accumulation of drusen and lipofuscin deposits, in the retinal pigment epithelium, and the macula's inability to clear them.[74] Macular degenerative diseases include a wide array of afflictions; such as Best's Disease, Stargardts disease, and Age-related macular degeneration (AMD).[75-77] AMD is the leading cause of blindness among people of European descent over the age of 65. There are currently more than 2 million cases of AMD in the United States, and it's predicted to reach 3 million cases by 2020. There are two forms of AMD, a neovascular age-related macular degeneration (wet) form and a geographic atrophy (dry) form. The dry form exhibits a minimal amount negative effects, but the wet form hinders central vision.

Figure 12 Macular Degenerative Diseases. The snap shots of the macula demonstrate the accumulation of lipofuscin shown in yellow. This accumulation leads to vision loss.

Stargardt's disease is a juvenile form of macular degeneration that can develop between the ages of six and twenty. Stargardt's disease is a rare form of macular degenerative diseases with close to 1 in 20,000-person frequency. The origin of this disease lies in the mutation of the ABCA4 gene; a membrane bound protein that helps transport N-retinylidene-phosphatidylethanolamine through the retina in the visual cycle.[76] With the inability to transfer N-retinylidene-phosphatidylethanolamine between the cells, these molecules can build up and form toxic dimers.

While some of the causes for macular atrophies have been demonstrated, there is a continued need for further exploration into what compounds cause retinal toxicity and inhibit the visual cycle. Identifying how these compounds are made and how they could be cleared into non-toxic byproducts are two methods to that could be used to treat the afflictions.

The Visual Cycle and its byproducts

Vision is originated by the photoreceptors of the rods and cones in animals with vertebrae.[78] The visual cycle is the process of recycling all-trans retinal (ATR) into 11-cis-retinal, which is required for pigment regeneration.[80] The photon capturing process of the visual cycle is achieved by rhodopsin, a light sensing chromophore covalently bound to opsin, a photoreceptor protein.[81] This chromophore undergoes isomerization to *all-trans* retinal (ATR) after it is connected with opsin, via Schiff base formation, and absorbs light into the retina. The photo-absorbance of the fluorophore leads to the conformational change of opsin and activates G-protein transduction, which facilitates vision.[79] A critical

aspect of the visual cycle is the regeneration of retinal starting material, as shown in Figure 13.

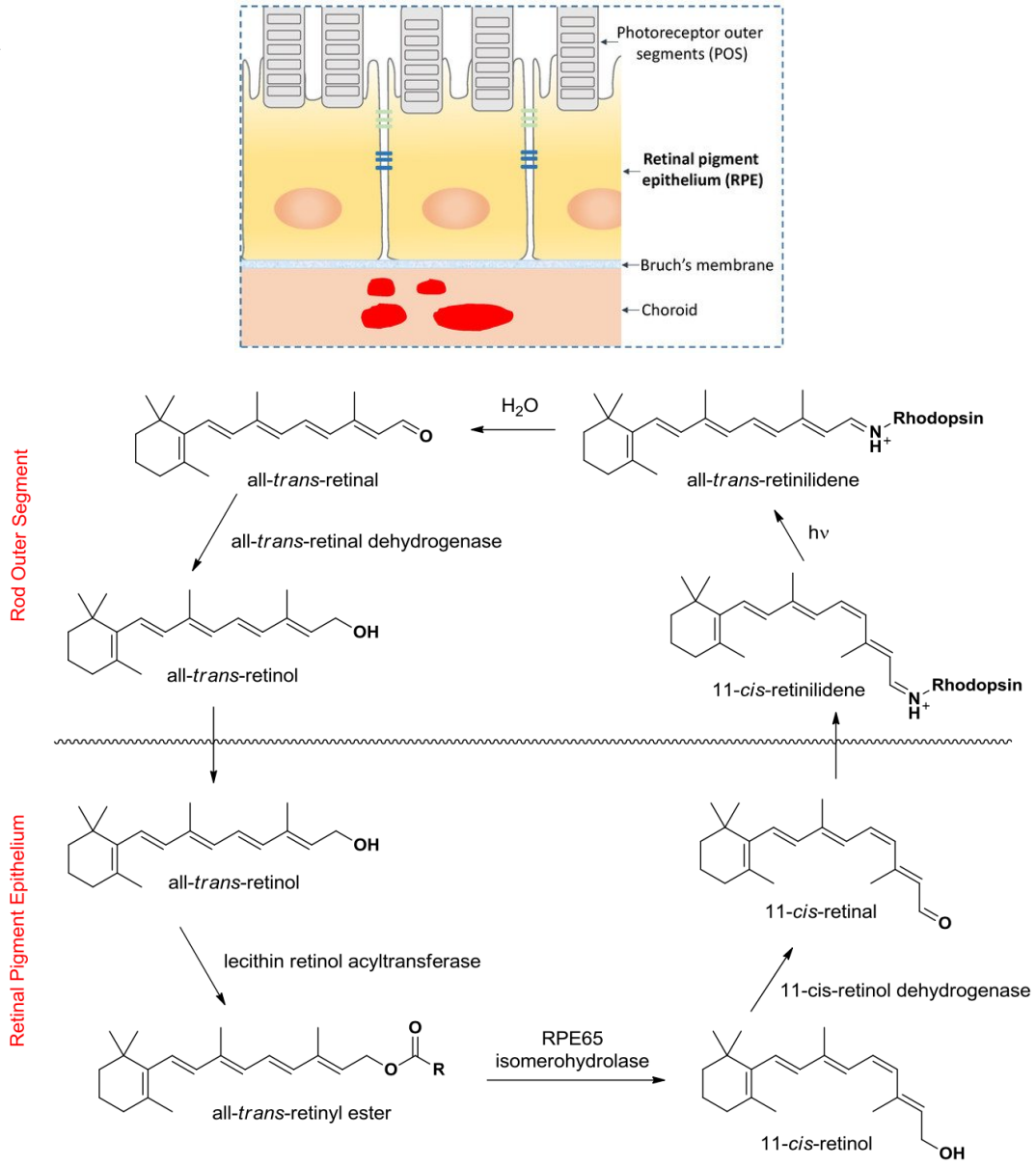

Figure 13 The human visual cycle. All-trans retinal and its derivatives cycle through the retinal pigment epithelium and rod outer segment with opsin or PE. The structural image of the retinal pigment epithelium and rod outer segment is also shown.[129]

The visual cycle is believed to originate with all-trans retinol, vitamin A, which is absorbed in the retinal pigment epithelium (RPE) through the blood stream. Retinol is then acylated by lecithin retinol acyltransferase (LRAT) and isomerized and hydrolyzed into 11-cis retinol in the RPE.[82,83] The 11-cis retinol then undergoes oxidation, attaches to opsin, via Schiff base formation, and migrates into the photoreceptor rich outer segment of the retina. ATR is generated after the retinol species is isomerized and hydrolyzed from opsin and released into the retina.[84]

As the visual cycle progresses, auto florescent byproducts of ATR form and accumulate inside the retina. The two biggest examples of these byproducts are the bisretinoid ATR dimers, A2E, and ATR-dimer (Cycloretinal).[85] A2E and cycloretinal have both been formed non-enzymatically. However, enzymes have been identified that are capable of catalyzing cycloretinal formation.

These compounds have been isolated from the lipofuscin of retinas and form from two molecules of ATR. The formation of either compound depends upon the stoichiometric ratio of amines present. The two bisretinoids are shown in figure 14. A2E has been extensively shown to form epoxides, when exposed to light of 430 nm, and cause retinal toxicity.[86] Since cycloretinal has the same conjugated chains that become oxidized in A2E, it is hypothesized that cycloretinal would undergo the same photo-oxidation and exhibit retinal toxicity.

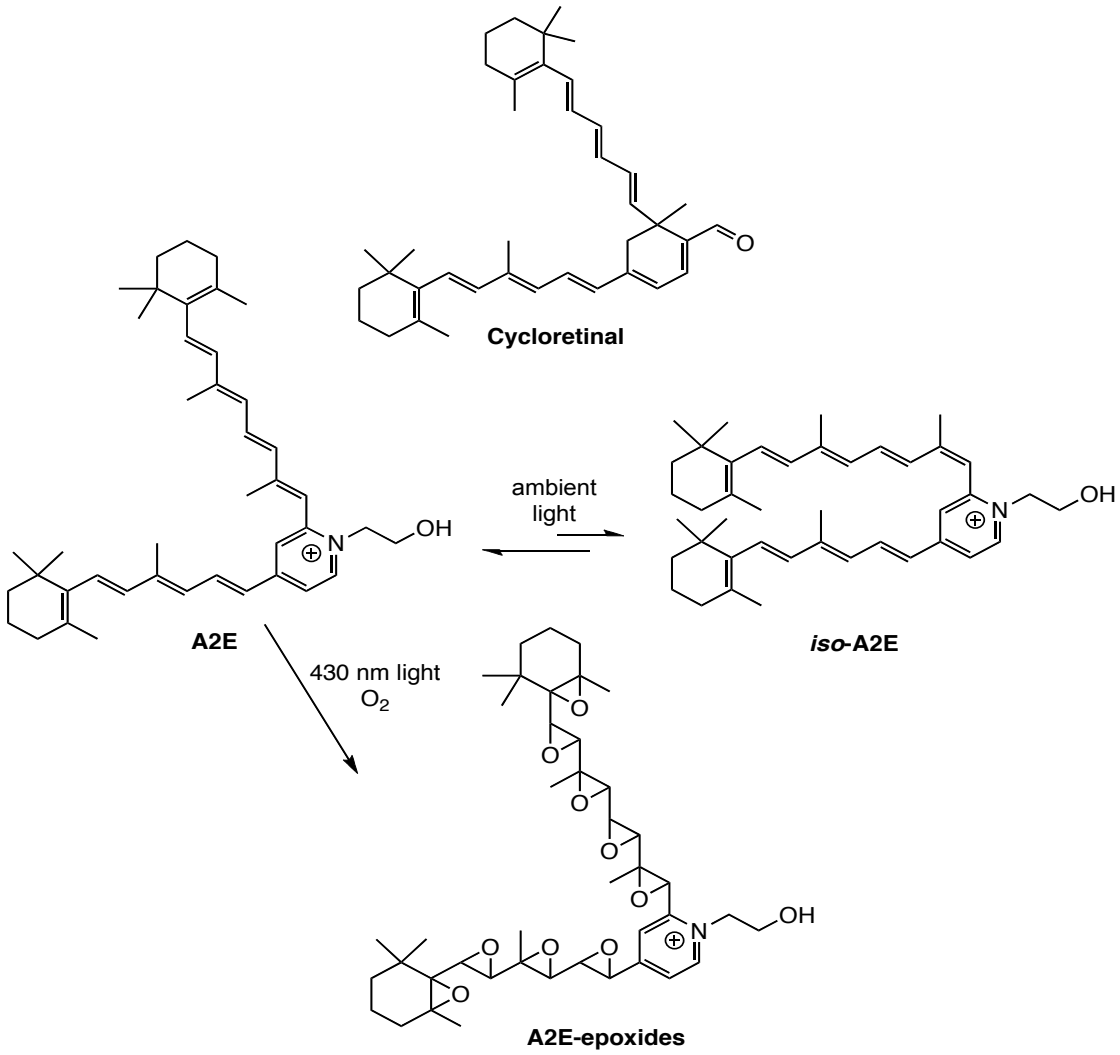

Figure 14 Lipofuscin formation and epoxidation from all-trans retinal monomers. A2E isomerizes from iso-A2E into A2E, which can form epoxides.

Oxidative toxicity of auto-fluorescent compounds

The accumulation of lipofuscin within the RPE has long been linked to macular degenerative diseases and the adduct A2E has been shown to induce blue-light mediated cell death.[87,88] The wavelength dependency on A2E toxic activation is concurrent with the excitation spectra of A2E and the known susceptibility of RPE cells to blue light exposure in animal models[89-91] A2E is capable of absorbing photons of specific energy by electron excitation to become photoactivated. Photoinduced damage can arise either through a direct reaction of the photoactivated molecule with cellular constituents and/or through the formation of reactive oxygen species.[92] The illumination of A2E with blue light leads to the formation of a specific pattern that involve the acceptance of oxygen.

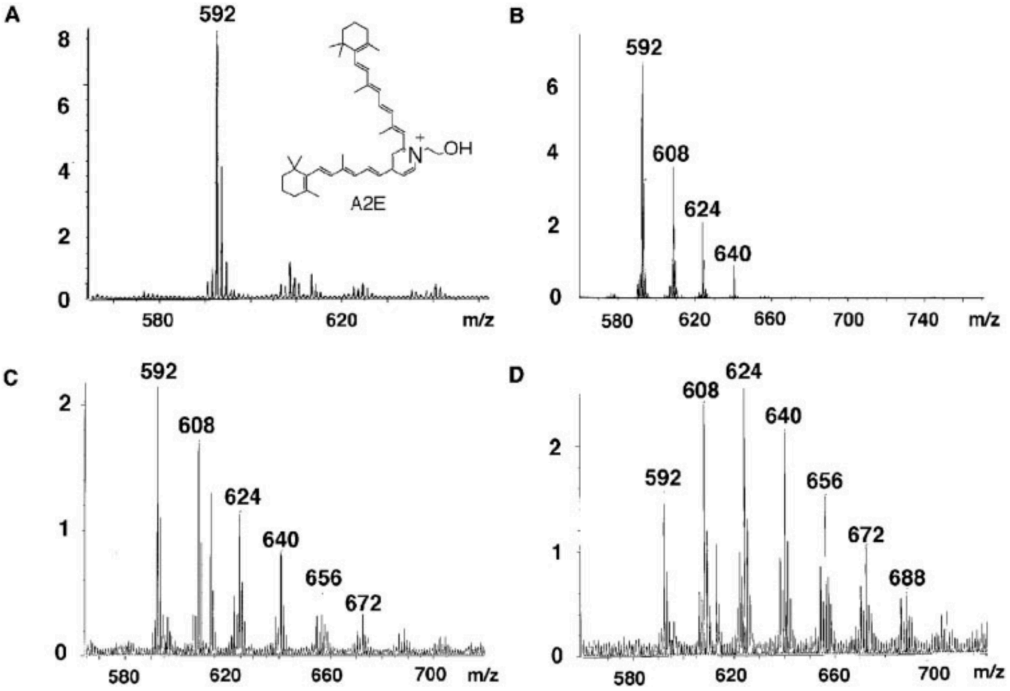

Figure 15 Oxidized Lipofuscin. FAB-MS analyzed of A2E illuminated at 430 nm of light. A.) A2E exposed to 0.075 mW/mm^2 for 10 min. B.) A2E with 0.095 mW/mm^2. C.) A2E with 0.15 mW/mm^2. D.) generated eries of molecular ion peaks for A2E. Each peak differed from the previous peak by a mass of 16.[92]

Figure 15 shows that as A2E is exposed to various intensities of light, it observes a mass increase of 16. These mass increases were eliminated when oxygen was removed from the media and A2E was irradiated in the presence of singlet-oxygen quenchers.[92]Given A2E's ability to form these epoxide moieties in the presence of oxygen and blue light, it is hypothesized that these conditions triggers oxidation of other lipofuscin and initiates death to the retinal pigment epithelium.

Synthetic and biosynthetic mechanisms for Cycloterpenal formation

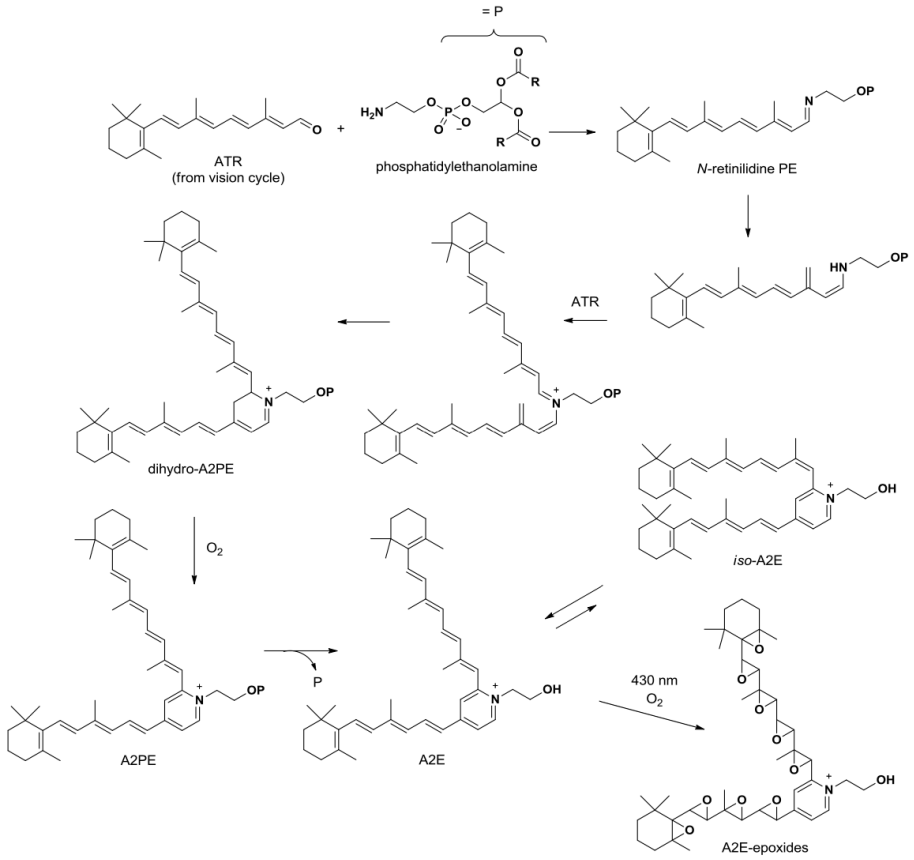

Figure 16 The formation of lipofuscin through all-trans retinal and a catalyst. Several steps occur in route to the formation of the dimers, A2E or cycloretinal.

The auto fluorescent bisretinoids A2E and cycloretinal have both been isolated from the lipofuscin of RPE and are created from a dimerization of ATR. The proposed mechanism for A2E synthesis is shown in Figure 16. ATR forms a Schiff base with phosphatidylethanolamine, a compound that allows ATR to move through the eye, and becomes deprotonated at the γ methyl group. This diene creates a secondary amine that can coordinate with another equivalent of ATR. This creates an open ring structure that becomes closed and deprotonated to create the final pyrimidine salt. It's hypothesized that cycloretinal forms under a similar mechanism as A2E. Two units of ATR can form Schiff bases with PE. The γ methyl group can also become deprotonated to create a diene structure. While one PE coordinates with two equivalents of ATR, cycloretinal forms when two equivalents coordinate with two equivalents of ATR. After the diene transition structure, two possible mechanisms were hypothesized and shown in Figure 17.

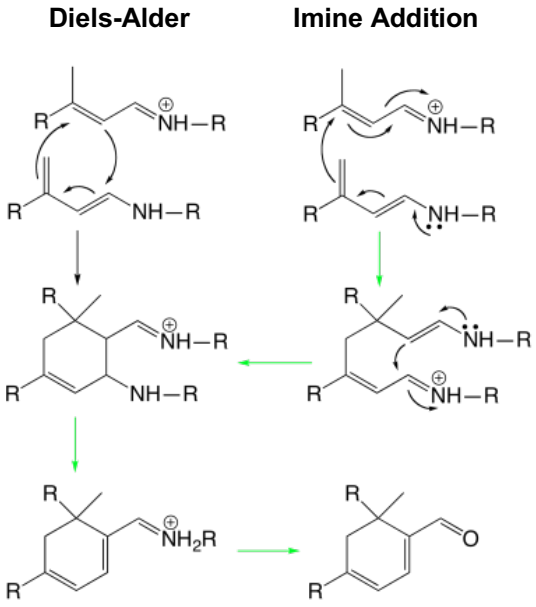

Figure 17 Proposed Cycloretinal Formation Mechanism

Once the diene forms, the closed cyclohexene ring forms through an aldol step-wise mechanism or a concerted, 4+2 cycloaddition. The challenge with these proposed mechanistic pathways is that both mechanisms create a cyclohexene intermediate.

Cycloretinal can also be created from the whey protein found in milk, β-Lactoglobulin (BLG). Schiff base formation can occur through lysine residues that are located within the hydrophobic cavity of BLG's active site. Elucidating the synthetic and enzymatic cycloretinal mechanism opens the possibility for the design of small molecule inhibitors. The ability to degrade or prevent lipofuscin from forming could prevent the negative physical effects that are associated with macular degenerative diseases.

The formation of natural products has been shown to demonstrate positive and negative effects in a wide array of biological systems. Through azinomycins anticancer properties, biosynthetic pathways can be characterized for the future purposes of engineering the pathway or developing site-specific delivery of azinomycin. The analysis of macular degenerative diseases identifies non-genetic factors that cause them. Discovering molecules that cause these diseases opens the door for identifying possible ways to treat these diseases. By identifying compounds that can combat and instigate disease, possible therapeutics can be developed that can be put towards clinical trials.

CHAPTER II

TRANSKETOLASE MEDIATED TWO CARBON EXTENSION IN THE CONSTRUCTION OF AN AZABICYCLE RING

Introduction

The construction of the azabicycle (aziridino[1,2-a] pyrrolidine) moiety is an essential aspect of azinomycin formation and its ability to display anti-tumor properties. A proposed biosynthetic route had been hypothesized and at least 11 different enzymatic steps have been predicted to be necessary for the formation of the azabicycle ring.

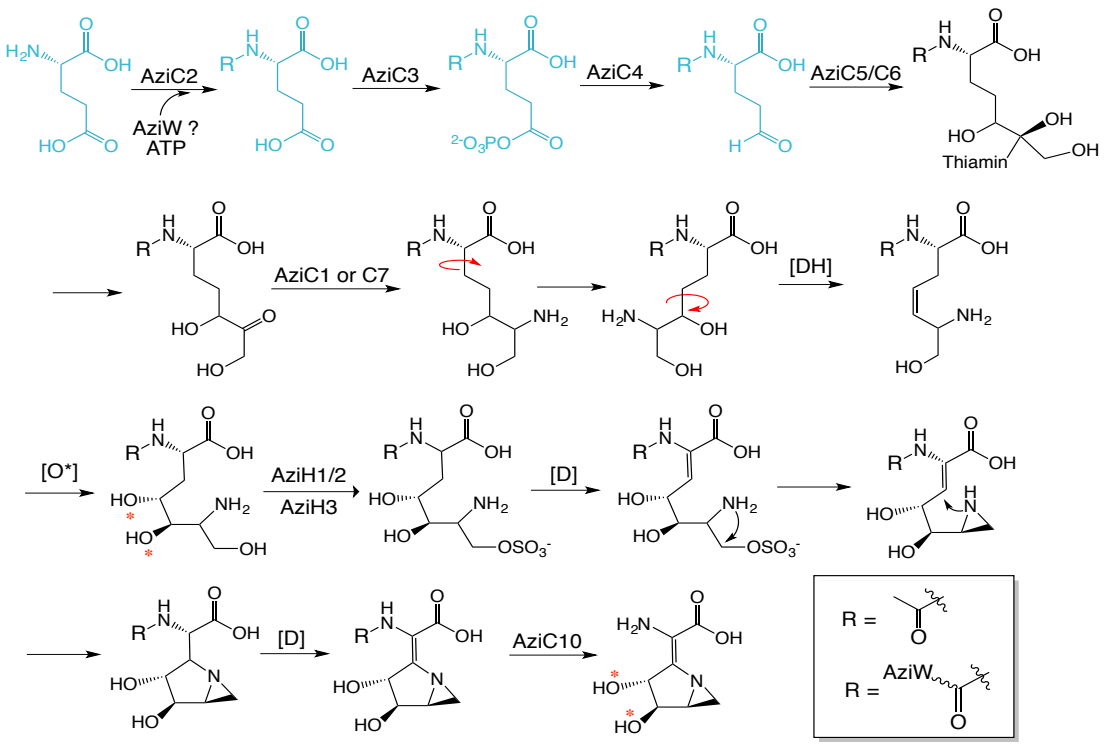

Scheme 1 Biosynthesis of the Azabicycle Moiety

Whole cell feeding studies with radiolabeled substrates indicated that glutamic acid is the precursor to the formation of the aziridine ring.[30] The blue highlighted

intermediates in Scheme 1 represent enzymatic steps that have been previously characterized. These enzymatic transformations are hypothesized to facilitate glutamic acids transformation into the aziridine ring. The free amine of glutamic acid interferes with the construction of hypothesized intermediates by undergoing intramolecular cyclization. In order to avoid the cyclization, the aziridine biosynthesis begins with AziC2 mediated acylation of the amine to give N-acetyl glutamic acid. Bioinformatic analysis has revealed that the addition of a protecting group to the amine is achieved with an amino group carrier protein, AziW. [93] After the protection of the amine group, AziC3 and ATP are able to phosphorylate the gamma carboxy group of glutamic acid. The creation of the acyl phosphate allows AziC4 and a reducing agent, NAD(P)H, to reduce that acyl phosphate and generate the glutamic acid semi-aldehyde intermediate.[94]

The proposed semi-aldehyde intermediate is lacking two carbons in comparison to the entire azabicycle moiety. A two-carbon extension step is necessary to transform glutamic acid semi-aldehyde into the ultimate azabicycle moiety. DNA annotation of the *Streptomyces sahachiroi* genome suggests that *aziC5* and *aziC6* encode the C- and N-terminal subunits of a transketolase enzyme. This is based on their high genetic similarity to the enzymes involved in ornithine and vazabitide biosynthesis.[93,95] Given the genetic similarity and the glutamic acid semialdehyde intermediate missing carbons, it was proposed that AziC5 and AziC6 use thiamin pyrophosphate and magnesium (II) to facilitate a transketolase mediated two carbon extension of glutamic acid semialdehyde to form 2-acetamido-5,7-dihydroxy-6-oxoheptanoic acid.

*Reproduced with permission from Washburn, L.; Foley, B.; Martinez, F.; Lee, R.; Pryor, K.; Rimes, E.; Watanabe, C. "Transketolase Activity in the Formation of the Azinomycin Azabicycle Moiety" *Biochemistry* **2019**, *58* (52), 5255-5258. 2020 American Chemical Society.

Preliminary research

aziC3, aziC5, and *aziC6* were successfully cloned, overexpressed, and purified in E. coli BL21 (DE3) to evaluate the next step of the pathway. *aziC4* was cloned in vector pET-21a (Rachel Lee). Synthesis of glutamic acid aldehyde was achieved following Scheme 2 (Flor Martinez). Diethyl 2-acetamidomalonate and sodium ethoxide were mixed under heat to generate an enolate. 3-chloro-Diethoxypropane was then slowly added to this solution to generate diethyl 2-acetamido-2-(3,3-diethoxypropyl) malonate. After subsequent basic and acidic treatments, the glutamic acid semialdehyde compound was synthesized.

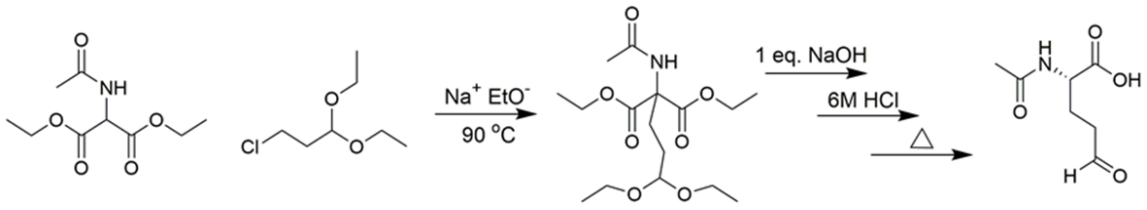

Scheme 2 Synthesis of AziC5/C6 Aldehyde Substrate

A homology study of human transketolase was performed and the binding pocket of the active site was found to contain a series of histidine's that help facilitate the cofactor thiamin pyrophosphate binding. The highly conserved residues His75, His129, His139, and His286 were hypothesized to have the largest role in this mechanism. His75 and

His139 of AziC5 are hypothesized to be involved in H-bonding with the aldose acceptor and keto-donor, while His139 and His286 are more directly involved in the mechanism. AziC5 and AziC6 are expected to form a tetramer of two homodimers. When overlaid with a human transketolase enzyme in Figure 18A, AziC5 and AziC6 revealed a similar structure to the human enzyme.

The histidine residues in the active site of AziC5/C6 are essential in the transketolase enzymes mechanism. To begin its enzymatic activity, AziC5/C6 takes the cofactor thiamin pyrophosphate into the active site and His286 of AziC5 deprotonates it to create the thiamin ylide. This ylide is capable of attacking the carbonyl carbon of the keto-donor substrate. Transketolase enzymes found in biological systems are capable of utilizing xylulose-5-phosphate or fructose-6-phosphate as the keto-donor substrate. However, hydroxy pyruvic acid (HPA) was utilized in assays due to the irreversibility of the reaction. The deprotonation facilitated by His286 can break a carbon-carbon bond of the keto donor substrate and create the dihydroxyl ethyl-thiamin enamine intermediate. This intermediate is capable of forming a carbon-carbon bond at the electrophilic carbonyl of the aldose acceptor. Deprotonation of a hydroxyl group by His129 of AziC6 breaks the thiamine-substrate bond and creates the α, α'-dihydroxy ketone product, 2-acetamido-5,7-dihydroxy-6- oxoheptanoic acid.

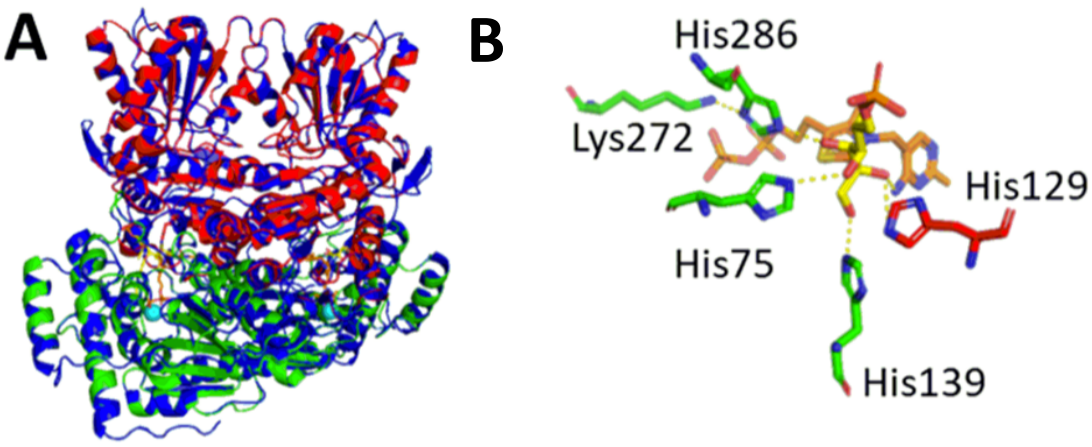

Figure 18 AziC5/C6 Model and Proposed Mechanism

A) Overlay of AziC5/C6 model with Human Transketolase (4KXU). Blue = 4KXU, Green = AziC5, Red = AziC6, Orange = thiamin pyrophosphate, Yellow = D-fructose-6-phosphate, Cyan = Mg2+. **B**) Zoom in on one catalytic site with conserved residues involved in substrate binding and enzymatic activity shown.

Transketolase enzymes role in multiple metabolic pathways allows them to utilize multiple keto donor molecules. Xylulose-5-phosphate (X5P) is employed in the pentose phosphate pathway and fructose-6-phosphate (F6P) is a crucial part of the Calvin cycle. The affinity of AziC5 and AziC6 towards each of these donor molecules and hydroxy pyruvic acid (HPA) was measured spectrophotometrically using potassium ferricyanide absorbance at 420 nm. In the presence of potassium ferricyanide, the α-carbanion intermediate of the thiamin-ketose donor complex is oxidized and ferricyanide is reduced, which leads to a decrease in absorbance at 420 nm.[96,97] The kinetic values demonstrate AziC5 and AziC6 have the highest affinity for their natural substrates, F6P and X5P, and

carried the lowest affinity for the irreversible keto donor substitute, HPA (Appendix Table 1).

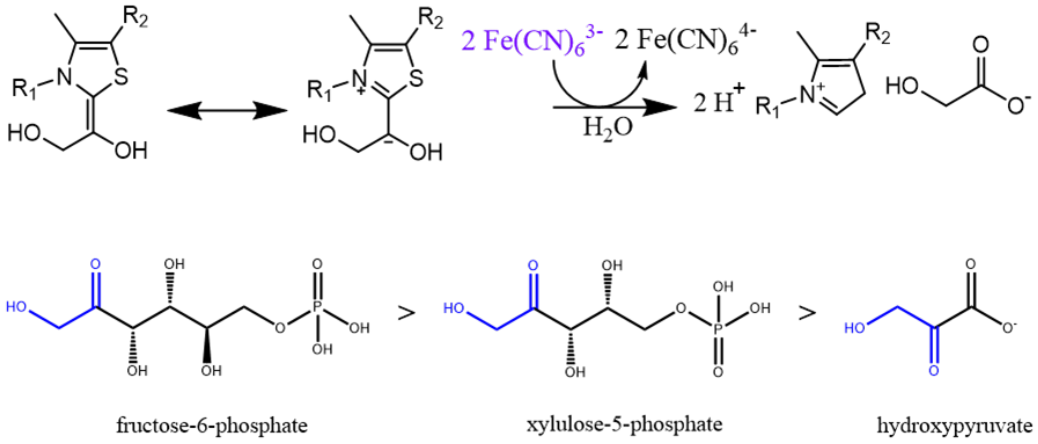

Figure 19 AziC5/C6 Donor Molecule Screening with molecules used in the pentose phosphate pathway, fructose-6-phosphate and xylulose-5-phosphate. Hydroxypyruvate provides an irreversible ketose donor

Results and discussion

Transketolase enzymes rely on the cofactor thiamine pyrophosphate (TPP) for the execution of their catalytic activity. TPP is able to be detected through several analytical techniques. The presence of TPP can be monitored by thiamin's activity within the UV range and thiamin's ability to become oxidized.[98,99] TPP was detected by observing its UV traces in a colorimetric assay and identifying its oxidized form with a thiochrome assay.

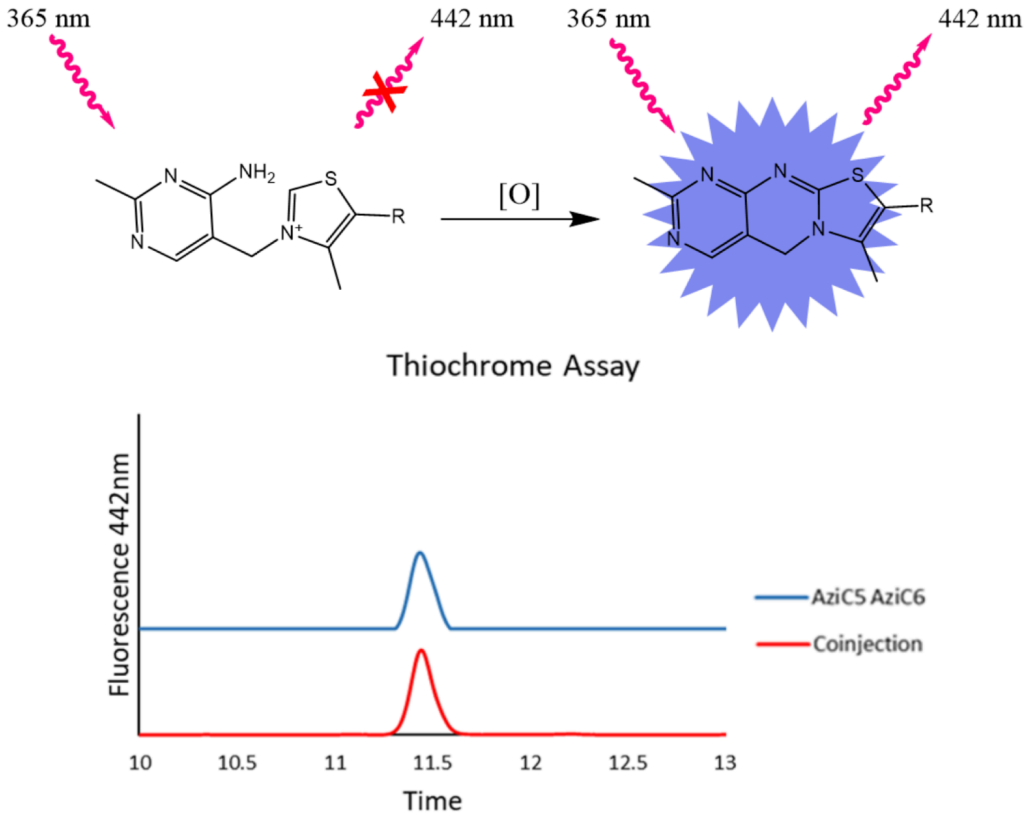

Figure 20 AziC5/C6 Thiochrome Assay with HPLC analysis. The denatured extract from AziC5/C6, shown in blue, was compared to the elution time of the synthesized thiochrome, shown in blue.

A thiochrome assay, which utilizes thiamin's ability to be oxidized, was performed with potassium ferricyanide. AziC5 and AziC6 were co-expressed, purified with a His-Trap column, and denatured with heat. The collected supernatant was exposed to the oxidizing environment of potassium ferricyanide and analyzed via HPLC to detect thiochrome's presence. The thiochrome product created from the enzymatic extraction was then compared to a synthetic standard, shown in Fig. 20. The co-injection of the enzymatic extraction and the synthetic standard were found to contain one peak at the

same retention time as the enzymatic extraction. This indicates that TPP was bound to AziC5 and AziC6 and is a necessary cofactor in its enzymatic activity.

A colorimetric assay, utilizing bromothymol blue, was also utilized to detect the presence of TPP. There is an acidic proton on the thiazolium ring of thiamin and it can be deprotonated in the presence of certain indicators. Bromothymol blue has two UV maxima in solution at 430 nm and 600 nm. AziC5 and AziC6 were denatured and exposed to a solution of bromophenol blue. The UV traces in Appendix Figure 13 demonstrate the I^{-2} state of the indicator decreased and the HI^{-} state increased. This indicates that thiamin is present because it changed the oxidation state of the indicator.

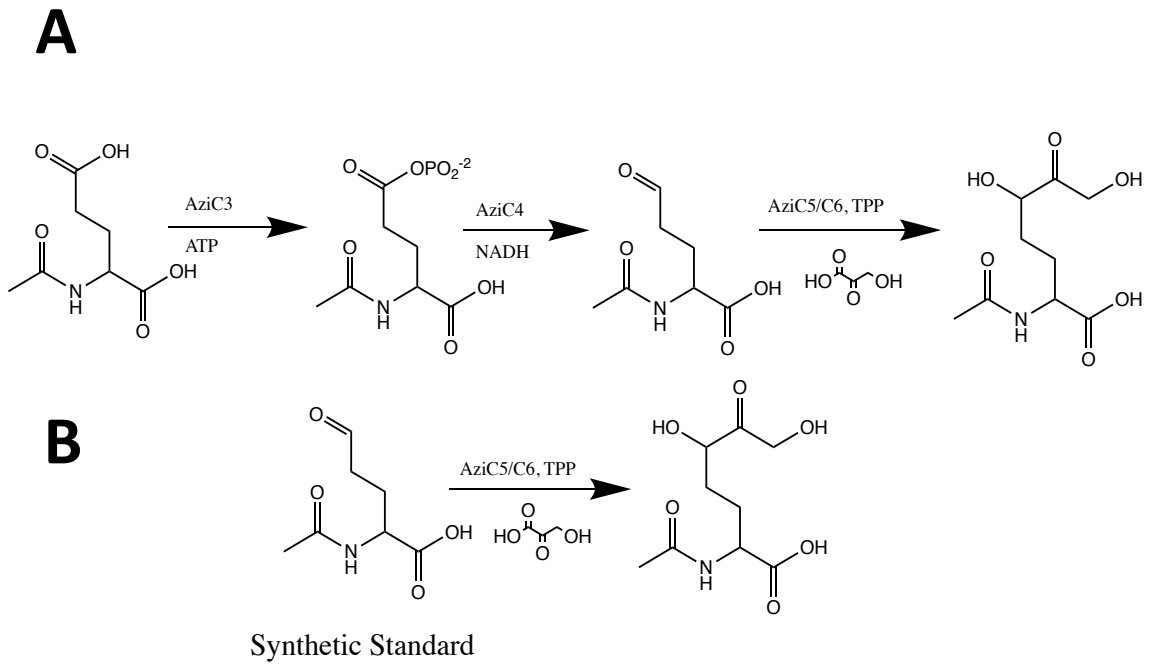

Scheme 2 Enzymatic and Synthetic routes to evaluate AziC5/C6 activity

The formation of the dihydroxy ketone product, 2-acetamido-5,7-dihydroxy-6-oxoheptanoic acid, was pursued through two routes, as shown in Scheme 2. A complete enzymatic assessment was performed with N-acetyl glutamic acid, AziC3, AziC4, AziC5 and AziC6. In addition, the synthetically achieved glutamic acid semi-aldehyde was directly exposed to AziC5 and AziC6. Both routes showed product formation as detected by electrospray ionization mass spectrometry (ESI-MS), giving masses of 233 [M + H] and 256 [M + Na], respectively. Synthetic semialdehyde and AziC5/C6 (route B) were used to obtain ESI-MS/MS data, giving the fragmentation seen in Figure 21. These fragmentation patterns are indicative of the desired dihydroxy ketone product.

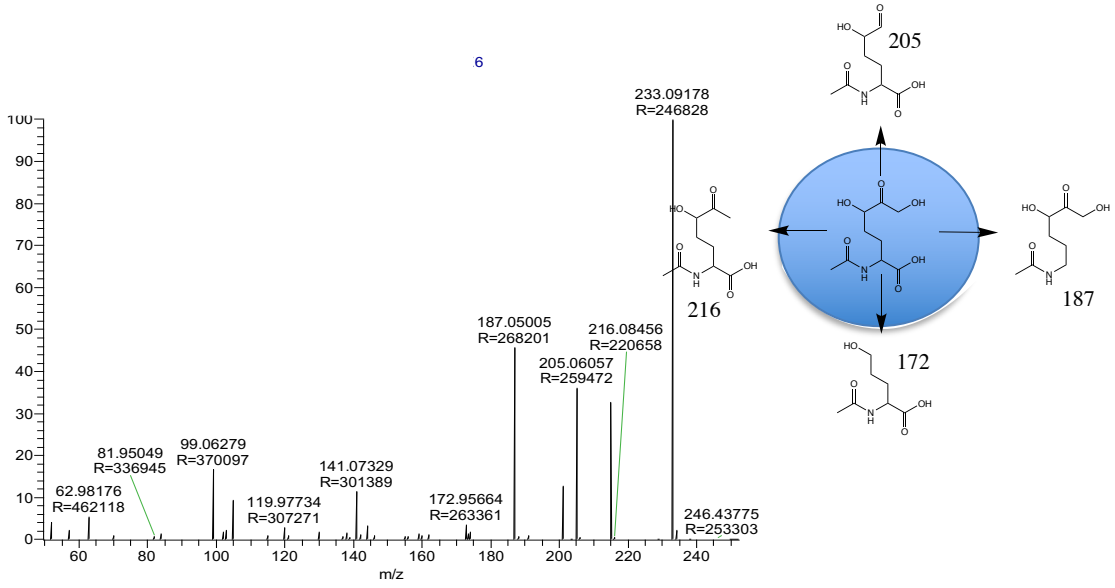

Figure 21 MS/MS fragmentation of AziC5/C6 product. The expected fragmentation was observed

To evaluate the necessity of both subunits in the reaction, controls were performed with one transketolase subunit at a time (AziC5 or AziC6). ESI-MS data can be found in

Appendix Figure 12. Minimal product formation is observed in the control reactions, likely catalyzed by TPP in solution. This confirms the need for both subunits in the enzymatic transketolase reaction.

The transketolase mediated formation of α, α'-dihydroxy ketones was also determined using a tetrazolium red, colorimetric assay.[100] When the dihydroxy ketone product is created in basic conditions, the hydroxyl groups are susceptible to deprotonation. The deprotonation forms a ketone and gives off a hydride anion, as seen in scheme 3. This reducing agent can react with a yellow tetrazolium dye to produce a red formazan precipitate (Figure 22). Trials were performed in the absence of enzyme, TPP, keto donor, and aldose acceptor. The only conditions that resulted in the red color change included AziC5/C6, TPP, glutamic acid semialdehyde, and HPA. This assay and mass spectrometry results demonstrates that both AziC5 and AziC6 are necessary for enzymatic activity.

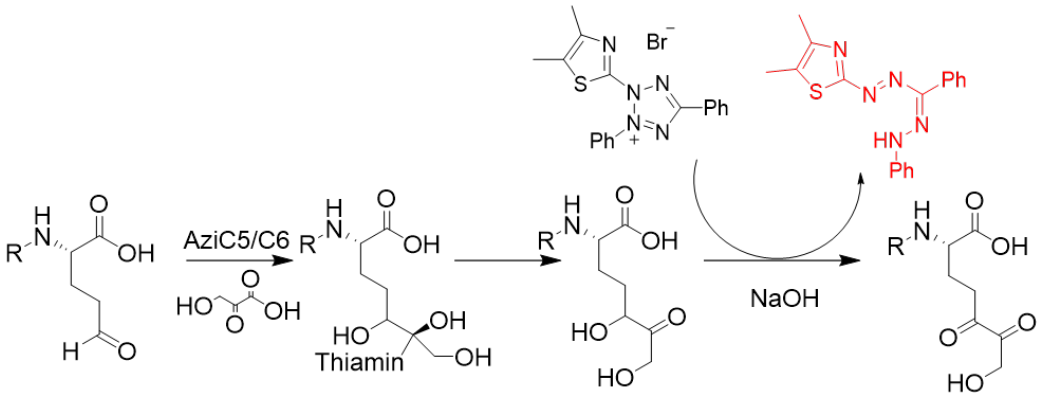

Scheme 3 Mechanism of transketolase assay

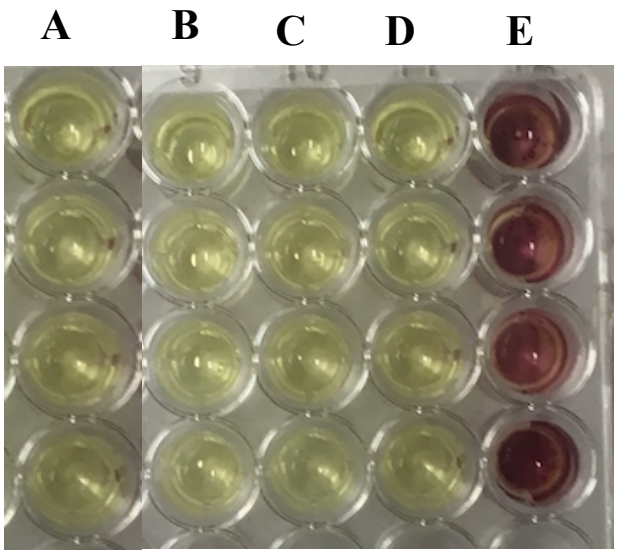

Figure 22 Transketolase assay with tetrazolium red
A. No enzyme, B. No substrate, C. No HPA, D. No TPP, E. Enzymes with substrates and cofactors

Significance

Elucidating the biosynthetic pathway of the aziridine ring in azinomycin is invaluable. This characterization provides an enzymatic route to creating a DNA binding reagent with potential therapeutic effects. Whole cell feeding studies revealed that glutamic acid is the precursor to the azabicycle. This work revealed the two-carbon extension that is necessary to form the azabicycle ring from glutamic acid. In addition, it was revealed that the two-carbon extension was achieved through a transketolase mediated

reaction. In order for this enzymatic reaction to proceed, thiamin pyrophosphate, a two-carbon donor molecule, and both AziC5 and AziC6 are needed. The enzyme was shown to bind thiamin after its presence was detected through a thiochrome assay. The identification of the 2-acetamido-5,7-dihydroxy-6- oxoheptanoic acid intermediate creates the opportunity to investigate the next steps in the aziridine biosynthesis. The proposed biosynthetic route, shown in Figure 1, indicates that after the creation of the dihydroxy intermediate, several of the remaining steps can be readily achieved synthetically. The dihydroxy ketone product allows for a semi-synthetic route that could create the azabicycle ring. Additionally, AziC5 and AziC6 achieve carbon-carbon bond formation, which is difficult to accomplish through synthetic means. AziC5 and AziC6 mediated creation of a dihydroxy ketone product enables the formation of an intermediate that is easily activated and utilized.

Materials and methods

Instrumentation and reagents

^{1}H & ^{13}C NMR spectra were recorded on an Avance III 400. ESI mass analysis was obtained with ion trap mass spectrometer (LCQ-DECA, ThermoFinnigan), at the Laboratory for Biological Mass Spectrometry at the Department of Chemistry, Texas A&M University. UV spectra were measured on a ThermoFisher GENESYS 10 Bio spectrophotometer. Adenosine-5'- triphosphate magnesium salt (ATP), β-nicotinamide adenine dinucleotide (NAD), reduced disodium salt (NADH), Potassium β-

hydroxypyruvate (HP), Thiamin Pyrophosphate (TPP), potassium ferricyanide, fructose-6-phosphate (F6P), xylulose-5-phosphate (X5P) and β–nicotinamide adenine dinucleotide phosphate hydrate (NADPH) were purchased from Sigma-Aldrich (St. Louis, MO, USA). N-acetyl-L-glutamic acid was obtained from Alfa Aesar, a Johnson Matthey Company, and New England Biolabs (NEB, Ipswich, MA, USA).

Cloning, expression, and purification of recombinant proteins

aziC3, *aziC5*, and *aziC6* were individually cloned into vector pET-24b; *aziC4* was cloned into vector pET-21a. Primers and restriction enzyme sites are provided below in Table S1. The construct was transformed in BL21 (DE3) *E. coli* strain for protein overexpression. A 10 mL overnight culture in LB medium containing 50 μg/mL kanamycin (100 μg/mL ampicillin for pET21a-aziC4) was added to 1 L of medium and grown until an OD_{600} of 0.8 was reached. The culture was induced with 1 mM IPTG and incubated at 16 °C for 22-24 h prior to harvest. The cells were centrifuged at 6,000 rpm for 20 min, washed twice with cold 50 mM phosphate buffer (300 mM NaCl and 10% glycerol at pH 7) and re-suspended in the same buffer containing 1 mM dithiothreitol (DTT) and 1 mM phenyl methylsulfonyl fluoride (PMSF). The cell pellets were sonicated on ice water bath using Branson Sonifier 450 (Branson Ultrasonics) fitted with a micro tip, output setting 6, duty cycle 50%, for 8 cycles for 30 sec each and centrifuged for 1 h at 12,000 rpm. The soluble protein was purified by Nickel affinity chromatography, His Trap TM FF 5 mL column (GE Healthcare Life Sciences), according to the instructions provided by the supplier. The purified fractions were desalted and concentrated using Amicon® 10K Ultra.

Synthesis of Glutamic Acid Semi-aldehyde

Diethyl acetamido malonate, 2.5 g (1 eq.) was mixed with 1.72 g (2.2 eq.) of sodium ethoxide in 30 mL of THF. The mixture was subsequently stirred and heated under reflux at 90 °C for 30 min. To the mixture, 1.92 mL (1 eq.) of 3-chloropropionaldehyde diethylacetal was added dropwise over 20 min. and the reaction allowed to stir with heat (90 °C) overnight. The mixture was subsequently allowed to reach room temperature and the resulting salt filtered. The filtrate was concentrated in vacuo and the oily residue diluted with water, extracted with ether, and dried over anhydrous sodium sulfate. Purification by column chromatography was completed on silica centrifugal filter (EMD Millipore) gel using 2:1 hexane: ethyl acetate. This afforded diethyl 2-acetamido-2-(3,3-diethoxypropyl) malonate (2.57 g, 64.4%) as characterized by ^{1}H and ^{13}C NMR (Appendix Figure 2-4). The product was subsequently treated with 1 equivalent of NaOH and mixture refluxed for 5 h. The reaction was cooled to room temperature and treated with 6 M HCl to a pH of 2. The mixture was lyophilized, dissolved in water and refluxed for an additional 3 h. The sample was lyophilized again to give N-acetyl-glutamate 5-semialdehyde as a yellow precipitate (0.98 g, 76.6%). NMR and mass characterization are provided in Appendix Figure 5-8. ~Note: Glutamic acid semialdehyde exists in equilibrium with its diol in D_2O as observed by NMR spectroscopy.

Enzymatic reaction of AziC3/C4/C5/C6 and product analysis

A reaction mixture consisting of 20 mM N-acetyl-L-glutamic acid (pH 7), 10 mM ATP, 2 mM NAD(P)H, 5 mM $MgCl_2$, 10 mM thiamin pyrophosphate, 10 mM β-hydroxypyruvic acid, 40 mM Tris-HCl (pH 7) and 0.2 mg/mL of purified AziC3/AziC4/AziC5/AziC6 protein was prepared and incubated in a 37 °C water bath overnight. The reaction was terminated with the addition of an equal volume of TCA (8%). The protein portion was pelleted by centrifugation to remove precipitates and the resulting aqueous solution was lyophilized to dryness and subjected to MS/MS analysis.

Enzymatic reaction of AziC5/C6 and product analysis

A reaction mixture consisting of 50 mM N-acetyl-glutamate 5-semialdehyde, 5 mM $MgCl_2$, 10 mM thiamin pyrophosphate, 10 mM β-hydroxypyruvic acid, 40 mM Tris-HCl (pH 7) and 0.2 mg/mL purified AziC5/AziC6 protein was prepared and incubated at 37 °C water bath overnight. The reaction was terminated with the addition of an equal volume of TCA (8%). The protein portion was pelleted by centrifugation to remove precipitates and the resulting aqueous solution was lyophilized to dryness and subjected to MS/MS analysis. To evaluate if both AziC5 and AziC6 subunits were necessary for product formation, controls lacking one subunit at a time were performed and analyzed by MS.

Thiochrome assay

The thiochrome assay involves conversion of thiamin phosphate to a thiochrome phosphate product. AziC5/C6 were expressed in the presence of 100 mM thiamin

pyrophosphate. The harvested protein was purified on a Ni-His Trap Column and the purified fractions desalted and concentrated with an Amicon 10K Ultra centrifugal filter (EMD Millipore). The isolated protein was quenched with an equal volume of TCA (8%) and centrifuged. To the resulting supernatant (100 μL) was added potassium acetate (50 μL of 4 M), followed by oxidative cyclization with the addition of a saturated solution of $K_3Fe(CN)_6$(50 μL) in 7 M NaOH, resulting in the formation of the desired thiochrome phosphate. Neutralized after 1 min with 6 M HCl and analyzed by HPLC.

Homology modeling of AziC5/C6

Homology modeling was performed using SWISS-MODEL. Model quality was evaluated by having a QMEAN score of less than 4. The model for AziC5/C6 was built upon the crystal structure of a human transketolase with D-fructose-6-phosphate bound and thiamin bound (PDB 4KXU).5 AziC5/C6 and 4KXU have 33 % sequence identity. The model was visualized using Pymol to identify residues that may play a role in transketolase activity of AziC5/C6.

Assay for Transketolase activity

The following methodology was used to assess transketolase activity. A 90 μL reaction mixture containing N-acetyl-glutamate 5-semialdehyde 6 (50 mM), lithium hydroxypyruvate (50 mM), TPP (2.4 mM), MgCl2 (9 mmol) and purified AziC5/C6 protein (5 mg/mL) in Gly-Gly (50 mM, pH 7.0) was incubated at 20 °C for 17 h. The reaction mixture (10 μL) was subsequently transferred to a microwell containing MP-

carbonate resin (Biotage AB) (10 mg) and Gly-Gly buffer (90 μL, 50 mM, pH 7.0) and the mixture incubated at 20 °C for 3 h. The mixture (50 μL) was diluted with Gly-Gly buffer (50 μL, 50 mM, pH 7.0), to which 3-(4,5-dimethylthiazol-2-yl)-2,5-diphenyl tetrazolium bromide (20 μL) and 3 M NaOH (10 μL) was added and mixed thoroughly. Four control experiments lacking in N-acetyl-glutamate 5-semialdehyde 6, lithium hydroxypyruvate, thiamin pyrophosphate, and AziC5/C6 proteins respectively, were performed.

CHAPTER III

PPTASE AND THIOESTERASE ACTIVITY

IN NAPHTHOATE PRODUCTION

Introduction

Although the aziridine ring and the epoxide moiety facilitate DNA crosslinking, the naphthoate ring is a vital part of azinomycin and stabilizes coordination. The hydrophobicity of the naphthoate fragment helps to augment interactions with DNA base pairs.[24] In addition, the epoxide and naphthoate fragments together have been observed to make DNA linkages without the aziridine or enol fragments.[21] The naphthoate fragment is created by a Polyketide Synthase (PKS) enzyme, AziB, and uses acetyl-CoA and malonyl-CoA to achieve the formation. However, AziB by itself is unable to produce the naphthoate fragment, but instead produces 2-methyl-benzoic acid. If the thioesterase (TE) domain of PKS is present, it produces the desired 5-methyl naphthoic acid.[10]

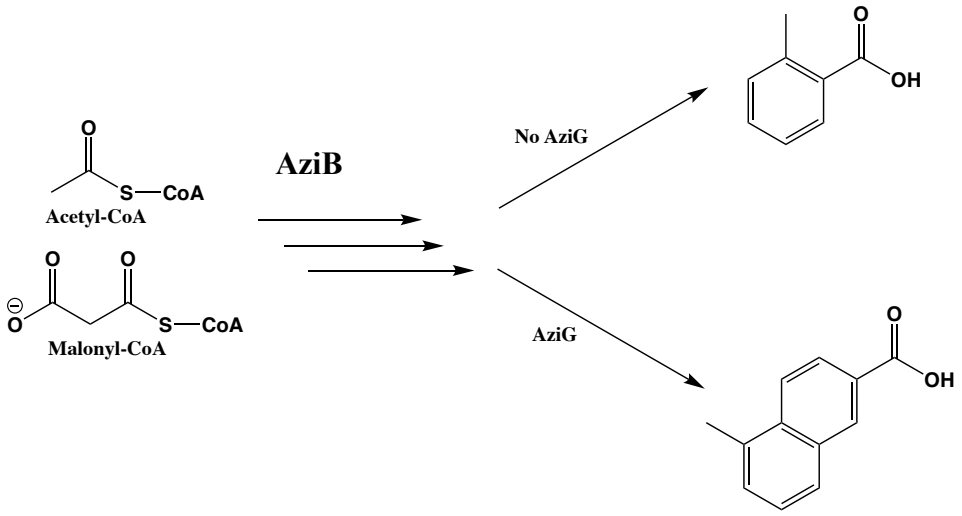

Figure 23 PKS product formation with and without the thioesterase domain

PKS enzymes contain multiple domains and initiate their activity after the posttranslational modification of the acyl carrier protein (ACP) domain with acetyl-CoA or other starter units. The CoA starter units are attached to the ACP domain via PPTase and Mg (II). After the CoA cofactor is attached to the ACP domain, it then carries the chain to the other domains of the PKS and promotes chain growth. The final domain involved in PKS enzymes is the TE domain. The TE domain of PKS enzymes performs multiple functions. It cleaves the thioester bond to release the final product from the PKS enzyme, facilitates chain elongation, and promotes chain cyclization. By expanding our understanding of how the PKS enzyme is post-translationally modified and how the TE domain is involved in cleavage from PKS and chain elongation, azinomycin production could be increased and naphthoate analogs could be developed to increase the hydrophobic interactions between DNA strands and azinomycin.

Preliminary research

AziB was previously expressed in a heterologous source, *E. coli*, and post-translationally modified by several PPTases. These include Svp and Sfp, from *Bacillus subtilis,* and FAS and NFAS, from *S. sahachiroi.* FAS and NFAS were cloned into *E. coli* but their expression was too low for regular usage (Dr. Lauren Washburn, Dr. Shogo Mori, and Dr. Huitu Zhang).[101,102] The ACP domain of AziB was previously expressed in *E. coli.*

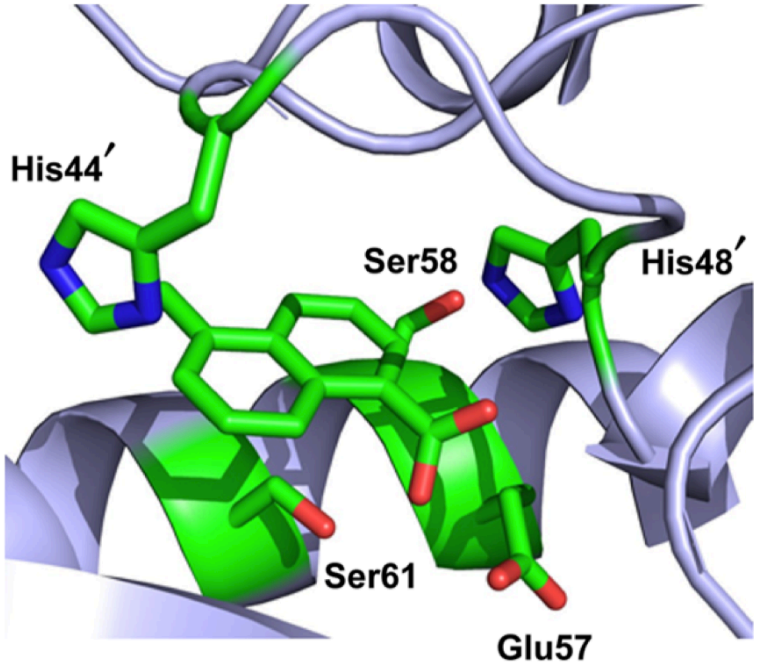

Figure 24 Crystal Structure of the thioesterase AziG
Depiction of the AziG active site with the substrate 5-methyl-naphthoic acid present. Ser58-H48-Glu57 form catalytic triad conserved amongst TE.[101]

The TE domain of AziB, AziG, was previously expressed in *E. coli.* A crystal structure of AziG was obtained and genomic analysis was utilized to evaluate the most essential residues within the active site, as seen in Figure 24.[101] TE domains utilize a conserved catalytic triad of serine, histidine, and aspartic acid. They operate in a cascading fashion as the aspartate activates histidine, which then activates the serine to hydrolyze the thioester bond. It was hypothesized that S58, H48, and E57 were the conserved residues of the TE catalytic triad within the active sites. The close vicinity of H48 to S58 and the small distance between S58 and the carboxyl group of 5-methyl-naphthoic acid were proposed to function like in Figure 11. An active site glutamic acid, Glu57, was hypothesized to perform the same function of aspartic acid in this mechanism.

Additionally, H44 and S61 were identified within the active site as remaining residues that could play a role in catalysis. These residues were mutated to alanine, incubated with AziB and its substrates, and analyzed by LC/MS to determine their effects on the production of 5-methyl-naphthoic acid.[30] None of the AziG mutants were able to eliminate the production of the 5-methyl-naphthoic acid as seen in Figure 25.

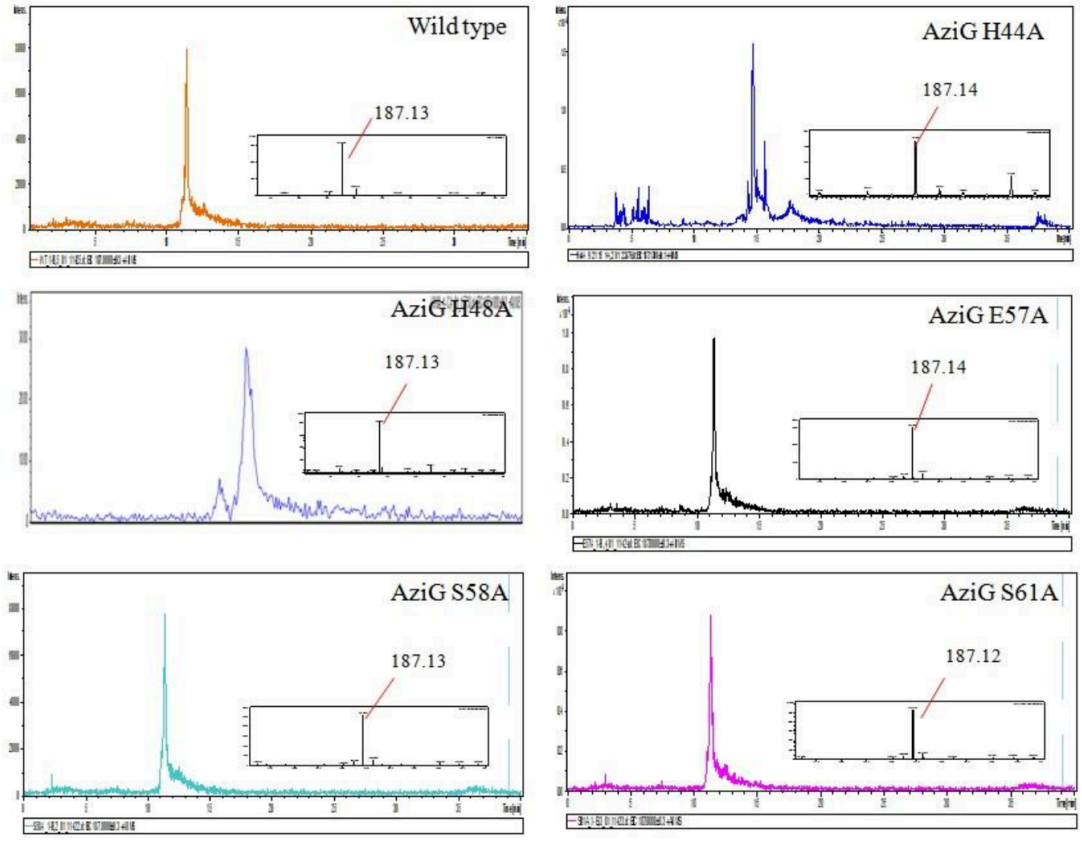

Figure 25 LC-MS analysis of AziB-AziG mutant products[101]
The product of AziB and AziG mutants was analyzed by LC-MS. The wild type AziG was used as the control.

The TE mediated rate of hydrolysis of thioester bonds was evaluated with AziG and its mutants. Kinetic analysis of these enzymes was determined utilizing a N-acetylcysteamine, SNAC mimic, but the measured catalytic activity of AziG and its mutants was low. In order to measure the actual hydrolytic cleavage of AziG, 5-methyl-naphthoate-CoA bound to the ACP domain of AziB was needed.

Results and discussion

In order to accurately measure the hydrolytic cleavage of 5-methyl-naphthoic acid from the ACP domain of AziB, the post-translational modification of AziB by PPTases needed to be optimized. Increasing the efficiency of Svp, Sfp, FAS, and NFAS mediated post-translational modification of AziB and the separated ACP domain was achieved through an enzyme linked immunosuppressant assay, ELISA, as shown in Figure 26.

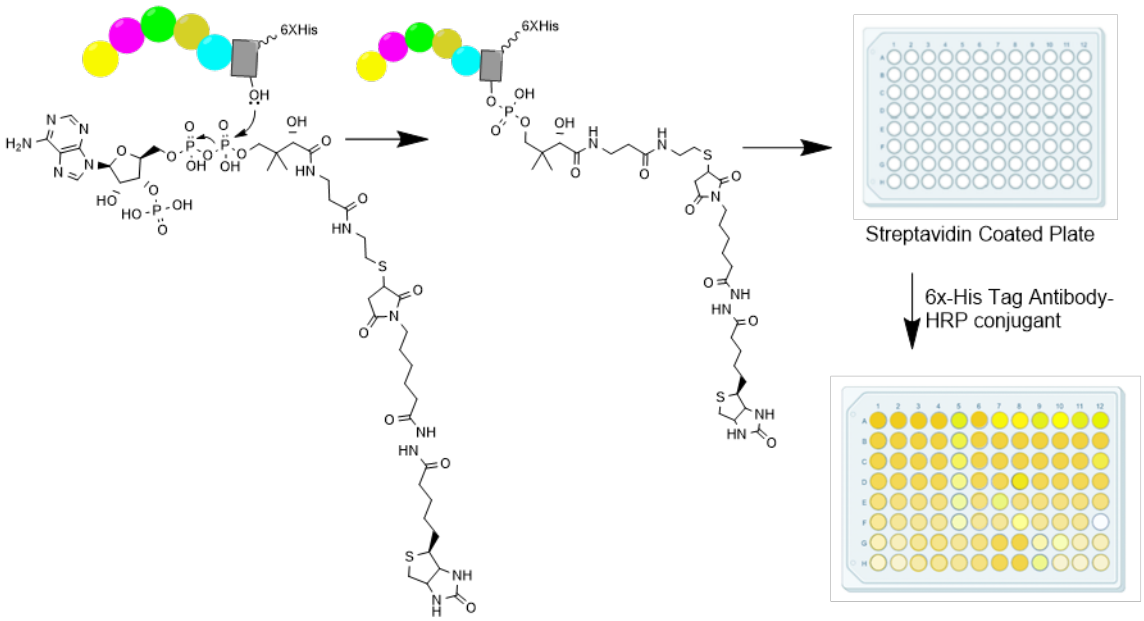

Figure 26 ELISA assay evaluating PPTase activity on AziB and the ACP domain

A streptavidin coated plate that binds biotin labeled substrates was used to assess the efficiency of post-translational modification. A biotin-CoA substrate was synthesized (Appendix Fig. 13), incubated with either AziB or the ACP domain, and treated with one of the four PPTases (Sfp, Svp, FAS, NFAS). Protein that is labeled with the biotin-CoA substrate binds to the streptavidin plate and unlabeled protein is removed with washes. A 6X-His Monoclonal Antibody – Horse Radish Peroxidase (HRP) Conjugant was used to coordinate with and quantify the labeled proteins. AziB and its ACP domain were expressed and purified utilizing a 6X-His-tag. This tag binds with the Monoclonal Antibody and protein labeling is determined by HRP activity. The amount of post-translationally modified ACP or AziB was measured by UV and is shown in Figure 27 and 28. The absorbance values and their standard deviation are shown in Appendix Table 4 and 5.

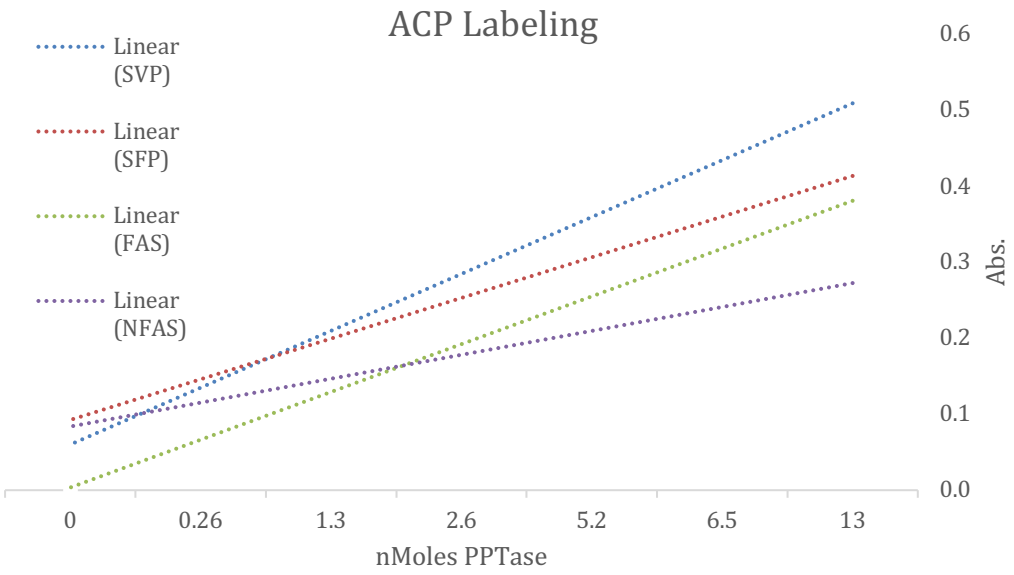

Figure 27 ACP domain of AziB labeling efficiency with different PPTases measured through ELISA.

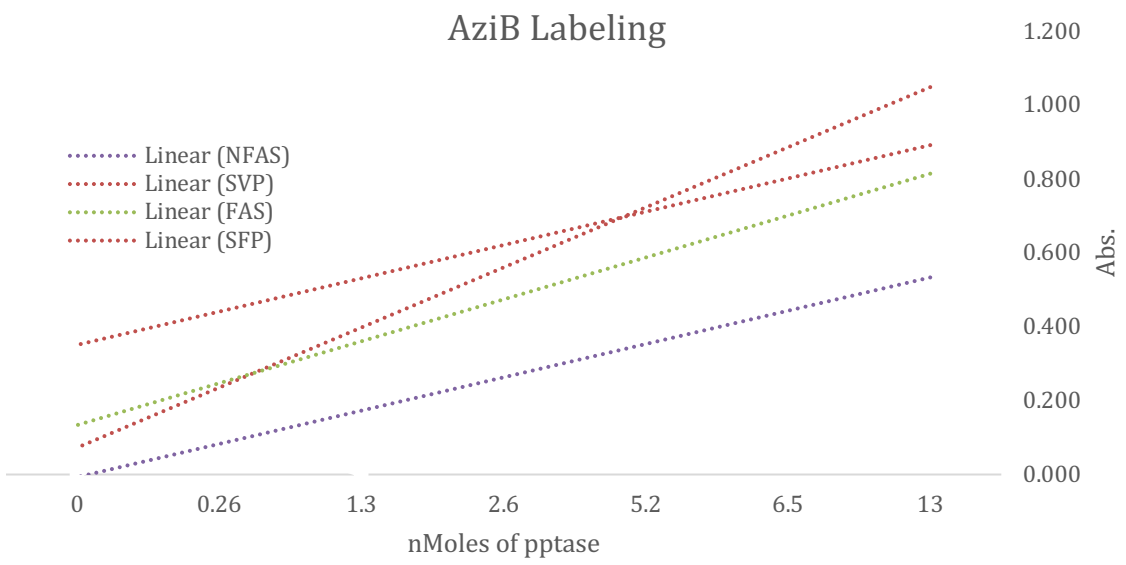

Figure 28 AziB labeling efficiency with different PPTases through ELISA

In the presence of HRP, 3,3′,5,5′-Tetramethylbenzidine (TMB) becomes oxidized and produces a blue color change. The peroxidase activity was quenched with acid and quantified using UV. The assay revealed that full AziB was labeled with a higher frequency than the isolated ACP at the same PPTase concentrations. Amongst the four PPTases, Svp was the most efficient followed by Sfp, FAS, and NFAS. This conclusion was made based on the slopes of each of the PPTases. Considering that Svp had the largest increase in absorbance per unit of protein, it shows that it possessed the greatest activity. The post-translational modification is not only dictated by PPTase. The modification is also dependent upon temperature, pH, and Mg concentration. ELISA was performed to analyze the optimal conditions for each variable. The conditions that provided the optimal

posttranslational modification were Sfp, at 37°C, at pH of 6.2, and with a Mg concentration above 1 mM, as shown in Table 1(Appendix Figures 15-19).

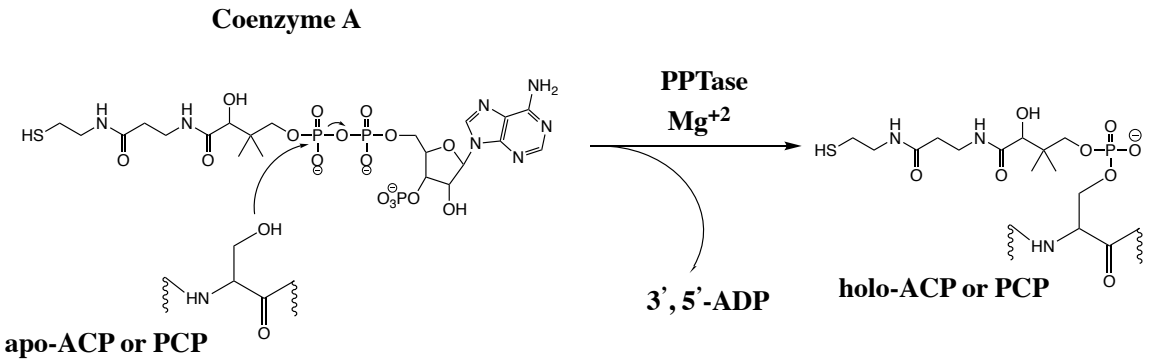

Figure 29 PPTase coordination of CoA to the ACP

	PPTase Type	Pptase : ACP or PCP	Rxn Time	pH	Mg^{2+} Conc.
Opt. Cond.	SVP, SFP, FAS, NFAS	1:8<	1 hr. ≤	6.2	1 mM ≤

Table 1 Optimal PPTase conditions measured through ELISA

After post-translational modification, a CoA analogue was synthesized by creating a thioester bond between 5-methyl-benzoic acid and the thiol of CoA (Appendix Figure

20) with isobutyl acetate. This synthetic analogue was post-translationally modified onto AziB utilizing the optimized conditions in Table 1. Once the post-translationally modified AziB was made, the rate of thioester hydrolysis was measured for AziG and its mutants. The rate of hydrolysis was determined using Ellmans reagent (5,5'-dithio-bis-(2-nitrobenzoic acid) or DTNB). Thioester hydrolysis releases a free thiol, which then breaks the disulfide linkage of DTNB. The resulting 2-nitro-5- benzoic acid can then be measured by UV. Although the bound CoA-Naphthoic Acid AziB hydrolysis is faster than SNAC experiments, the kinetic values are still lower than other thioesterases.[103,104] The predicted mechanism for thioester cleavage is a base mediated hydrolysis, where the activated serine can deprotonate a water molecule, which acts as a nucleophile. The kinetic values seen in Table 2 are not able to definitively support this conclusion. Although two residues within the proposed catalytic triad, H48 and S58, give the lowest values upon mutation, the hydrolysis values between all of the mutants does not definitively support a hydrolysis mechanism or confirm a catalytic triad of S58-H48-E57.

AziG Thioesterase	**k_{cat}/K_m (M^{-1} s^{-1})**	**k_{cat}/K_m (M^{-1} s^{-1}) w/ SNAC**
WT	1.26 ± .02	1.11± .04
H44A	0.53±.04	0.56± 0.02
H48A	0.48±.03	0.36 ± 0.03
E57A	0.74±.03	0.40 ± 0.03

Table 2 k_{cat}/K_m values for AziG and its mutants with AziB bound substrate

Given the low kinetic values, it's hypothesized that the hydrolysis rates are low because there is no separation and differentiation between unlabeled and labeled AziB, the substrate for the reaction. The most efficient post-translational modification of AziB was pursued so that this problem could be avoided, but the substrate concentration was based on how much of the protein substrate was present, independent of whether it was labeled or not. Since we were unable to identify whether or not all of the protein was labeled, unlabeled protein could have acted as a competitive inhibitor that drives rates down.

The expected mechanism of hydrolysis for TE is a base hydrolyzed mechanism. In order to investigate this hypothesis, the kinetic values of the AziG mutants were evaluated over a range of pH. The results in Figure 30 demonstrated that the higher the pH, the faster the hydrolysis values for AziG and its mutants. The glutamate mutant consistently had the smallest effect on the rate of hydrolysis. The H48A and S58A mutants exhibited the largest effects on hydrolysis as the pH dropped, which was expected since they were hypothesized to be in the catalytic triad. Their kinetic activity approached zero as the pH got to 6.7. The decrease in kinetic activity as the pH decreases supports the conclusion that TE cleavage is done by base mediated hydrolysis.

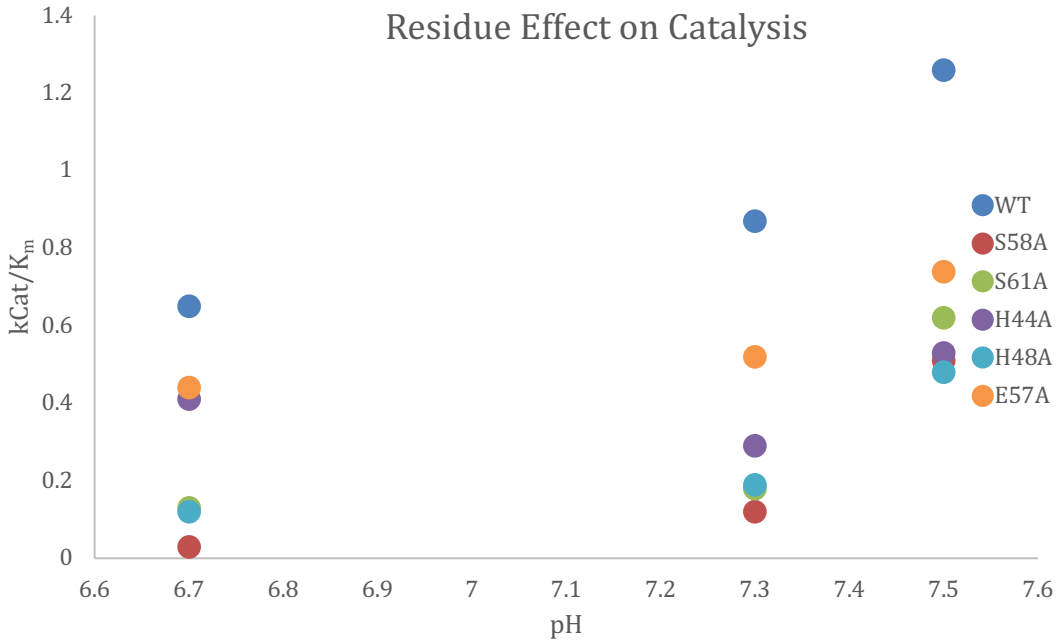

Figure 30 pH effects on kinetic activity for AziG and its mutants

The purposes of the TE domain include hydrolysis, chain elongation, and cyclization. Figure 25 shows that all five mutants were able to effectively produce the naphthoic acid product. The five active site mutants were examined on their ability to affect the quantity of 5-methyl-naphthoic acid produced. The quantity of 2-methyl benzoic acid and 5-methyl-naphthoic acid formed was evaluated by LC/MS and shown in Figure 31. The mutant that least affected naphthoate production was E57A. Given glutamic acid isn't included in the Ser-His-Asp conserved triad for TE, its minimal effect on naphthoate production was expected. The histidine and serine mutants appeared to affect naphthoate production equally in two tiers. The serine mutants produced minimal quantities of 5-methyl-napthoic acid and four times less than the glutamic acid mutant. In

addition, no 2-methyl benzoic acid was able to be detected by any of the mutants. These results do not support the conclusion that only the catalytic triad is involved with naphthoate production. S61A had a larger impact than S58A and H44A had then H48A. Chain elongation may proceed through a more complex process than hydrolysis.

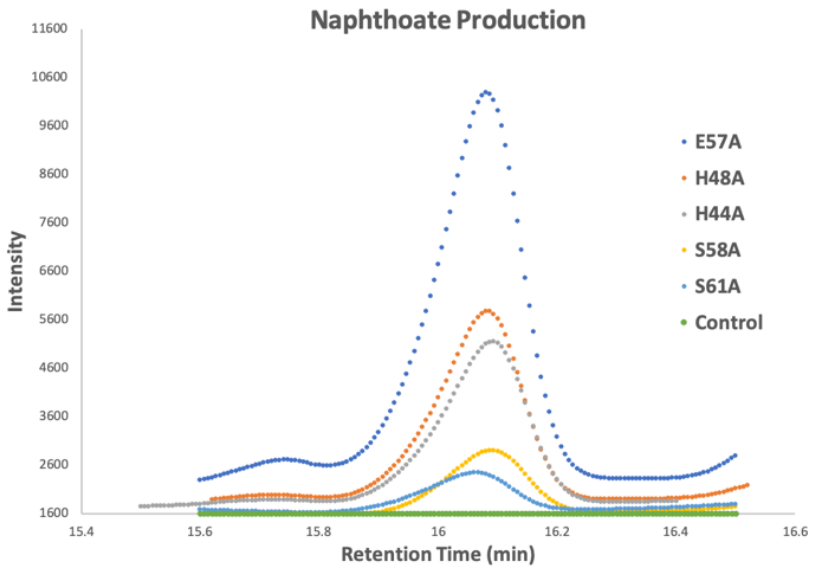

Figure 31 LC/MS analysis of naphthoate production for AziG mutants

Lastly, the naphthoate ring has several hypothesized intermediates. The isolation and identification of intermediates was pursued to provide insight into the naphthoate rings mechanism of formation (Appendix Figures 23-28). A large-scale reaction of AziB with unlabeled substrates was performed and hydrolyzed over a period of times. By hydrolyzing the enzyme at different time intervals, potential intermediates were cleaved off AziB and detected by LC/MS.

Significance

Previous attempts at determining the rate of hydrolysis by AziG were much lower than other thioesterases, so a substrate bound enzyme was created to more accurately measure the hydrolysis. While these kinetic values were slightly higher, they did not match similar TE enzymes. However, the kinetic values of the AziG mutants were unable to help support the conclusion that the thioester is cleaved by a base hydrolysis mechanism. S58A and H48A, hypothesized members of catalytic triad, had the lowest kinetic values with H44A also having a substantial decrease in hydrolysis. The kinetic values of the AziG mutants were observed across a range of pH and were found to substantially decrease as the pH became more acidic. The hydrolysis rate of H44A, H48A, and S58A all approached zero as the pH reached 6.7. The decrease in hydrolysis as pH decreases strongly supports the conclusion that AziG cleaves the thioester bond with a base mediated hydrolysis.

The optimization of the post-translational modification of AziB was achieved by evaluating two promiscuous PPTase enzymes, Svp and Sfp, against PPTases native to *Streptomyces*, FAS and NFAS. Svp was found to be the most effective at modifying AziB and the ACP domain of AziB. AziB was found to post-translationally modify to a higher extent than the isolated ACP domain. In addition, PPTase tethering to the serine of the ACP domain was dependent upon pH and Mg2+ concentration.

The AziG mutants were found to have varying effects on the production of 5-methyl-naphthoic acid. Glutamate had the lowest effect, while the histidine mutants had the second lowest. The serine mutants had a substantial impact on production of naphthoic acid, creating the hypothesis that serine plays a substantial role in its formation. While the

histidine mutants had the largest effect on hydrolysis, the serine mutant effects indicate involvement in chain elongation. Lastly, intermediates were isolated during naphthoate production. Masses of the chain were found with 4 Malonyl CoA units that were uncyclized, while the cyclized 2-methylbenzoic acid was also found. This suggests that the chain is cyclized before it progresses to the final product.

Materials and methods

General Info

All chemicals from Sigma-Aldrich, all bacterial media were purchased from Becton-Dickinson, and ELISA and PCR reagents were purchased from ThermoFisher Scientific. Molecular biology reagents were purchased from New England Biolabs. Mass Spectra were obtained at the Laboratory for Biological Mass Spectrometry or at the Department of Chemistry, Texas A&M University. A Phenomenex column (Prodigy 5 µm C18 150 Å, 150 x 4.6 mm) was used during HPLC and LC-MS purification and analysis. LC-MS was performed on a Thermo Scientific Ultimate 3000 UHPLC with a Thermo Fisher Scientific Q Exactive Focus mass spectrometer. UV light absorption was measured by GENESYS 2 UV-Vis Spectrophotometer (Thermo Fisher Scientific, Waltham, Massachusetts, USA).

Cloning of Phosphopantetheinyl Transferases

The two PPTases located in the genomic DNA of *S. sahachiroi*, FAS PPTase and NFAS PPTase, were codon optimized for expression in *E. coli* by Genescript. They were

cloned into a pET21 expression plasmid using NdeI and XhoI as restriction enzymes. T4 DNA Ligase was used to ligate the final constructs.

Overexpression and purification of PPTases

E. coli BL21 (DE3) containing a PPTase expression vector was grown in 5 ml of LB medium with 50 µg/ml ampicillin overnight. The culture was used to inoculate 1 L of LB medium and culture at 37 °C at 250 rpm until an OD600 of 0.6 was reached. Induction was performed by the addition of 1 ml of 1 M IPTG. The cultures were incubated at 16 °C for 24 h at 250 rpm. The cells were harvested by centrifugation at 6500 rpm and resuspended in buffer containing 20 mM potassium phosphate, 500 mM NaCl, 1 mM DTT, 5 mM imidazole, and 20% glycerol, pH 7.4. The cells were lysed by sonication, clarified using centrifugation to remove cellular debris. The supernatant containing the PPTase was purified using a HisTrap FF 5 ml column (GE Healthcare Life Sciences). The purified protein was concentrated using a 10 kDa centrifugal ultrafiltration unit (Amicon Ultra centrifugal filter unit, Millipore)

Characterization of PPTase activity using modified ELISA

To synthesize Biotin-Coenzyme A, 25 mg of Biotin-Maleimide was dissolved in 500 µl DMSO and added to a solution containing 45 mg Coenzyme A in 2 ml of Phosphate buffer pH 6.0. The reaction was stirred at room temperature overnight. The reaction was lyophilized and analyzed by LC-MS to confirm product formation (Appendix Figure 14). To perform phosphopantetheinylation reactions, the four PPTase (Sfp, Svp, NFAS

PPTase, and FAS PPTase) were purified along with AziB and the ACP domain of AziB. 100 μM Biotin-Coenzyme A, 1 μM PPTase, and 50 μM ACP containing protein were combined in 100 μl of 50 mM HEPES Buffer pH 7.5 with 10 mM $MgCl_2$. The reaction was incubated at 37 °C for 1 hr. A streptavidin coated plate was washed three times with 25 mM Tris, 150 mM NaCl pH 7.2 with 0.1% BSA and 0.05% Tween 20. Serial dilutions of the 100 μl PPTase reaction were made and 100 μl of each was added to one well and incubated for 2 hours at room temperature. The wells were washed three times. 100 μl of 6x-His Tag Monoclonal Antibody-Horse Radish Peroxidase conjugant was added to each well and incubated for 30 minutes. The wells were washed three times to remove excess antibody. 100 μl of 3,3',5,5'-tetramethylbenzidine (TMB) substrate was added to each well and incubated for 30 minutes to develop color. 100 μl of 2 M sulfuric acid was added to stop the reaction and the UV was recorded at 450 nm.

Overexpression of AziB, Svp, AziG, and AziG mutants

AziB, Svp, AziG, and AziG mutants were overexpressed in the same manner. E. coli strains which contain their expression plasmids were cultured in 5x5 mL LB media for AziB, 3x5 mL for Svp and 2x5 mL for each AziG overnight with proper antibiotics, which are 50 μg/mL kanamycin for AziB and AziG, and 100 μg/mL ampicillin for Svp. Each of the 5 mL overnight cultures was inoculated into 1 L LB medium and grown until OD600 reaches 0.6-0.8. The production of the proteins was induced by 1 mM Isopropyl β-D-1-thiogalactopyranoside (IPTG) and incubation in 16 C^o at 250 rpm for 22 hours. The resulted cells were harvested by centrifugation at 7000 rpm for 15 min. After discarding

the supernatant, the cells were washed with 250 mL of DI water and centrifuged down again by the same condition. The supernatant was discarded, and the cells were washed again with 30 mL of AziB- Svp reaction buffer (75 mM Tris-HCl, pH 8.0, 10 mM MgCl2, 5 mM dithiothreitol (DTT), and 20% glycerol). It was centrifuged down again at 9900 rpm for 15 min, and the supernatant was discarded. The remaining steps were performed on ice. The cells were resuspended into the AziB-Svp reaction buffer of 30 mL and each AziG and total 100 mL for AziB and Svp which were subsequently mixed together. Phenylmethanesulfonylfluoride (PMSF) was added into each solution to the final concentration of 1 mM shortly before the cells were lysed by sonication with Branson Sonifier 450 (Branson Ultrasonics, Danbury, CT) fitted with a 5 mm micro-tip, output setting 6, duty cycle 60%, and 5 cycles for 30 sec each. The lysed cells were removed by centrifugation at 9900 rpm for 45 min twice to remove the cell residues completely. The supernatants which consist of water-soluble proteins were stored in 4 ^{o}C.

Posttranslational modification of AziB with Svp and Coenzyme A

Approximately 90 mL of apo-AziB and Svp crude protein extract was obtained following cell lysis and centrifugation. Apo-AziB was converted to the holo-form by adding 5 μmol of coenzyme A, giving a final concentration of ~5.5 μM. The sample was incubated at 28 ^{o}C and 250 rpm for 1 h. Any resulting precipitation formed during incubation was removed by centrifugation, 9900 rpm for 45 min. Holo-AziB/Svp were purified by nickel affinity chromatography. A HisTrap FF 5 mL column was equilibrated with PPT buffer and subsequently loaded with the protein mixture at a rate of 0.25

mL/min. The column was washed with 200 mL of PPT column buffer (1 mM DTT, 500 mM NaCl, 40 mM imidazole, 75 mM Tris-HCl, pH 8.0, and 20% glycerol) and eluted with 30 mL of PPT column buffer supplemented with 250 mM imidazole. The buffer was exchanged to the AziB-AziG reaction buffer (50 mM potassium phosphate, pH 7.5, and 20 % glycerol). The purity and quantity of holo-AziB and Svp were assessed by 8 % (v/v) SDS-PAGE and Bradford assay utilizing the Bio-Rad Protein Assay kit (Bio- Rad Laboratories, Hercules, CA, USA); bovine serum albumin (BSA) was implemented as a standard.

Purification of AziB-Svp, AziG, and AziG mutants

The crude solutions, which contained AziG, were applied to pre-equilibrated HisTrap FF 5 mL columns at 0.25 mL/min. The loaded columns were treated as follows: For AziG and its mutants the column was washed with 200 mL of column buffer supplemented with 60 mM imidazole and eluted with 30 mL of column buffer supplemented with 250 mM imidazole. The buffer was exchanged to AziB-AziG reaction buffer (potassium phosphate: 50 mM, glycerol: 20 %, pH 7.5) by centrifugal ultrafiltration units for 10 kDa (Amicon Ultra - 15). The buffer was exchanged to sephadex column buffer (20 mM sodium phosphate, 150 mM NaCl, pH 7.5). The sephadex G-50 fine (size exclusion) column with 200 mL volume about 1 m height was equilibrated with the sephadex column buffer.

Production of 5-Methyl-1-Naphthoic Acid by AziB and TE domains

A 25 mL of the reaction solution consists of 50 μM of acetyl coenzyme A, 250 μM of malonyl coenzyme A, 10 μM of NADPH, about 10 mg of AziB-Svp mixture, and about 10 mg of AziA6 or AziG in the AziB-AziG reaction buffer. The reaction solution was incubated in 30 ^{o}C overnight. The product was cleaved from the protein by basification of the solution with NaOH till pH about 12, and it was subsequently acidified by HCl till pH below 5 for the following extraction. The acidified product was extracted with the equal volume of ethyl acetate three times. After dried over anhydrous sodium sulfate, ethyl acetate was evaporated off in vacuo and gentle flow of dry nitrogen gas. In case of AziG mutant assays, the solution after the reaction was neither basified nor acidified. Alternatively, the reaction solution was filtered out with centrifugal ultrafiltration units for 3 kDa, and the filtrate was extracted with the equal volume of ethyl acetate three times and solidified by the same method.

LC-MS Analysis of AziB or AziG products

The product was analyzed by LC-MS. It was dissolved in 100 μL of methanol, and 10-30 μL of the sample was injected into the reversed-phase HPLC column (Phenomenex, Columbus 5μ C8 100A, 250 x 3.20 mm 5 μ) which was pre-equilibrated with 80% A (water) and 20% B (75% methanol and 25% isopropanol). The liquid chromatography was run by the following program: Time 0 min A-80% B-20%; 1 min A-80% B-20%; 15 min A-0% B-100%; 30 min A-0% B-100%; 32 min A-80% B-20% till 40 min at the flow rate

0.75 μL/min. It was monitored by UV at 254 nm wavelength and by mass at around 136 m/z (2-methylbenozoic acid) and 187 m/z (5-methyl-1- naphthoic acid).

CHAPTER IV

LIPOFUSCIN TOXICITY AND DEGRADATION

Introduction

The over accumulation of lipofuscin and drusen in the retinal pigment epithelium is associated with age related macular degeneration (AMD). In addition to AMD, diseases that trigger early onset blinding are also associated with the buildup of lipofuscin. However, diseases like Stargardts and Bests disease contain mutations in essential retinal genes like *ELOVL4*, *BEST-1*, and *ABCA4* that allow the accumulation of lipofuscin to occur.[105-107] The term lipofuscin represents a large set of compounds originating from the monomer all-trans retinal. These compounds include A2E, A2E isomers, A2-dihyropyridine-ethanolamine, A2-dihydropyridinephophatidylethanolamine, cycloretinal, and all-trans retinal dimer phosphatidylethanolamine, listed in Figure 16.[108] These lipofuscin form as by-products of the visual cycle and form epoxides along the conjugated chain when exposed to 430 nm of light. These epoxides demonstrate cytotoxic effects in the form of DNA or essential protein damage.[85]

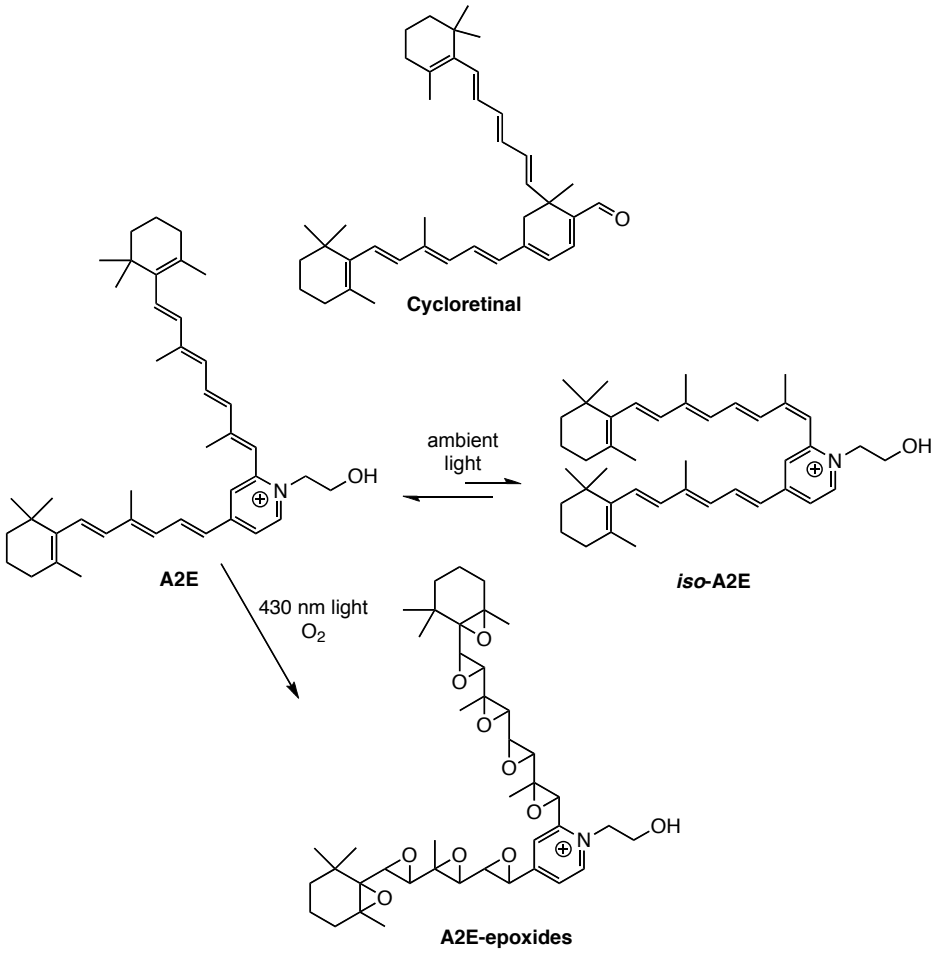

Figure 32 Lipofuscin found in the retina after exposure to 430 nm of light hypothesized to form toxic epoxides

Retinal cells of mice have been analyzed for the quantity and type of lipofuscin present in several macular diseases. Mice with Stargardts disease were found to contain approximately 40 pmoles/eye of A2E, while the all-trans retinal dimer, cycloretinal, was found in 120 pmoles/eye quantities.[85] The toxicity of A2E has been extensively reported, but the concentration and length of exposure has varied. A concentration of 200 pmoles/cell were seen to trigger complete cell death after 10 days,

while 30 μM can facilitate complete toxicity after 16 hours.[109,110] The toxicity of cycloretinal has yet to be determined. Given its chemical similarity with A2E, it is hypothesized that cycloretinal induces retinal cell death through the photooxidation of its conjugated chain.

In order to combat the toxic effects of lipofuscin accumulation, several different treatment methods have been utilized. Small molecule inhibitors, gene therapy treatments, and protein delivery systems have been used to either prevent the formation of these compounds or degrade them once they form.[111-113] The elimination of the harmful compounds that accumulate in the retina could alleviate vision loss of people with macular degenerative diseases. Possible enzymes were evaluated on their ability to break down the lipofuscin, so that these genes could eventually be employed in gene therapy trials.

Screening of enzymes that could degrade lipofuscin into non-toxic by-products was performed by analyzing enzymes that degrade β-carotene. Carotene is a terpene natural product that can produce derivatives of vitamin A upon oxidation.[114] While a wide array of enzymes has been found to oxidize and degrade β-carotene, their activity is low and the mechanism of degradation remains unknown.[115-117] An extracellular peroxidase enzyme from a basidiomycete *Marasmius scorodonius* (garlic mushroom), MsP1, was selected based on its thermostability properties and its ability to degrade long terpene chains.[118,119]

Preliminary research

A gene coding for *MsP1* was synthesized *de novo*, cloned and overexpressed in E. coli to give MsP-BL21 cells. Both MsP-BL21 and BL21 were incubated with cycloretinal as the only carbon source in minimal medium. Decolorization was observed only in tubes containing MsP-BL21. Given its low expression, MsP1 was expressed as an MBP fusion protein. Figure 33 demonstrates that MsP1 was able to effectively catabolize cycloretinal within two hours.

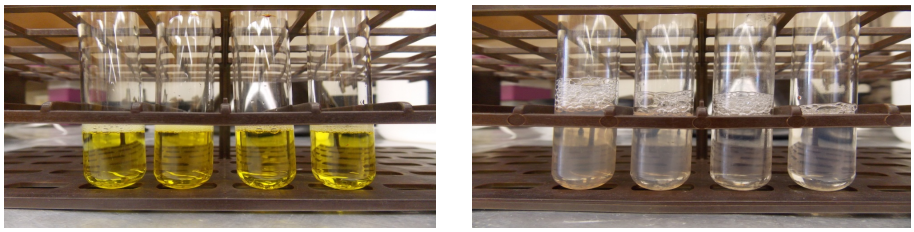

Figure 33 Demonstration of Cycloretinal Catabolism with MsP1-BL21 cells: A] Time 0, cycloretinal is yellow in solution B] After 2 h of incubation, clearance observed.

In order for MsP1 to be an effective enzyme in degrading lipofuscin linked with macular degenerative diseases, it must break apart the conjugated chains into non-toxic byproducts. To identify the degradation products, cycloretinal and A2E were incubated (1 h) with MsP1 in the presence of hydrogen peroxide. Following incubation, the reaction mixture was extracted and analyzed by gas chromatography mass-spectrometry (GC/MS).

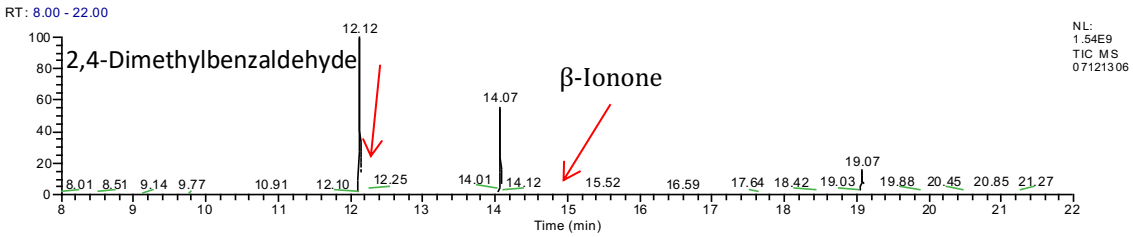

Figure 34 GC/MS Analysis of Cycloretinal Degradation

The observed degradation of cycloretinal and A2E in the presence of MsP1 resulted in two major products that are shown in Figure 34 and Figure 35.

Not only does MsP1 effectively break apart lipofuscin macromolecules, but it also exhibits a consistent modality of degradation. Both A2E and cycloretinal were seen to become oxidized at the two terminal tails to produce β-Ionone. Additionally,2,4-dimethylbenzaldehyde was also detected in the degradation of cycloretinal. This represents the cleavage of the central cyclohexadienal moiety from the larger macro-structure.

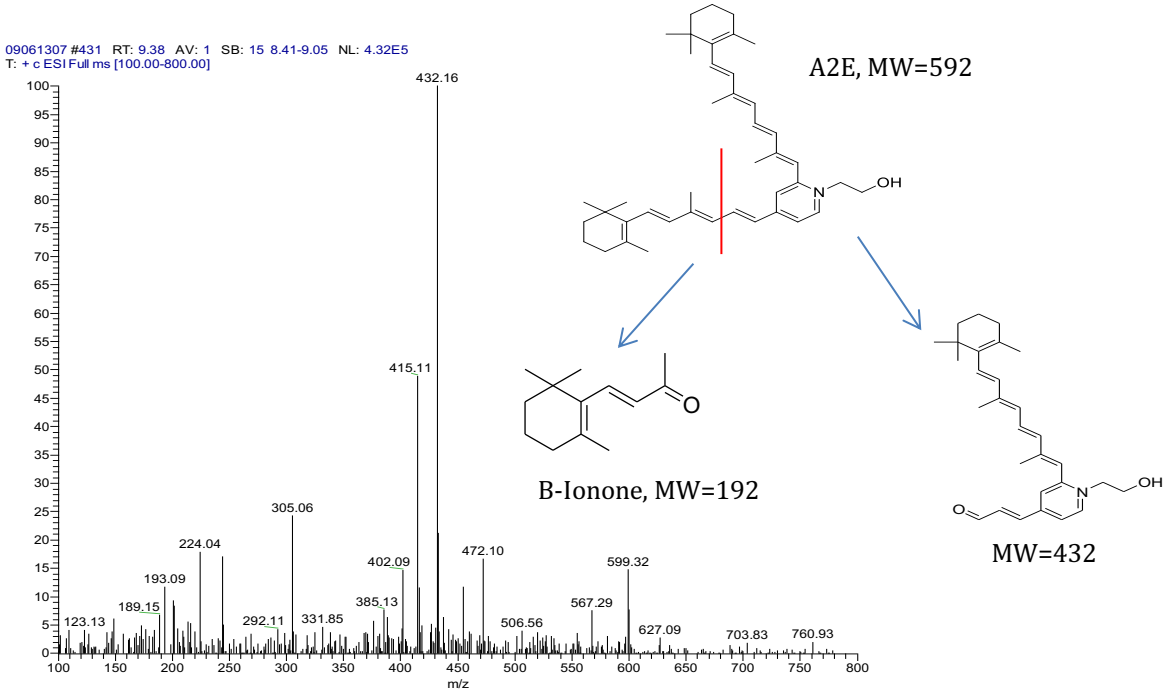

Figure 35 GC/MS Analysis on A2E Degradation indicating β-Ionone formation (Irum Perveen)

Results and discussion

The extent of cycloretinal toxicity on retinal cell was evaluated on ARPE-19 cells with synthesized cycloretinal. However, cycloretinal is an unstable compound that doesn't easily penetrate mammalian cell membranes. In order to effectively introduce cycloretinal into the cell, a liposomal delivery system was synthesized. Figure 36 demonstrates the successful incorporation of cycloretinal into the liposome. Without the necessary components of the liposome, cycloretinal degrades and is unable to be seen via HPLC.

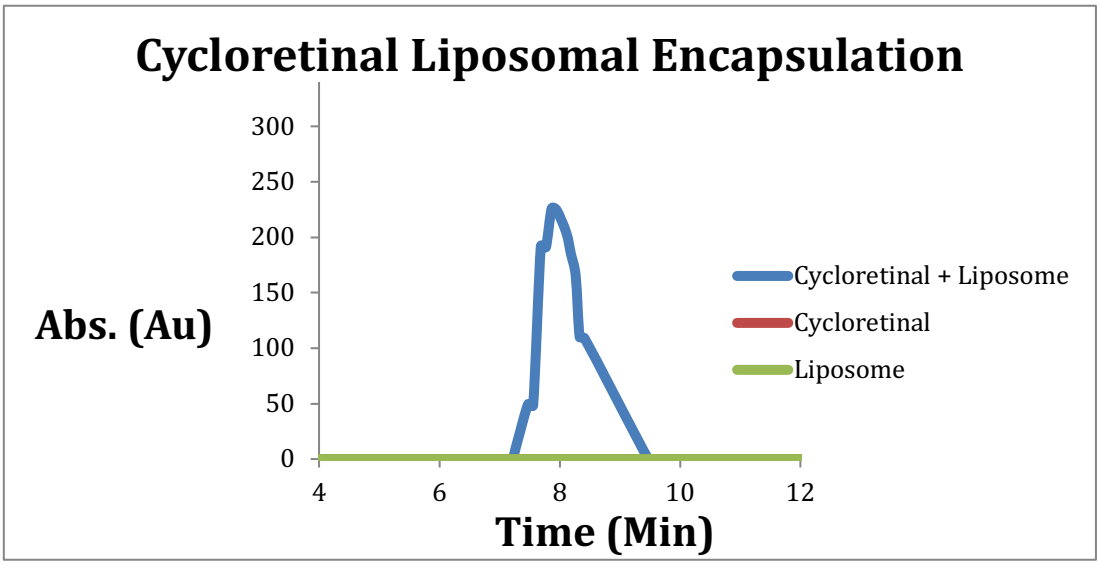

Figure 36 HPLC trace of cycloretinal liposomal encapsulation

After the liposomal encapsulation of cycloretinal was complete, the liposomal complexes containing the lipofuscin were exposed to darkness or 430 nm of light (blue light) to demonstrate whether photoactivation would facilitate the formation of the toxic epoxides. ARPE-19 cells were exposed to concentrations between 0 and 200 μM of

cycloretinal and incubated for four days. As seen in Figure 37, Cycloretinal was observed to be toxic to retinal cells and exposure to 430 nm of light lowered the concentration threshold of toxicity. Under 430 nm of light, cycloretinal started to demonstrate toxic effects at 60 μM and continued its effects until it eliminated all cell viability at 130 μM. When retinal cells were prevented from any light exposure and were incubated with cycloretinal, they also observed the loss of cell viability, but at higher concentrations. Cell viability began to drop at 70 μM and complete cell death did not occur until 200 μM.

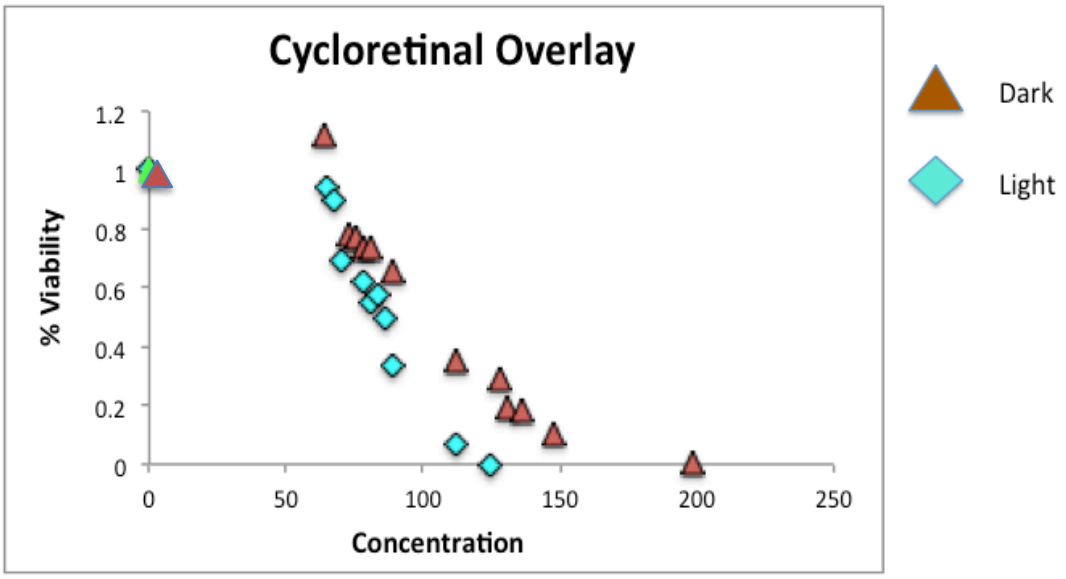

Figure 37 Cycloretinal cytotoxicity assessed with ARPE-19 cells utilizing the MTT assay. Cells were either left in complete darkness or irradiated with 430 nm of light.

While Figure 37 successfully displays that cycloretinal causes retinal cell death, it has some limitations. While the liposomal encapsulation facilitates the delivery of the lipofuscin into retinal cells, the efficiency in which it does is unknown. Therefore, the

concentration of cycloretinal toxicity could be much lower than the observed values. In addition, the toxicity of cycloretinal was observed on a fixed time scale of 4 days. These results indicate that if retinal cells are exposed to a concentration above 60 μM for 4 days, they begin to lose viability. Since macular degenerative diseases are defined by the accumulation of these lipofuscin for prolonged periods of time, negative visual effects could be observed from lower concentrations if they are allowed to reside in the retina for longer periods of time.

While MsP1 was observed to successfully degrade two types of lipofuscin into smaller subunits, the efficaciousness of MsP1 as a possible gene therapy target was still unknown due to the unknown toxicity of β-Ionone and 2,4-dimethylbenzaldehyde. In order to demonstrate the MsP1 could potentially be used for gene therapy the toxicity of β-Ionone and 2,4-dimethylbenzaldehyde were assessed and shown in Figure 38.

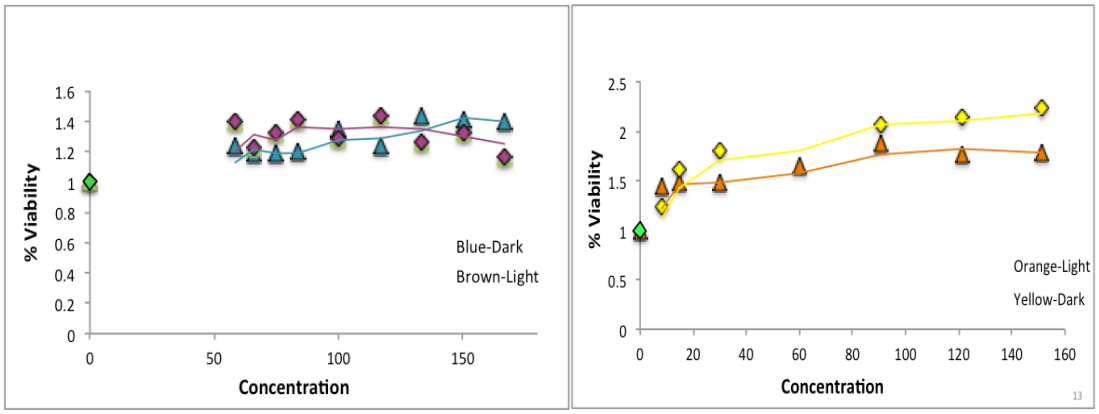

Figure 38 Cytotoxicity of β-Ionone and 2,4-dimethylbenzaldehyde in light or dark conditions on ARPE-19 cells

Both of these compounds were encapsulated by liposomes, like cycloretinal, so that they could be effectively inserted into ARPE-19 cells. When these two compounds

were incubated with retinal cells, they were exposed to two separate conditions. One set of cells was exposed to 430 nm of light at 40 V intensity for 30 seconds, while the other set of cells was left in complete darkness. After four days of incubation, the cells viability was monitored and quantified with the MTT Assay.

As seen in Figure 38, β-Ionone and 2,4-dimethylbenzaldehyde were not able to exhibit toxic effects on ARPE-19 cells under varying conditions. In addition to not exhibiting toxic effects, these two compounds were seen to facilitate cell growth with the retinal cell samples. Part of this increase in viability can be attributed to the fact the cells are assessed when they've reached 80% confluence. If the compounds exhibit no toxic effects, the cells can continue to grow to complete confluence and demonstrate increased viability. Additionally, the liposomes themselves contain nutrients for cell growth (cholesterol, lipids, etc.), so they, in conjunction with the two degradation products, could help increase cell growth within the retinal cell cultures. However, liposomal controls with no compound present inside were not found to strongly affect cell viability.

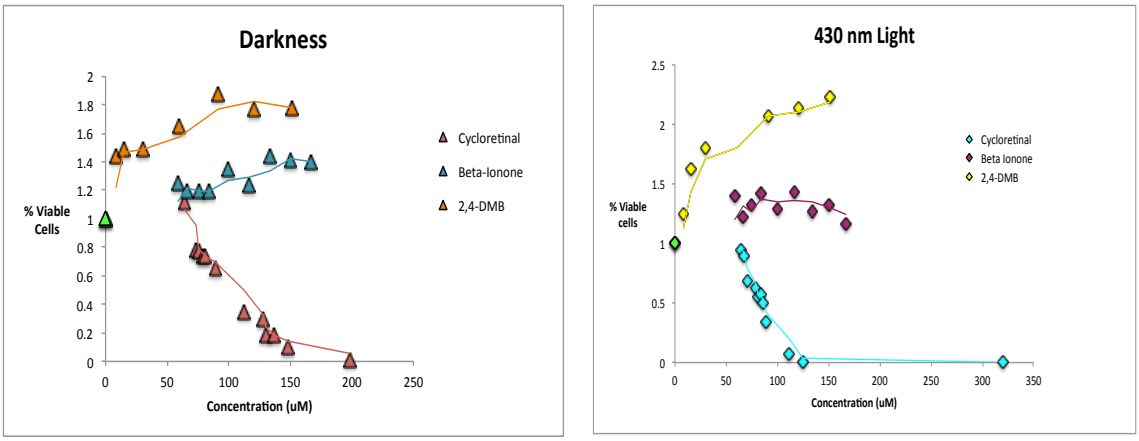

Figure 39 Comparison replot between cycloretinal and its degradation products toxicity in light or darkness

Significance

The lipofuscin compound cycloretinal has exhibited a toxicity slightly above the toxicity threshold for A2E. The lipofuscin compound A2E had shown that 430 nm of light could activate the conjugated chains into toxic, epoxide intermediates.[88,92] Given the formation of epoxides under these conditions and the molecular similarity between A2E and cycloretinal, cycloretinal is hypothesized to initiate toxicity under the same mechanism. Due to the increased toxicity effects on the retinal cells under that specific wavelength of light, it's assumed that cycloretinal can form the same epoxide chain that A2E can and trigger cell death. In addition, cycloretinal has exhibited toxicity of retinal cells at a lower toxicity than A2E. With a lower toxicity threshold and 3 times the amount of A2E in patients with Stargardts disease, cycloretinal could play a much more significant role in macular degenerative diseases than A2E.

A liposomal delivery system was designed to introduce large molecules into the retinal pigment epithelium. Toxicity was not observed for retinal cells exposed to cycloretinal without the liposome. This encapsulation method allowed for the molecules to be introduced into the cell and increased stability. This liposomal encapsulation has the potential to incorporate other large molecules for delivery into other mammalian cell lines.

Due to MsP1's ability to degrade B-carotene, another macromolecule in the family of terpenoids, it was selected to break down retinal lipofuscin. MsP1 degraded both A2E and cycloretinal into B-ionone, while cycloretinal additionally produced a byproduct of 2,4-dimethylbenzaldehyde. To determine if MsP1 could effectively be employed as therapeutic in gene therapy, the toxic effects of the byproducts were needed to be

juxtaposed to the actual lipofuscin. Under both light and dark conditions, the degradation products of lipofuscin from MsP1 did not exhibit toxic effect on retinal cells. Due to the lack of toxicity for β-Ionone and 2,4-dimethylbenzaldehyde on retinal cells, MsP1 is a desirable enzyme to be employed on retinal cells affected by macular degenerative diseases. With gene therapy treatments, MsP1 could be selected to be expressed into ARPE-19 cells and to clear accumulated lipofuscin.

EXPERIMENTAL SECTION

Preparation of All-trans Retinal Dimer, Cycloretinal

Cycloretinal was prepared according to the published procedure. A mixture of 100 mg All-trans retinal (.3 mmol), 62 mg L-Proline (.5 μmol), and 400 μL triethylamine (2.9 mmol) were suspended in ethanol and stirred at room temperature for 24 hours. The crude mixture was purified by flash column chromatography (1:19 EtOAc: Hex).

Synthesis of Liposomal Cycloretinal, B-Ionone, and 2,4-Dimethylbenzaldehyde

The liposomal complexes were prepared according to a modified version of the published procedure. Cycloretinal (10 mg), β-Ionone (20 mg), and 2,4-Dimethylbenzaldehyde (20 mg) were separately dissolved in 1 mL ethanol. A solution of Cholesterol (56 mg), Tween 80 (252 mg), and L-**α**-Phosphatidylcholine (365 mg) were dissolved in 8 ml of chloroform. Two milliliters of this solution were added to each of the reagents dissolved in ethanol. The solvents were removed under vacuum with a rotovap and charged with nitrogen. Each of the flasks were then mixed with 5 ml of water and

stirred at 60°C for 1 hr. Each solution was then placed on ice and sonicated with a probe sonicator (15s on/ 15s off) for 5 min. The solutions were centrifuged at 11,000 x g for 30 min and filtered through a 0.2 um filter. To evaluate the final concentrations, 10 μL of each of the solutions was added to 1 mL ethanol and measured using the absorption of the UV-Vis spectroscopy. The extinction coefficients used were 9970 $M^{-1}cm^{-1}$, 26343 $M^{-1}cm^{-1}$, and 13476 $M^{-1}cm^{-1}$ for Cycloretinal, 2,4-dimethylbenzaldehyde, and β-Ionone.

HPLC was used to confirm the encapsulation of the three compounds and ensure that Cycloretinal didn't undergo any degradation or oxidation.

Retinal cell growth

Retinal Pigment Epithelial Cells (ARPE-19 from CRL-2302, American Type Culture Collection (ATCC)) were grown in Dulbecco's Modified Eagle medium/ nutrient mixture F12 (DMEM/F12) with 10% Fetal bovine Serum in accordance with the manufacturer's instructions. Cells were grown at 37°C under 5% CO_2 with 1% gentamycin (50 mg/ml). Cells were harvested for assay at near confluence with Trypsin/EDTA after being washed with Dulbecco's Phosphate Buffered Saline.

Evaluating Cytotoxicity of Cycloretinal, β-Ionone, and 2,4-Dimethylbenzaldehyde

ARPE-19 cells were grown to confluence in 24-welled plates with 900 μL DMEM/F12 (10% FBS). Aliquots of 100 μL of the Cycloretinal liposomal complexes were applied in triplicates to the 24-welled plates at various concentrations (10-320 μM) and the cells were incubated for 24 hours. Using only media and water, controls were

generated for each plate. The same conditions were used to assess the cytotoxicity of β-Ionone and 2,4-Dimethylbenzaldehyde. The range of concentrations used for β-Ionone was 58.4-166.9 μM and the range for 2,4-Dimethylbenzaldedhyde was 8-151 μM.

After 24 hr. incubation with the liposomal complexes, light induced cell damage was determined by exposing cells to 10 min. irradiation (70W lamp) through a 430 nm bandpass filter (Thor labs, 340±2 nm). The cells were then left for 72 hours, the media was removed, and the plates were washed three times with DPBS and left in 200 uL of the buffer.

To evaluate non-light induced toxicity, near confluent cells, in 900 μL media, were exposed to the same concentrations of liposomal complexes and allowed to incubate for 96 hours. The cells were then washed three times with DPBS and left in 200 μL of the buffer.

MTT assay

Cell viability was determined by the MTT cell proliferation assay. The MTT assay utilizes a yellow tetrazolium MTT (3-(4, 5-dimethylthiazolyl-2)-2,5-diphenyltetrazolium bromide) that is reduced by metabolically active cells. The viability was determined by the manufacturer's suggested protocol. The MTT reagent was added in 10 uL aliquots and incubated at 37^{o}C under 5% CO_2 for four hours. Then 100 uL of the detergent reagent was added to each well and was left in the dark at room temperature for two hours. The absorbance was then evaluated at 570 nm using a microplate reader (FLx800 Microplate Fluorescence Reader, BioTek Insturments Inc.)

CHAPTER V

MECHANISTIC INVESTIGATION OF LIPOFUSCIN

Introduction

The formation of lipofuscin results in conjugated chains that can undergo oxidation and form toxic byproducts that are lethal to the retina.[88] Macular degenerative diseases are defined by lipofuscin accumulation and the retinas inability to break them down. Gene therapy has been pursued and successfully achieved to combat retinal degeneration. Voretigene neparvovecrzyl (Luxturna) was approved by the FDA in 2017 and remains one of the few gene therapy treatments that have been approved for use on human beings.[120] While removing lipofuscin through degradation has seen positive results, preventing cycloretinal from forming could reduce the effects of these diseases. With the cycloretinal mechanism in hand, inhibitors for lipofuscin formation could be designed.

Vitamin A derivatives move throughout the eye while coordinated to phosphatidylethanolamine (PE) or connected to opsin.[121] Both of these routes require the aldehyde form of vitamin A, all trans-retinal, to create a Schiff base with the terminal amine group of phosphatidylethanolamines or a lysine residue located on opsin. Opsin is a retinal protein that combines with 11-cis-retinal to form rhodopsin and initiates the visual cycle.[125] This transformation into the Schiff base is crucial, because it allows for the deprotonation of the γ-methyl group of all-trans retinal to create a diene structure. This structure could then react with another monomer of all-trans retinal to create one of the two dimeric, toxic lipofuscins. There are two possible mechanisms that were considered

for cycloretinal formation. It could form from a synchronized 4+2 cycloaddition or it could be created by a stepwise type aldol addition. The proposed mechanisms of formation for these compounds are shown below in Figure 40.

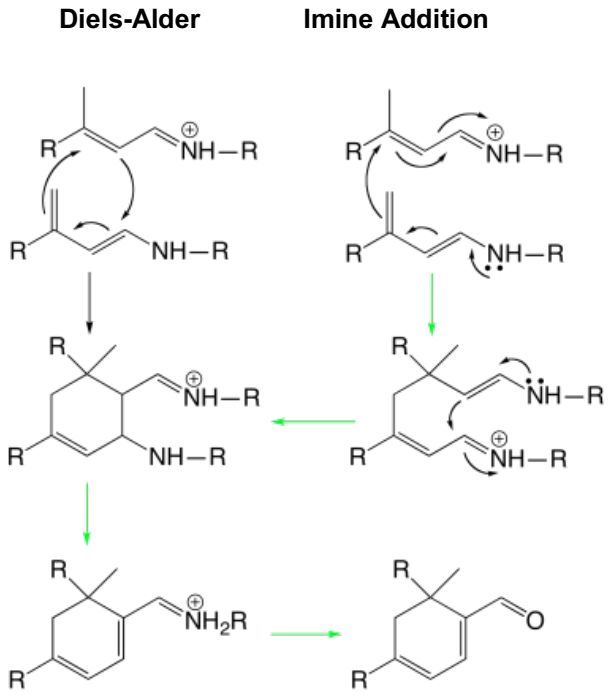

Figure 40 Hypothesized mechanism of cycloterpenal formation

The challenging aspect of determining which of these mechanisms persists is that both mechanisms would create the closed cyclohexene ring in Figure 40. The only difference between these potential mechanisms is that the step-wise, addition mechanism creates the open ring structure intermediate, shown in the second row of Figure 40.

Preliminary results

Since cycloretinal can be formed non-enzymatically with free amines found in the retina, mimicking the non-enzymatic construction of cyclohexadienal rings allowed for further investigations into the mechanism of formation of cycloretinal. L-Proline and its derivatives were found to serve as extremely efficient catalysts for aldol additions to aldehydes.[122] Prolines ability to form a Schiff base with aldehydes and facilitate aldol additions made it a desirable catalyst to employ for mechanistic investigations of cycloretinal. Additionally, proline serves as an effective catalyst for dimerization of cyclohexadienals because it is a secondary amine. Primary amines are capable of intramolecular cyclization which forms a pyridine ring, similar to A2E. A methodology to synthetically achieve the formation of cycloretinal with L-proline was achieved. This methodology was applied to create homo-dimeric units of α, β-unsaturated aldehydes. The all-trans retinal dimer and molecules with the similar hydrophobic chains were found to display the highest percent yields. [123]

In addition to enabling the homodimerization of α, β-unsaturated aldehydes into cyclohexadienal moieties, proline was also shown to facilitate the dimerization of different monomeric units. The same methodology used to create homodimers was also employed to create heterodimeric complexes. A series of heterodimeric complexes were synthesized, creating a library of cyclohexadienal compounds with different substituents.[124]

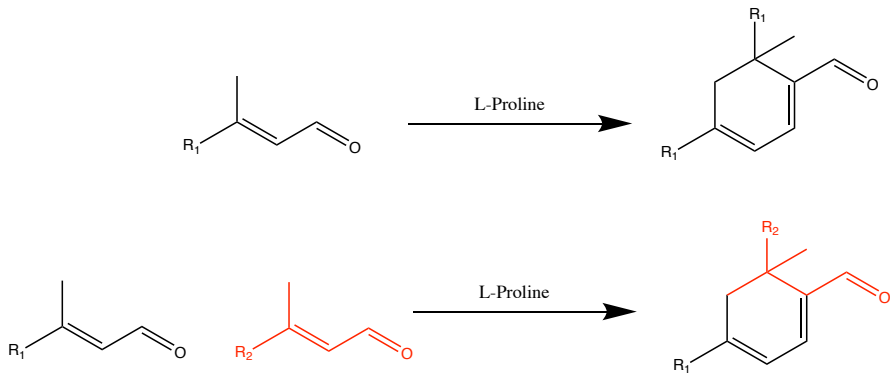

Figure 41 Proline Mediated Formation of Homo- and Hetero-dimers

In addition to forming within the presence of amine catalysts, cycloretinal is capable of forming through enzymatic means. A whey protein found in milk, Bovine β-lactoglobulin (BLG), is a stable enzyme that makes up approximately 15% of milk. BLG is highly promiscuous enzyme with multiple enzymatic capabilities. BLG has shown the ability to catalyze the homodimerization of α, β-unsaturated aldehydes.[126] Cycloretinal is one of the cyclohexadienal homodimers capable of being catalyzed by BLG. The enzymatic formation of cyclohexadienal rings was optimized and cycloretinal was amongst the highest yielding compounds.[126] BLG catalyzes cycloretinal formation by utilizing two lysine residues within a hydrophobic cavity to form a Schiff base, which activates the all-trans retinal.[127] Since the BLG mediated production of cycloretinal was observed *in vivo* and *in vitro* and proline acts as a catalyst that promotes cyclohexadienal formation, elucidating the enzymatic and non-enzymatic mechanism of formation for cycloretinal provides insight as to how it is formed in the eye and leads to potential inhibitors.[126]

Results and discussion

The two predicted mechanisms for the catalysis of the cyclohexadienal moiety of cycloretinal were a Diels-alder 4+2 cyclo-addition or a step-wise type aldol addition. In order to demonstrate which mechanism persists, isolating possible intermediates was attempted and unsuccessful. Therefore, (*Z*)-3-bromo-3-phenylacrylaldehyde and (*E*)-3-(naphthalen-2-yl) but-2-enal were designed and synthesized. These compounds would yield different products based on the mechanism that persisted, which is shown in Figure 42.

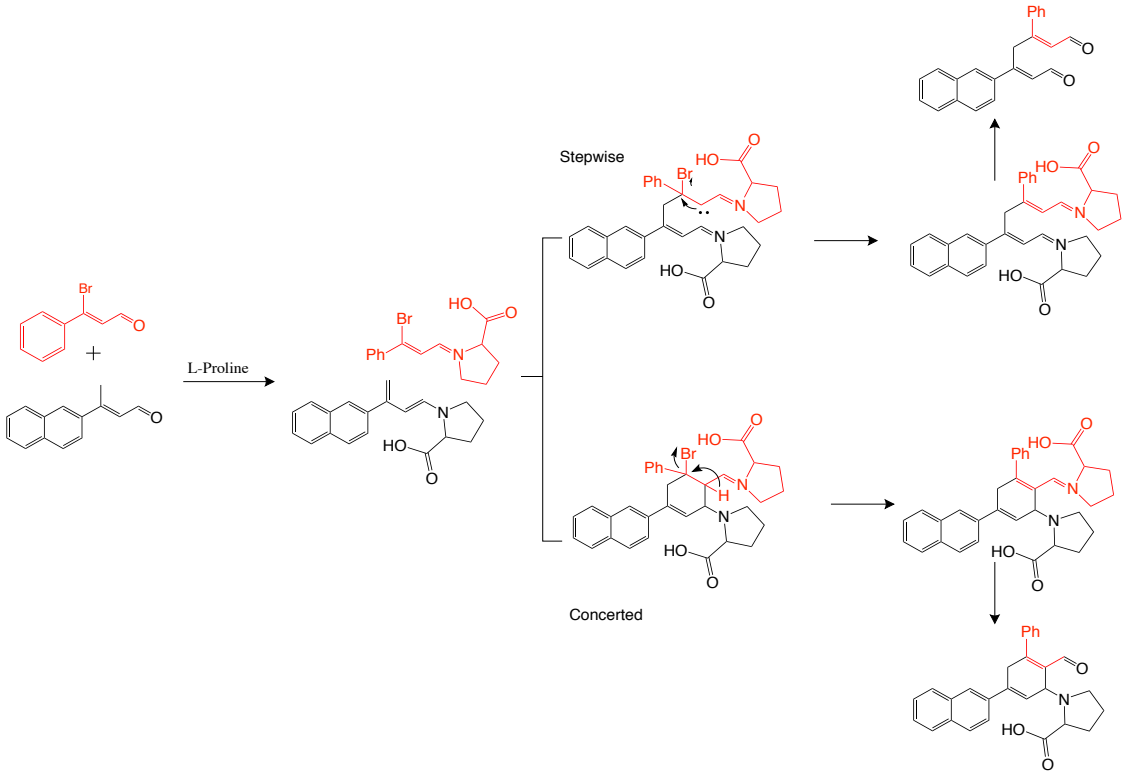

Figure 42 Trapping Experiment to Elucidate Proline Catalyzed Mechanism

If a Diels-alder type mechanism forms the cyclohexadienal ring, the lower mechanism occurs and a cyclohexene ring with proline bound is created. In the hetero- and homodimerization reactions, the acidic α-hydrogen to the proline attached carbon

becomes deprotonated and eliminates the proline molecule to create the cyclohexadiene ring. However, instead of cleaving proline from the cyclohexene ring, the acidic α-hydrogen would eliminate the halogen from (*Z*)-3-bromo-3-phenylacrylaldehyde. After hydrolysis, the product that would remain would be the cyclohexadienal ring with proline attached.

If the stepwise mechanism persisted, the upper route of Figure 42 would be undertaken. With this predicted mechanism no central ring should form and a dialdehyde compound should be created. In figure 40, the imine, step-wise mechanism is hypothesized to have the lone pair of nitrogen on one substrate push down to form an imine. This pushes electrons to act as a nucleophile and attack the imine carbon of the other substrate. This action forms the cyclohexyl ring of cycloretinal. However, using the bromo-phenylacrylaldehyde substrate leads to the elimination of the halogen instead of the ring forming carbon-carbon bond. After hydrolysis, this would create a dialdehyde product.

Although we anticipated the creation of a dialdehyde or proline coordinated molecule, we were unable to observe either of the hypothesized products. Instead, ^{1}H and ^{13}C confirmed that we catalyzed the formation of 1-(naphthalen-2-yl) ethan-1-one (Appendix Figure 35). This compound indicates that a retro-aldol reaction occurred. Under acidic or basic conditions, aldol reactions can revert into retro aldol reactions.[128] The cleavage of bromine from (*Z*)-3-bromo-3-phenylacrylaldehyde creates an acidic reaction environment. The retro aldol reaction that occurred under acidic conditions indicates that this reaction proceeds with a step-wise, imine type, aldol addition.

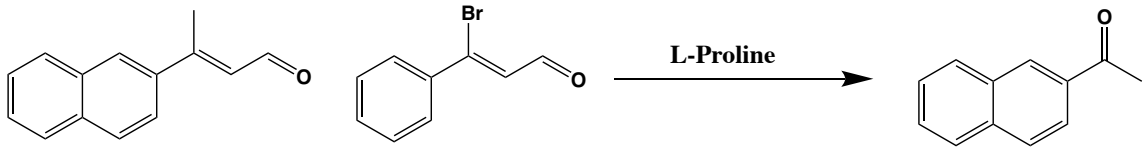

Figure 43 Product from Proline Catalysis

In the reaction of heterologous cyclohexadienal formation, the alkene acceptor is in a 2.2:1 ratio with the diene donor. This ratio is employed to prevent competition with homodimer formation. When the heterodimerization reaction is performed with the halogenated substrate, we still observe some homodimerization occurring. However, when we increase the halogenated substrate ratio to 3:1, 1-(naphthalen-2-yl) ethan-1-one forms but no homodimerization is observed.

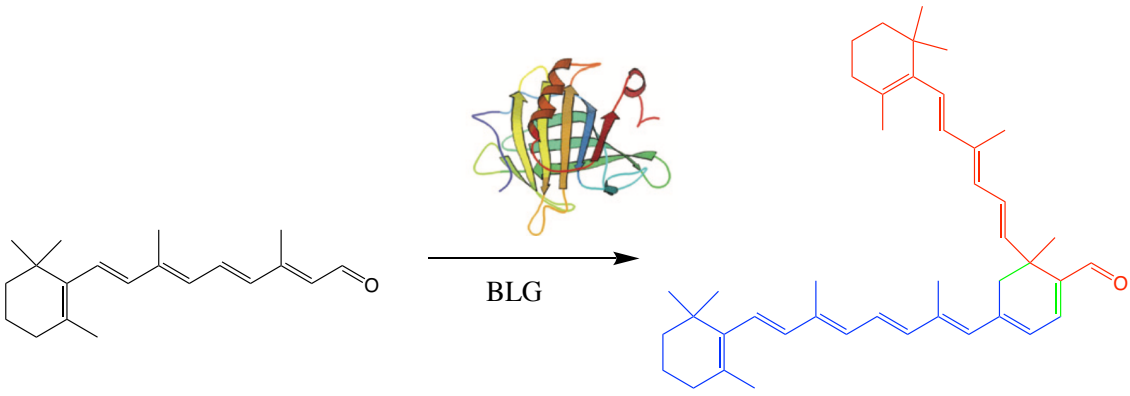

Figure 44 BLG catalyzed formation of Cycloretinal

3-Bromo-3-phenylacrylaldehyde and (*E*)-3-(naphthalen-2-yl) but-2-enal were also used to determine the mechanism of cycloretinal formation with BLG. The proposed creation of cycloretinal involved two active site lysine residues that form Schiff bases with

all-trans retinal.[127] After coordination to lysine, one of the gamma methyl groups would become deprotonated to generate the diene that facilitates either the Diels alder reaction or the step-wise aldol type reaction. When the halogenated aldehyde and the α, β-unsaturated aldehyde were incubated with BLG, the products shown in Figure 45 were hypothesized to form.

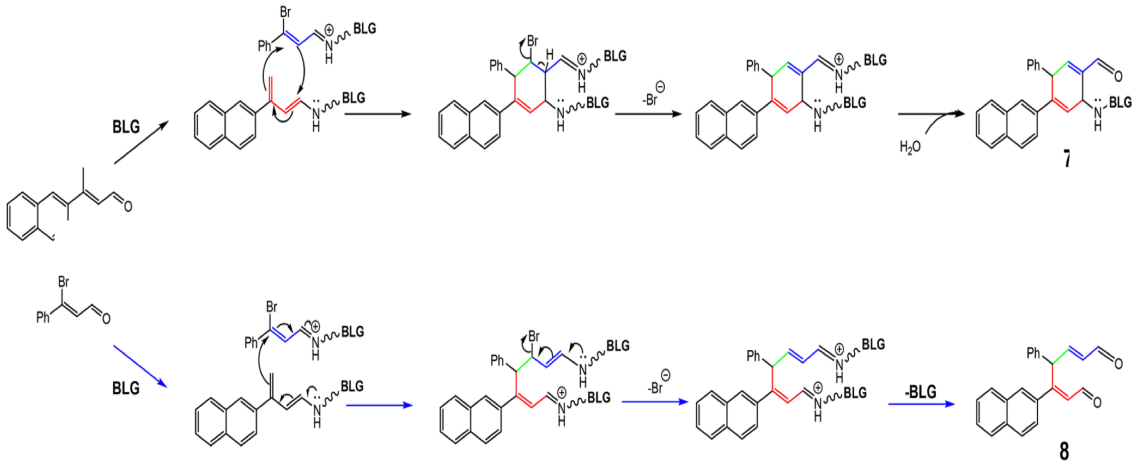

Figure 45 Trapping Experiment to Demonstrate BLG Mechanism

The BLG mediated formation of cyclohexadienal was hypothesized to form similar products to the proline mediated formation. A dialdehyde or a complex bound product was hypothesized to form. BLG was incubated with the naphthaldehyde and the bromo-aldehyde compound in a ratio of 1:1.5. Although two compounds were expected to form, neither of these products were observed. In the same fashion as the proline mediated catalysis, 1-(naphthalen-2-yl) ethan-1-one was the observed product. Since the enzyme bound product would be unable to be detected by extraction, trypsin digestion and peptide analysis by ESI-MS was implemented. Instead of seeing the naphthalene-cyclohexene

bound product, the bromo-phenylacrylaldehyde substrate mass, without the bromine, was observed on the K90 and K61 position of the active site. The brominated aldehyde was proposed to act as an inhibitor as shown in Figure 45.

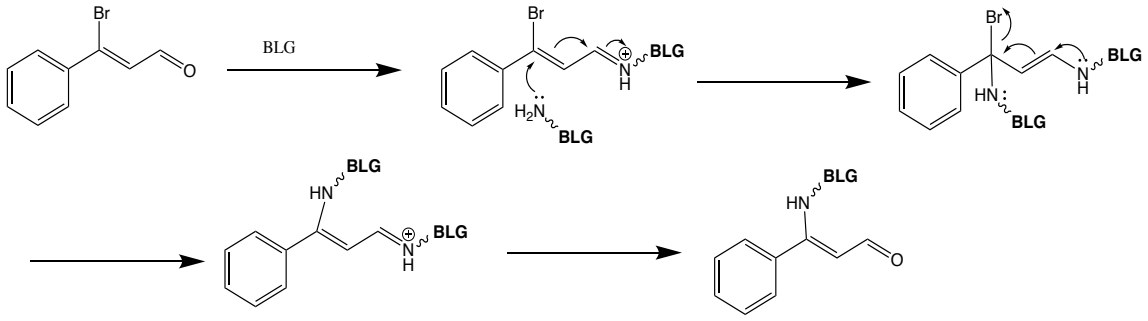

Figure 46 Proposed Mechanism of Inhibition of BLG

The presence of the brominated aldehyde within the BLG mediated dimerization facilitated a retro aldol reaction. In order to investigate the effects, the brominated compound has on BLG's catalytic ability, a series of compounds were incubated with the bromo-aldehyde. A series of α, β-unsaturated aldehydes were synthesized with varying non-polar side chains to see if the presence of the brominated compound triggers retro aldol activity. When incubated with the brominated compound, all the reactions created

retro-aldol products. The rate of retro-aldol production with different hydrophobic side chains is listed in Table 3.

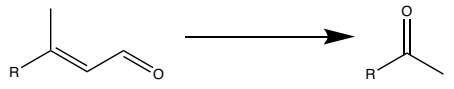

R group	TTN (uM product per mM BLG)
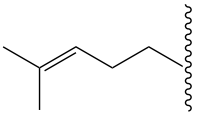	0
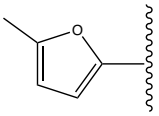	0.003
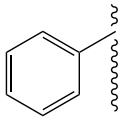	8.80
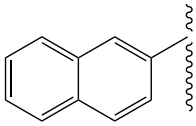	6.93
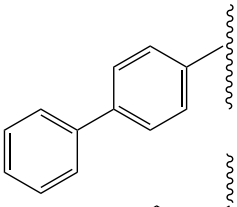	0.67
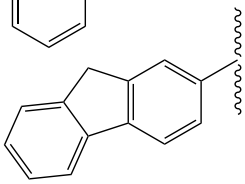	2.27

Table 3 BLG Catalysis of Retro Aldol Reactions on Different Substrates

The most effective side chains were connected aromatic rings. The smaller sized rings resulted in higher total turnover numbers. The furanyl and alkyl group observed

almost zero retro aldol activity. BLG was also tested with (*Z*)-3-bromo-3-(naphthalen-2-yl) acrylaldehyde to see if other brominated aldehydes would drive retro aldol activity of BLG. The naphthalene halogenated aldehyde also binds to a lysine residue within the active site, indicating the electrophilicity of the halogenated carbon serves as a good inhibitor and "switches" BLG into a retro aldolase.

Significance

The lipofuscin cycloretinal exhibits toxic effects in the retina and is formed through a step-wise, aldol type reaction. This mechanism was demonstrated enzymatically and non-enzymatically. When exposed to particular substrates, the proline and BLG catalysts initiate the retro aldol reaction of the substrate aldehyde. It's predicted that the brominated substrate acts as an electrophile and inactivates proline and active site lysine in BLG. Once this inactivation occurs, the Schiff base form of the aldehyde substrate can undergo hydrolysis to facilitate a retro-aldol reaction. The BLG mediated retro-aldol reaction was performed over a series of substrates with hydrophobic side arms. Connected aromatic rings were observed to have the highest retro-aldol turnover rate, with the smaller aromatic rings being more active. Since BLG is an extremely cheap and abundant substance, it possesses vast potential as a carbon-carbon bond breaking biocatalyst. In addition, the brominated α, β-unsaturated aldehyde compounds were shown to alter the L-proline and BLG product formation. At high enough concentrations, the brominated α, β-unsaturated aldehydes can completely inactivate homo-dimerization. Cycloretinal is synthesized within the eye as a dimer of

vitamin A. Given multiple brominated substrates induced retro-aldol activity, this brominated compound could potentially be employed as an inhibitor to cycloretinal activity and to lysine dependent enzymes.

Materials and methods

General methods

All reactions were carried out in flame-dried glassware unless otherwise noted. All non-enzymatic reactions were magnetically stirred and monitored by thin layer chromatography (TLC), performed using glass-backed silica gel plates Analtech (#47011). Flash column chromatography was performed using 60Å Silica Gel (Silacycle, 230-400 mesh) as a stationary phase. H & C NMR spectra for synthesized compounds were recorded on a Varian Inova 300 unless otherwise noted. H NMR chemical shifts are reported as δ values in ppm relative to CDCl3 (7.26 ppm), coupling constants (J) are reported in Hertz (Hz).

Compounds obtained from enzymatic reactions using substrate 3 were purified on a Varian ProStar chromatography system and analyzed by NMR spectrometry. NMR spectra were acquired on a Bruker Avance III 500 MHz spectrometer equipped with a 5 mm H-C-N cryoprobe (Bruker Corporation, Billerica, Massachusetts, USA) at 500 MHz for 1H NMR and 125 MHz for 13C NMR in CDCl3. Mass spectra (ESI) were obtained at the Laboratory for Biological Mass Spectrometry at the Department of Chemistry, Texas A&M

University, with API QStar Pulsar, MDS Sciex (Toronto, ON, Canada) Quadrupole-TOF hybrid spectrometer.

Materials

Commercial solvents, reagents, Phosphate Buffer Saline (PBS) salts and acetonaphthone standards were used as received from Sigma- Aldrich. β-lactoglobulin was obtained from Davisco Foods International, Inc. (JE-003-6-922, La Sueur, MN, 93.6% BLG).

General method for trypsin digestion and mass spectrometric analysis

Trypsin digest, liquid chromatography-mass spectrometry (LC-MS) and the associated data mining procedures were each carried out at the Laboratory for Biological Mass Spectrometry at Texas A&M University. Aliquots (75 μL) of each sample were desalted using a Micro Bio-Spin P30 column (BioRad, Hercules, CA). Protein concentration was adjusted to 0.1 mg/mL with (NH4)2HCO3 buffer and reduced with 5 mM dithiothreitol at 60 °C for 1 h. Subsequent protein alkylation was achieved using 20 mM iodoacetamide at room temperature for 10 min. Protein samples were then digested with trypsin overnight (protein: enzyme ratio of 1:50) at 37 °C. Separation and mass spectrometry were carried out on a NanoFrontier LC-MS (Hitachi High Technologies, Dallas, TX) equipped with a nanospray ESI source. A 200 ng peptide sample was separated on a Vydac C18 capillary column (Grace Davison Discovery Sciences, 150 x 0.075 mm) at a flow rate of 200 nL/min under the following gradient routine employing

water/acetonitrile and 0.1% formic acid in all conditions: 2% water/acetonitrile for 5 min, 2-10% over 0.1 min, 10-40% over 29.9 min, 40-60% over 10 min, 60- 98% over 5 min, 98% for 6 min, 98-2% over 1 min, 2% for 13 min. MASCOT-assisted predictions for modified lysine and carbamidomethyl groups on peptide fragments were used in manual examination of tandem MS/MS data.

Protein samples were dialyzed into 50 mM ammonium acetate using Millipore centrifugal filters. The samples were then analyzed by injecting 30 μL of each sample onto an API QStar Pulsar, MDS Sciex (Toronto, ON, Canada) Quadrupole-TOF hybrid spectrometer. The obtained spectra were deconvoluted to obtain mass spectra as a function of intensity vs m/z.

Generic assay conditions for BLG with α, β unsaturated aldehydes

Assays with BLG were carried out according to procedures reported by Bench, et.al. BLG (150 μM) was added to 500 mL of PBS (10 mM phosphate buffer, 27 mM potassium chloride and 137 mM sodium chloride, pH 7.4) along with the α, β unsaturated aldehyde (450 μM), dissolved in ethanol. The 1L flask was covered in foil and shaken at 250 rpm, 37 °C in an incubator shaker for 4 days. The reaction was quenched by adding 500 mL of water and the solution extracted twice with 250 mL of ethyl acetate. The ethyl acetate fraction was dried over sodium sulfate and concentrated in vacuo. The resulting compound was stored at -80 °C until further analysis. Prior to analysis by HPLC the organics were dissolved in 200 μL of methanol. Assay with brominated compound was

repeated in the same manner except that 35.5 mg of compound was added to the reaction mixture.

HPLC analysis conditions

All samples with the exception of the reaction with 5 were analyzed on a Thermo ScientificTM UltiMateTM 3000 Rapid Separation HPLC system with a Prodigy 5µm ODS-2 150 Å, LC column 250 mm×4.6 mm (Phenomenex) and a mobile phase comprising water (with 0.1% formic acid) as inlet A and 75%:25% Methanol:Isopropanol (with 0.1% formic acid) as inlet B. Separation was achieved with the following conditions: 0-1 min: 80% A; 1-23 min: gradient change to 0% A; 23-33 min: maintain 0% A. A wavelength of 280 nm was used as it afforded the best signal to noise ratio.

The reaction assay of 3-methyl-3-naphthalene-propenalwith BLG was analyzed using a Varian ProStar Liquid Chromatography system with a Luna 5 silica column (10 x 250 mm, 5 µm, 100 Å, Phenomenex) and a mobile phase gradient of 40% hexane in ethyl acetate to 20% hexane in ethyl acetate over 30 min. with a 2 mL/min flow rate. A wavelength of 280 nm was used as it afforded the best signal to noise ratio.

Total Turnover Number (TTN) analysis

The amount of ketone product produced using wild type BLG was quantified using standard curves generated with synthetic standards. The amount of ketone product in

micromoles was then divided by the number of millimoles of protein added to the reaction mixture to obtain TTN in terms of μM per mM of protein.

Synthesis of α, β unsaturated aldehydes

The α, β unsaturated aldehydes used in this study were synthesized according to previously reported procedures. They were characterized by comparing H-NMR to previously reported H-NMR data.

Synthesis of (Z)-3-bromo-3-naphthylacrylaldehyde

3-bromo-3-naphthylacrylaldehyde was synthesized similarly to the synthesis of compound 8. A solution of dimethylformamide (15 mmol, 3.0 equiv.) in CHCl3 (10 ml) was cooled to 0 ºC and PBr3 (13.5 mmol, 2.7 equiv.) was added to the solution over 15 min. The reaction mixture was stirred at room temperature for 1 h. Acetonaphthone (5 mmol, 1 equiv.) was added to the solution and was allowed to stir overnight. The reaction mixture was then poured into ice water, neutralized with K2CO3 to a pH of 8 and extracted with Et2O (20 ml x 3). The organic phase was washed with brine, dried over MgSO4, and concentrated in vacuo. The compound was purified by flash column chromatography (1:30, EtOAc: hexanes). H NMR (300 MHz, CDCl3) δ 9.96 (d, 1H), 8.05 (s, 1H), 7.75-7.62(m, 4H), 7.51-7.46(m, 2H), 6.73(d, 2H) 13C NMR (300 MHz, CDCl3) δ 193.6, 144.9, 134.6, 134.4, 132.7, 129.5, 129.1, 128.6, 128.2, 127.7, 127.6, 127.2, 124.0 HRMS (ESI) calculated for C13H9BrO

CHAPTER VI

CONCLUSION

The isolation and extraction of chemically unique natural products has served as an invaluable tool to combat diseases and ailments. However, the identification and characterization of natural products with biological applications was an incredibly slow and inefficient process. Technological advances in the 20th century, like whole cell feeding studies and low-throughput fermentation, opened the door for the quick identification of natural products from microorganisms. Discovering these natural products led to the formation of combinatorial libraries of molecules that had similar chemical structures to existing natural products. An overwhelming majority of the compounds from libraries lacked complexity and exhibited no biological applications. The characterization and investigation of the biosynthetic pathways of existing natural products allowed for the identification of enzymes that give certain natural products biological applications. Investigations into the biosynthesis of the anti-tumor compound, azinomycin, and the retinal lipofuscin molecule, cycloretinal, led to the identification of enzymes and chemical compounds that can exhibit positive effects in biological systems.

Azinomycin A and B display anti-tumor capabilities due to their electrophilic epoxide and aziridine rings. The aziridino- [1,2-a] pyrrolidine moiety of azinomycin is extremely rare amongst natural products and has strong potential as a therapeutic. Identifying the enzymes that catalyze the formation of the aziridine ring allows for the implementation of this bioactive moiety in other molecules. Whole cell feeding studies

with *Streptomyces sahachiroi* revealed that glutamic acid is the precursor to azabicycle formation. A series of genes within the *Streptomyces* genome were identified and expressed to elucidate the first several enzymatic steps towards azabicycle formation. The last intermediate isolated within the proposed mechanism pathway was glutamic acid semi-aldehyde. However, this intermediate is missing two carbons from the ultimate azabicycle ring. Given their genetic similarity to other transketolase enzymes, *aziC5* and *aziC6* were hypothesized to mediate a thiamin pyrophosphate dependent, two-carbon extension of glutamic acid semi-aldehyde.

The transketolase activity of AziC5 and AziC6 was evaluated through a complete enzymatic and semi-synthetic route. N-acetyl-glutamic acid was incubated with AziC3/C4/C5/C6 and all of the necessary cofactors, while a synthetic glutamic acid semi-aldehyde was incubated with AziC5/C6. Both routes were analyzed with ESI-MS and revealed a mass that correlates to 2-acetamido-5,7-dihydroxy-6-oxoheptanoic acid. Further MS/MS analysis was utilized to reveal a fragmentation pattern matching the α, α'-dihydroxyketone product. A colorimetric assay was developed to detect transketolase products with tetrazolium red. This assay revealed that AziC5/C6, the ketose donor, the aldose acceptor, and thiamin pyrophosphate were essential to catalytic activity. Without any of these reagents, the α, α'-dihydroxyketone product did not form. Additionally, transketolase enzymes are thiamin dependent enzymes. The two enzymes were expressed in the presence of thiamine, purified, and denatured to see if thiamin could be isolated. A thiochrome assay revealed, by HPLC analysis, that the denatured extract did contain thiamin after it was co-injected with a synthetic standard.

Although azinomycin derives its toxicity from the epoxide and aziridine ring, the naphthoate ring helps to form noncovalent interactions that help facilitate coordination between the DNA strands. The left half of azinomycin is able to form DNA adducts, but the epoxide ring does not coordinate unless the naphthoate ring is attached. The multi-domain polyketide synthase, AziB, is able to form the naphthoate fragment. However, the naphthoate ring only forms in the presence of the thioester domain, AziG. When the TE domain of AziB is missing, the naphthoate ring is not produced and 2-methyl benzoic acid is produced. The thioesterase domains role in PKS activity was evaluated against several mutant forms of AziG.

In order to determine the rate of hydrolysis by the TE domain, the post-translational modification of the ACP domain was optimized. The promiscuous PPTase Svp was found to post-translationally modify AziB and its ACP domain the most efficiently. After the optimization of the post-translational modification was achieved, a 5-methyl-naphthoic acid-CoA analog was synthesized and tethered to AziB. The creation of the AziB-substrate bound complex allowed the rate of thioester hydrolysis to be observed for AziG and its mutants.

Thioesterase enzymes conserve a triad of Ser-His-Asp residues that facilitate thioester hydrolysis. The hypothesized AziG catalytic triad S58, H48, and E57 were expected to have the largest effects on hydrolysis, but kinetic values were unable to support that hypothesis. E57A was hypothesized to play a similar role to aspartic acid in TE activity, but this mutation had a minimal effect on activity. The AziG mutants were also used to investigate their effects on AziB mediated production of 5-methyl-naphthoic

acid. S58A and S61A were shown to exhibit the largest effects with H44A and H48A displaying the second largest effects. Once again, E57A had the lowest impact on PKS activity. These results indicate that serine has the largest impact on product formation. While H48, S58, and E57 were hypothesized to function as the catalytic triad, the kinetic results were unable to support that conclusion.

Although Azinomycin and thousands of other natural products have been shown to have beneficial effects on human biological systems, other natural products can have deleterious effects. Macular degenerative diseases have been linked to impaired visual abilities and the accumulation of lipofuscin. Lipofuscin form in the retina naturally as dimers of all-trans retinal, a necessary cofactor in the visual cycle. These dimers are formed to create A2E and cycloretinal. Cycloretinal has been shown to exist in much higher concentrations than A2E in certain macular diseases, but the extent of its toxicity has never been displayed. Liposomal complexes containing cycloretinal were synthesized and incubated with ARPE-19 in the presence and absence of 430 nm of light. Both of these conditions mediated retinal cell death, but the 430 nm of light caused the viability to decrease at a lower concentration. In addition, cycloretinal was observed to initiate retinal cell death at lower concentrations than some reported instances of A2E.

In order to combat the toxicity of cycloretinal formation, enzymatic degradation and synthetic inhibition was pursued. The peroxidase enzyme, MsP1, was shown to break apart cycloretinal into 2,4-dimethylbenzaldehyde and β-Ionone, while A2E was broken into β-Ionone. The toxicity of these compounds was measured after liposomal encapsulation. Both of these molecules exhibited no toxicity in light or dark conditions.

This reveals that MsP1 is an effective lipofuscin degradation enzyme that could be deployed into the retina with gene therapy.

The dimerization of cycloretinal can occur enzymatically and non-enzymatically through the formation of a central cyclohexadienal moiety. These rings form with a proline catalyst or the milk protein BLG. (*Z*)-3-bromo-3-phenylacrylaldehyde and (*E*)-3-(naphthalen-2-yl) but-2-enal were synthesized in a trapping experiment in order to reveal the mechanism of formation for cyclohexadienals. Both catalysts yielded a retro aldol product which introduces a step-wise mechanism. The brominated aldehyde was observed to inhibit the enzyme and proline catalyst, while preventing homodimer formation. In addition, a series of substrates were created and treated with BLG and the brominated inhibitors to show that BLG is able to catalyze the retro aldol, two-carbon cleavage from a series of hydrophobic α, β-unsaturated aldehydes.

The investigations into the biosynthesis of azinomycin can outline the enzymes and intermediates involved that enable its construction. This information can pave the way for the increased production of azinomycin *in vivo, in vitro,* and *in situ.* The characterization of AziC5 and AziC6 as a transketolase enzyme and its ability to facilitate a two-carbon extension of the intermediate glutamic acid semi-aldehyde. By characterizing this intermediate, we identified an enzyme that can convert the azabicycle precursor, glutamic acid, to the correct carbon length as the aziridine ring. In addition, further hypothesized steps can be achieved synthetically, so a semi-synthetic approach could be employed to create the aziridine ring. The thioesterase domain of the PKS AziB was observed to have effects on naphthoate ring production and the rate of hydrolysis from

the enzyme. Cycloretinal toxicity of retinal cells was determined and an enzymatic gene therapy target was found to degrade cycloretinal into non-toxic byproducts. Additionally, the mechanism of cycloretinal formation was determined and inhibitors were designed for its enzymatic and non-enzymatic formation. The identification and characterization of natural products not only creates possible treatment plans for certain diseases, but also identifies harmful compounds that originate within human beings. By characterizing azinomycin and cycloretinal biosynthesis, the knowledge of natural products was utilized to help ameliorate diseases.

REFERENCES

1. Maplestone, R. A.; Stone, M. J.; Williams, D. H., *Gene* **1992,** *115* (1), 151-157.
2. Der Marderosian, A.; Beutler, J.A. *The Review of Natural Products*, **2002**; 13–43.
3. Aniszewski, T. Alkaloids—Secrets of Life. In *Alkaloid Chemistry, Biological Significance, Applications and Ecological Role*; Elsevier Science: Amsterdam, The Netherlands, **2007**; p. 334.
4. Mann, J. *Murder, Magic, and Medicine*; Oxford University Press: New York, NY, USA, **1994**; pp. 164–170
5. Katz, L.; Baltz, R. H., Natural product discovery: past, present, and future. *Journal of Industrial Microbiology & Biotechnology* **2016,** *43* (2), 155-176.
6. Shen, B., *Cell.* **2015** ;163(6):1297-300.
7. Newman, D. J., *Journal of Medicinal Chemistry* **2008,** *51* (9), 2589-2599.
8. Henkel, T.; Brunne, R. M.; Muller, H.; Reichel, F. Statistical investigation into the structural complementarity of natural products and synthetic compounds. *Agnew. Chem., Int. Ed.* **1999**, *38*, 643– 647.
9. Newman, D.; Cragg, G., *J. Nat. Prod.* 2016, **79**, 629−661
10. Paulus, Constanze et al. sp. MP131-18." *Scientific reports* vol. 7 42382, **2017.**
11. Liu, R.; Deng, Z.; Liu, T., Streptomyces species: Ideal chassis for natural product discovery and overproduction. *Metabolic Engineering* **2018,** *50*, 74-84.
12. Hopwood, D., Streptomyces in Nature and Medicine: the Antibiotic Makers. *Oxford University Press* **2007**.
13. Watve, M.G., Tickoo, R., Jog, M.M. *et al.* How many antibiotics are produced by the genus *Streptomyces*. *Arch Microbiol,* **2001,** 176, 386–390
14. Hata, T., Koga, F., Sano, Y., Kanamori, K., Matsumae, A. et al., I. *J. Antibiot., Ser. A* 7, 107-112
15. Nagaoka, K., Matsumoto, M., Oono, J., Yokoi, K., Ishizeki, S. et al. azinomycin A and B, new antitumor antibiotics I. Producing organism, fermentation, isolation, and characterization. *J. Antibiot,* **2008** 39, 1527-1532.
16. Yokoi, K.; Nagaoka, K.; Nakashima, T., azinomycin A and B, new antitumor antibiotics. II. Chemical structures. *Chem Pharm Bull (Tokyo)* **1986,** *34* (11), 4554-
17. Casely-Hayford, M.A., Pors, K., James, C.., Patterson, L.H., Hartley, J.A. et al. Design and synthesis of a DNA-crosslinking azinomycin analogue. *Org. Biomolec. Chem.,* **1985,** 3, 3585-3589

18. Ishizeki, S., Ohtsuka, M., Kazuhiko, I., Kukita, K., Nagaoka, K. et al. Azinomycin A and B, new antitumor antibiotics III. Antitumor activity. *J. Antibiot.*, **1987**40, 60-65

19. Coleman, R.S., Perez, R.J., Burk, C.H. & Navarro, A. Studies on the mechanism of action of azinomycin B: Definition of regioselectivity and sequence selectivity of DNA cross- link formation and clarification of the role of the naphthoate. *J. Am. Chem. Soc.,* **2002,** 124, 13008-13017.

20. Armstrong, R. W.; Salvati, M. E.; Nguyen, M., Novel interstrand cross-links Induced by the antitumor antibiotic carzinophilin/azinomycin B. *Journal of the American Chemical Society* **1992**, 114 (8), 3144-3145.

21. Fujiwara, T.; Saito, I.; Sugiyama, H., Highly efficient DNA interstrand crosslinking induced by an antitumor antibiotic, carzinophilin. *Tetrahedron Letters* **1999,** *40* (2), 315-318.

22. LePla, R.C., Landreau, C.A.S., Shipman, M., Hartley, J.A. & Jones, G.D.D. Azinomycin inspired bisepoxides: influence of linker structure on in vitro cytotoxicity and DNA interstrand cross-linking. *Bioorg. Med. Chem*. **2005**, Lett. 15, 2861-2864 (2005).

23. Musser, S., Pan, T.M., Egorin, M., Kyle, D., Gallery, P., *Chem. Res. Toxicol.* **1992**, 5, 95-99

24. Coleman, R. S.; Burk, C. H.; Navarro, A.; Brueggemeier, R. W.; Diaz-Cruz, E. S., Role of the Azinomycin Naphthoate and Central Amide in Sequence-Dependent DNA Alkylation and Cytotoxicity of Epoxide-Bearing Substructures. *Organic Letters* **2002,** *4* (20), 3545-3548.

25. Mao, Y., Varoglu, M. & Sherman, D.H. Molecular characterization and analysis of the biosynthetic gene cluster for the antitumor antibiotic mitomycin C from Streptomyces lavendulae NRRL 2564. *Chem. Biol*., **1999** 6, 251-263.

26. Ogasawara, Y. & Liu, H.-w. Biosynthetic studies of aziridine formation in azicemicins. *J. Am. Chem. Soc*., **2009**, 131, 18066-18068.

27. Zhao, Q., He, Q., Ding, W., Tang, M., Kang, Q. et al. Characterization of the azinomycin B biosynthetic gene cluster revealing a different iterative type I polyketide synthase for naphthoate biosynthesis. *Chem. Biol*. **2008** 15, 693-705.

28. Van Lanen, S.G., Oh, T.-j., Liu, W., Wendt-Pienkowski, E. & Shen, B. Characterization of the maduropeptin biosynthetic gene cluster from Actinomadura madurae ATCC 39144 supporting a unifying paradigm for enediyne biosynthesis. *J. Am. Chem. Soc*., **2008** 129, 13082- 13094.

29. Sweeney, JB *Chem. Soc. Rev.*, **2002**,31, 247-258

30. Mori, S., Nepal, K., Kelly, G., Sharma, V., Watanabe, C., *Biochemistry* **2017**, 56, 6, 805-808.

31. Corre, C. & Lowden, P.A.S. The first biosynthetic studies of the azinomycins: Acetate incorporation into azinomycin B. *Chem. Commun*., **2004**, 990-991.

32. Corre, C., Landreau, C.A.S., Shipman, M. & Lowden, P.A.S. Biosynthetic studies on the azinomycins: The pathway to the naphthoate fragment. *Chem. Commun*., **2004**, 2600-2601.

33. Kelly, G. T.; Sharma, V.; Watanabe, C. M. H., An improved method for culturing Streptomyces sahachiroi: Biosynthetic origin of the enol fragment of azinomycin B. *Bioorganic Chemistry* **2008,** *36* (1), 4-15.

34. Zhao, Q., He, Q., Ding, W., Tang, M., Kang, Q. et al. Characterization of the azinomycin B biosynthetic gene cluster revealing a different iterative type I polyketide synthase for naphthoate biosynthesis. *Chem. Biol.,* **2008**, 15, 693-705.

35. Hu, C. W., Chang, Y. L., Chen, S. J., Kuo-Huang, L. L., Liao, J. C., Huang, H. C., & Juan, H. F. (2011). Revealing the functions of the transketolase enzyme isoforms in Rhodopseudomonas palustris using a systems biology approach. *PloS one*, **2011**, *6*(12).

36. G. Schenk et al, *Journal of Biochemistry & Cell Biology*, 30,**1998** 1297±1318.

37. M. Walfridsson, J. Hallborn, M. PenttilaÈ, S. KeraÈ nen, B. Hahn-HaÈ gerdahl, Xylose-metabolizing Saccharomyces cerevisiae strains overexpressing the TKL1 and TAL1 genes encoding the pentose phosphate pathway enzymes transketolase and transaldolase, *Appl. Environ. Microbiol*. 61, **1995**, 4184±4190.

38. T. Wood, The pentose phosphate pathway. *Academic Press*, **1985**.

39. C.F. Hawkins, A. Borges, R.N. Perham, A common structural motif in thiamin pyrophosphate-binding enzymes, *FEBS Lett.,* 255 **1989**, 77±82.

40. M. Reynen, H. Sahm, Comparison of the structural genes for pyruvate decarboxylase in different Zymomonas strains, *J. Bacteriol.* ,170, **1988** 3310±3313.

41. M. S. Hasson, A. Muscate, M. J. McLeish, L. S. Polovnikova, J. A. Gerlt, G. L. Kenyon, G. A. Petsko, D. Ringe, The crystal structure of benzoylformate decarboxylase at 1.6A resolution: diversity of catalytic residues in thiamin diphosphate-dependent enzymes, *Biochemistry* ,37, **1998,** 9918±9930.

42. Y. Lindqvist, G. Schneider, U. Ermler, M. SundstroÈ m, Three-dimensional structure of transketolase, a thiamine diphosphate dependent enzyme, at 2.5 A resolution, *EMBO J.* 11 **1992** 2373±2379.

43. L. Meshalkina, U. Nilsson, C. Wikner, T. Kostikowa, G. Schneider, Examination of the thiamin diphosphate binding site in yeast transketolase by site-directed mutagenesis, *Eur. J. Biochem*. 244 **1997**, 646±652.

44. M. Nikkola, Y. Lindqvist, G. Schneider, structure of transketolase from Saccharomyces cerevisiae at 2.0 A resolution*, J. Mol. Biol*. 238 **1994**, 387±404.

45. G. Schneider, Y. Lindqvist, Enzymatic thiamine catalysis: mechanistic implications from the three-dimensional structure of transketolase, *Bioorg. Chem* 21 **1993**, 109± 117.

46. R.F. Butterworth, J.F. GigueÁ re, A.M. Besnard, Activities of thiamine-dependent enzymes in two experimental models of thiamine deficiency encephalopathy: 1. the pyruvate dehydrogenase complex, *Neurochem. Res.* 10, **1985** 1417±1428.

47. R.F. Butterworth, J.F. GigueÁ re, A.M. Besnard, Activities of thiamine-dependent enzymes in two experimental models of thiamine-deficiency encephalopathy: 2. a-ketoglutarate dehydrogenase, *Neurochem. Res.* 11 ,**1986,** 567±577.

48. G.E. Gibson, H. Ksiezak-Reding, K.F.R. Sheu, V. Mykytyn, J.P. Blass, Correlations of enzymatic, metabolic, and behavioral deficits in thiamine deficiency and its reversal, *Neurochem. Res*. 9, **1984**, 803±814.

49. G.E. Gibson, K.F.R. Sheu, A.C. Baker, K.C. Carlson, B. Harding, P. Perrino, J.P. Blass, Reduced activities of thiamine-dependent enzymes in brains and peripheral tissues of Alzheimer's patients, *Arch. Neurol*. 45 **1988**

50. B. Ganem, from glucose to aromatics: recent developments in natural products of the shikimic acid pathway, *Tetrahedron,* 34, **1978,** 3353±3383.

51. G. Gosset, J. Yong-Xiao, A. Berry, A direct comparison of approaches for increasing carbon¯ow to aromatic biosynthesis in Escherichia coli, *J. Ind. Microbiol*., 17, **1996,** 47±52.

52. G.R. Hobbs, M.D. Lilly, N.J. Turner, J.M. Ward, A.J. Willets, J.M. Woodley, Enzyme catalyzed carbon-carbon bond formation: use of transketolase from Escherichia coli, *J. Chem. Soc*. ,1, 1993, 165±166.

53. Du, L.; Lou, L., PKS and NRPS release mechanisms. *Natural Product Reports* **2010**, *27* (2), 255-278.

54. *Nat. Prod. Rep.*, *2014*, 31, 61-108

55. S. Borchert, T. Stachelhaus and M. A. Marahiel, *J. Bacteriol.*, **1994**, 176, 2458–2462

56. S. Borchert, T. Stachelhaus and M. A. Marahiel, *J. Bacteriol.*, **1994**, 182, 4468–4471

57. J. N. Copp and B. A. Neilan, *Appl. Environ. Microbiol.*, **2006**, 72, 2298–2305

58. Du, L., Lou, L., *Nat. Prod. Rep.*, **2010**,27, 255-278

59. P. Caffrey, B. Green, L. C. Packman, B. J. Rawlings, J. Staunton and P. F. Leadlay, *Eur. J. Biochem*., **1991**, 195, 823–830.

60. S. C. Tsai, L. J. Miercke, J. Krucinski, R. Gokhale, J. C. Chen, P. G. Foster, D. E. Cane, C. Khosla and R. M. Stroud*, Proc. Natl. Acad. Sci. U. S. A*., **2001**, 98, 14808–14813.

61. R. M. Kohli, C. T. Walsh and M. D. Burkart, *Nature*, **2002**, 418, 658–661.

62. C. N. Boddy, T. L. Schneider, K. Hotta, C. T. Walsh and C. Khosla, 459. *J. Am. Chem. Soc.,* **2003**, 125, 3428–3429.

63. R. M. Kohli, M. D. Burke, J. H. Tao and C. T. Walsh, *J. Am. Chem. Soc*., **2003**, 125, 7160–7161.

64. J. Grunewald and M. A. Marahiel, *Microbiol. Mol. Biol. Rev*., **2006**, 70, 121–146.

65. D. A. Miller, L. S. Luo, N. Hillson, T. A. Keating and C. T. Walsh, *Chem. Biol*., **2002**, 9, 333–344.

66. B. K. Hubbard and C. T. Walsh, *Agnew. Chem., Int. Ed*., 2**003**, 42, 730–765.

67. M. F. Byford, J. E. Baldwin, C. Y. Shiau and C. J. Schofield, *Chem. Rev*., **1997**, 97, 2631–2650.

68. Y.T. Kim, Y.R. Lee, J. Jin, K.H. Han, H. Kim, J.C. Kim, T. Lee, S. H. Yun and Y. W. Lee, *Mol. Microbiol.,* **2005**, 58, 1102–1113.

69. H. Zhou, J. Zhan, K. Watanabe, X. Xie and Y. Tang*, Proc. Natl. Acad. Sci. U. S.* A., **2008**, 105, 6249–6254.

70. L. Robbel, K. M. Hoyer and M. A. Marahiel, *FEBS J*., **2009**, 276, 1641–1653.

71. S. Dawson, J. P. Malkinson, D. Paumier and M. Searcey*, Nat. Prod. Rep*., **2007**, 24, 109–126.

72. A. M. Gehring, I. Mori and C. T. Walsh, *Biochemistry*, **1998**, 37, 2648–2659.

73. Lihua Y. Marmorstein, Francis L. Munier, Yvan Arsenijevic, Daniel F. Schorderet, Precious J. McLaughlin, Daniel Chung, Elias Traboulsi, Alan D. Marmorstein, *PNAS,* 2**002**, 99 (20) 13067-13072

74. Fine, S. L., Berger, J. W., Maguire, M. G. & Ho, A. C. *N. Engl. J. Med.,* **2002,** 342, 483– 492.

75. Allikmets, R., Shroyer, N., Singh, N., Seddon, J., Lewis, A., Bernstein, P., *Peiffer, A*.,**1997**: Vol. 277, Issue 5333, pp. 1805-1807.

76. Stone, E., Nichols, B., Streb, L. *et al*. Genetic linkage of vitelliform macular degeneration (Best's disease) to chromosome 11q13. *Nat Genet*, **1992** 1**,** 246–250

77. Lim, S., Wong, T., *The Lancelet*379, Issue 9827, 2012**,** Pages 1728-1738.

78. Wald, G. *J Gen Physiol.* **1935** 19 (2): 351–371.

79. Palczewski, K., G protein-coupled receptor rhodopsin. *Annual Rev Biochem*. **2006,** 75, 743-767.

80. Kuhn, H., Wilden, U., Deactivation of photoactivated rhodopsin by rhodopsin- kinase and arrestin. *J Recept. Res*., **1987** 7, 283-298.

81. Harosi, F.I., Absorption spectra and linear dichroism of some amphibian photoreceptors. *J Gen Physi*ol., **1975** 66, 357-382.

82. Mondal, M.S., Ruiz, A., Bok, D., Rando, R.R. Lecithin retinol acyltransferase contains cysteine residues essential for catalysis. *Biochemistry*. **2001,** 39, 5215-5220.

83. Ruiz, A., Winston, A., Lim, Y.H., Gilbert, B.A., Rando, R.R., Bok, D., 1999. Molecular and biochemical characterization of lecithin retinol acyltransferase. *J Bio. Chem.,* **1999** 274,

84. Jang, G.F., McBee, J.K., Alekseev, A.M., Haeseleer, F., Palczewski, K.. Stereo- isomeric specificity of the retinoid cycle in the vertebrate retina. *J Biol. Chem.,* **2000** 275.

85. Kim, S., Young, P., Jang, P., Jockusch, S., Fishkin, N., Turro, N., Sparrow, J., *PNAS,* **2007**, 104 (49) 19273-19278.

86. Donstov, A., Sakina, L., Golubkov, A., Ostrovsky, M., Doklady, M. *Biochemistry and Biophysics*; Moscow Vol. 425, IS. 1, **2009**: 98-10

87. Sparrow JR, Nakanishi K, Parish CA. The lipofuscin fluorophore A2E mediates blue light-induced damage to retinal pigmented epithelial cells. *Invest Ophthalmic. Vis Sci.* **2000**; 41:1981–1989.

88. Schutt F, Davies S, Kopitz J, Holz FG, Boulton ME. Photodamage to human RPE cells by A2-E, a retinoid component of lipofuscin. *Invest Ophthalmol Vis Sci.* **2000**; 41:2303–2308.

89. Ham WTJ, Allen RG, Feeney-Burns L, et al. The involvement of the retinal pigment epithelium. In: Waxler M, Hitchins VM, eds. *CRC Optical Radiation and Visual Health*. Boca Raton, FL: CRC Press; **1986**.

90. Ham WTJ, Mueller HA, Ruffolo JJJ, et al. Basic mechanisms under- lying the production of photochemical lesions in the mammalian retina. *Curr Eye Res.* **1984**; 3:165–174.

91. Ham WTJ, Ruffolo JJJ, Mueller HA, Clarke AM, Moon ME. Histologic analysis of photochemical lesions produced in rhesus retina by short-wavelength light. *Invest Ophthalmol Vis Sci.* **1978**;17: 1029 –1035.

92. Sparrow, J., Zhou, J., Ben-Shabat, S., Vollmer, H., Itagaki, Y., Nakanishi, K., *Invest. Ophthalmol. Vis. Sci.* **2002**;43(4):1222-1227

93. Hasebe, F.; Matsuda, K.; Shiraishi, T.; Futamura, Y.; Nakano, T.; Tomita, T.; Ishigami, K.; Taka, H.; Mineki, R.; Fujimura, T.; Osada, H.; Kuzuyama, T.; Nishiyama, M., Amino-group carrier-protein-mediated secondary metabolite biosynthesis in Streptomyces. *Nature Chemical Biology* **2016,** *12* (11), 967-972.\

94. Keshav K. Nepal, Rachel P. Lee, Yohannes H. Rezenom, and Coran M. H. Watanabe *Biochemistry* **2015** *54* (29), 4415-4418

95. Zhao, Q.; He, Q.; Ding, W.; Tang, M.; Kang, Q.; Yu, Y.; Deng, W.; Zhang, Q.; Fang, J.; Tang, G.; Liu, W. *Chemistry & Biology* **2008**, 15, 693-705

96. Joshi, S.; Singh, A. R.; Kumar, A.; Misra, P. C.; Siddiqi, M. I.; Saxena, J. K., Molecular cloning and characterization of Plasmodium falciparum transketolase. *Molecular and Biochemical Parasitology* **2008,** *160* (1), 32-41.

97. Aymard, C. M. G.; Halma, M.; Comte, A.; Mousty, C.; Prévot, V.; Hecquet, L.; Charmantray, F.; Blum, L. J.; Doumèche, B., Innovative Electrochemical Screening Allows Transketolase Inhibitors to Be Identified. *Analytical Chemistry* **2018,** *90* (15), 9241-9248.

98. Brown S. B., Honeyfield D. C., Vandenbyllaardt L., *Am. Fish. Soc. Symp*. **1998**, 21, 73–81

99. Liu S., Zhang Z., Liu Q., Luo H., Zheng W., *J. Pharm. Biomed. Anal*. **2002**, 30, 685–694

100. Smith, M. E. B., Kaulmann, U., Ward, J. M., and Hailes, H. C. A colorimetric assay for screening transketolase activity. *Bioorg. Med. Chem.*, **2006** 14, 7062−7065.

101. Mori, S., et. al., Watanabe, C., *Biochemistry* **2016,** 55, 4, 704–714

102. Huang, Y., Wendt-Pienowski, E., Shen, B., *The Journal of Biological Chemistry,* 281, 40, 29660–29668, **2006**.

103. Lu, H., Tsai, S., Khosla, C., Cane, D., *Biochemistry*, Vol. 41, No. 42, **2002**

104. Zhihao Zhuang, Feng Song, Wenhai Zhang, Kimberly Taylor, Angela Archambault, Debra Dunaway-Mariano, Jian Dong, and Paul R. Carey *Biochemistry* **2002** *41* (37), 11152-11160

105. Mir, H., Raza, S.I., Touseef, M. *et al.* A novel recessive mutation in the gene ELOVL4 causes a neuro-ichthyotic disorder with variable expressivity. *BMC Med Genet*, **2014**, 15.

106. Lin, Y., Gao, H., Liu, Y., Liang, X., Liu, X., Wang, Z., Zhang, W., Chen, J., Lin, Z., Huang, X., Liu, Y. "Two novel mutations in the bestrophin-1 gene and associated clinical observations in patients with best vitelliform macular dystrophy". M*olecular Medicine Reports* 12.2 **2015**: 2584-2588.

107. Maugari, A., Hyong, C., Cremers, F. *The American Journal of Human Genetics*, Volume 67, Issue 5, **2000**, 1365-1371

108. Fishkin, N., Sparrow, J., Allikmets, R., Nakanis, J., *Proceedings of the National Academy of* Sciences **2005**, 102 (20) 7091-7096

109. Mihai, D., Washington, I. Vitamin A dimers trigger the protracted death of retinal pigment epithelium cells. *Cell Death DiS.* **2014**, 5, e1348

110. Maeda, A., Maeda, T., Golzak, M., Chou, S., Desai, A., Hoppel, C., Palczewski, K *Jour. Biol. Chem.,* **2009** VOL.284, NO.22, pp.15173–15183.

111. Catherine Y. MD, PhD[*]; Francis, Jasmine H. MD[†]; Brodie, Scott E. MD, PhD[†, ‡]; Marr, Brian MD[†]; Pulido, Jose S. MD[§]; Marmor, Michael F. MD[¶]; Abramson, David H. MD[†, **] RETINAL TOXICITIES OF CANCER THERAPY DRUGS, Retina: **2014** - Volume 34 - Issue 7 - p 1261-1280

112. Rolling, F. Recombinant AAV-mediated gene transfer to the retina: gene therapy perspectives. *Gene Ther*, **2004**11, S26–S32.

113. Wu, Y., Zhou, J., Fishkin, A., Rittman, B., Sparrow, J., *J. Am. Chem. Soc.* **2011**, 133, 4, 849–857

114. Schwartz SH, Cai Tan B, Gage DA, Zeevaart JAD, McCarty DR *Science,* **2001,** 276:1872–1874

115. Rodríguez-Bustamante E, Maldonado-Robledo G, Ortiz MA, Diaz-Avalos C, Sánchez S **2005**. *Appl. Microbiol Biotechnol.* 68:174–182

116. Rodríguez-Bustamante E, Sánchez S **2007**, *Crit. Rev Microbiol* 33:211–230

117. Marasco EK, Vay K, Schmidt-Dannert C **2006** Identification of carotenoid cleavage dioxygenases from *Nostoc* spp. PCC 7120 with different cleavage activities. *J Biol. Chem* 281:31583–31593

118. Scheibner, M., Hülsdau, B., Zelena, K. *et al.* Novel peroxidases of *Marasmius scorodonius* degrade *β*-carotene. *Appl. Microbiol Biotechnol* ,**2008** 77, 1241–1250

119. Szweda, Renata T., Katharina Schmidt, and Holger Zorn *European Food Research and Technology* **2013**: 377-384.

120. Darrow, J., *Drug Discovery Today,* **2009** Volume 24, Number 4

121. Schichi, H., Somers, R., *The Journal of Biological Chemistry,* **1998,**249, 65706577.

122. List, B., Lerner, R., Barbas, C., *J. Am. Chem. Soc.,***200** Vol. 122, No. 10.

123. Bench, B., Liu, C., Evett, C., Watanabe, C., *J. Org. Chem.* **2006**, 71, 25, 9458–9463

124. Bench, B., Tichy, S., Perez, L., Benson, J., Watanabe, C. *Bioorganic & Medicinal* Chemistry 16 **2008** 7573–7581

125. Scheerer, P., Park, J., Hildebrand, P. *et al.* Crystal structure of opsin in its G-protein-interacting conformation. *Nature* **2008,** 455 497–502.

126. Bench, B., Foulke-Abel, J., Watanabe, C., *Mol. BioSyst.*, **2011**, 7**,** 162-168

127. Gowda, V., Bench, B., Foulke-Abel, J., Chen, J., Watanabe, C., *Biochemistry* **2017**, 56, 43, 5715–5719

128. Guthrie, J.P.; Cooper, K.J.; Cossar, J.; Dawson, B.A.; Taylor, K.F. "The retroaldol reaction of cinnamaldehyde". *Can. J. Chem.* **1984**, 62 (8): 1441-1445.

129. Beranova-Giorgianni, S., Giorgianni, F.,*Proteomes* **2018**, *6*(2), 22

APPENDIX

SUPPORTING FIGURES AND TABLES

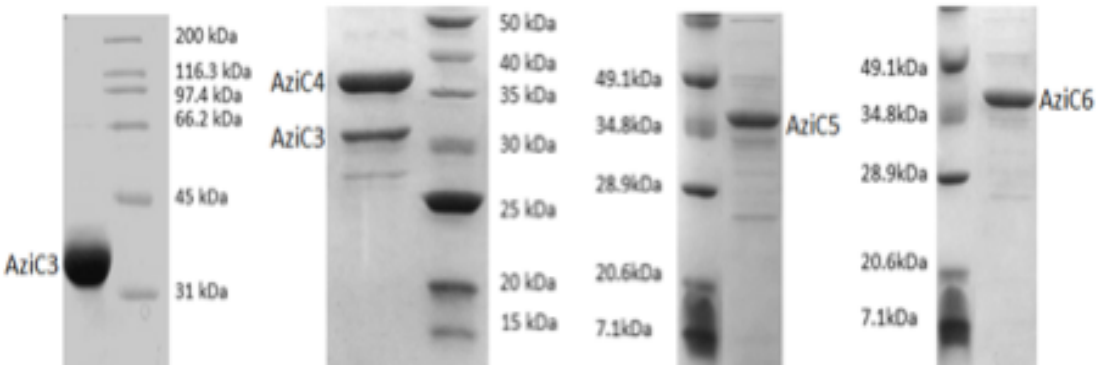

Appendix Figure 1 Purification of AziC3, C4, C5, and C6 protein

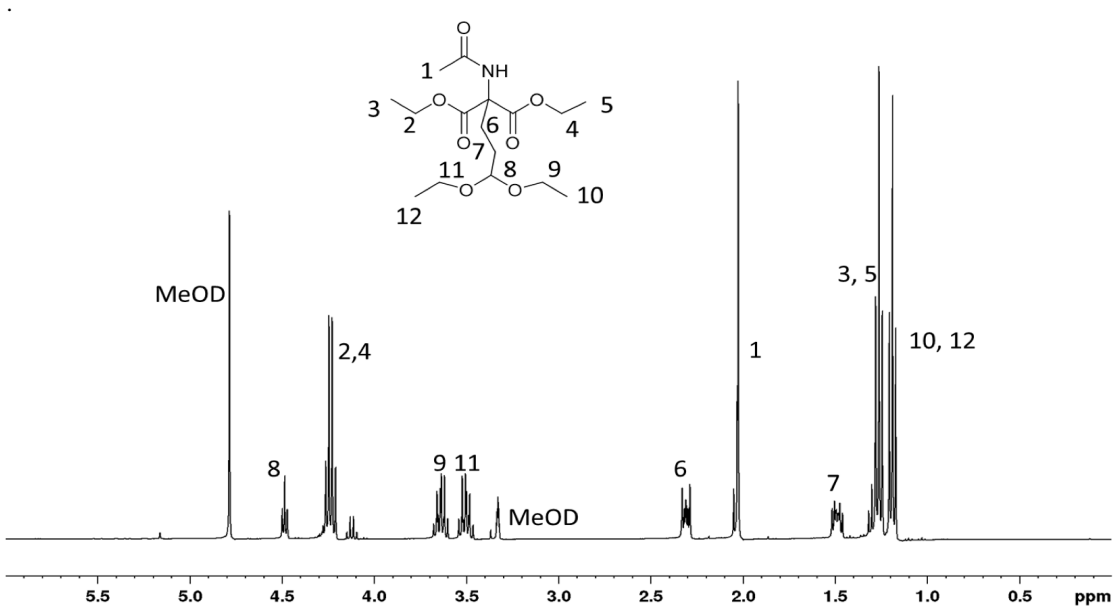

Appendix Figure 2 δ^1H (400 Hz) of diethyl 2-acetamido-2-(3,3-diethoxypropyl) malonate in MeOD

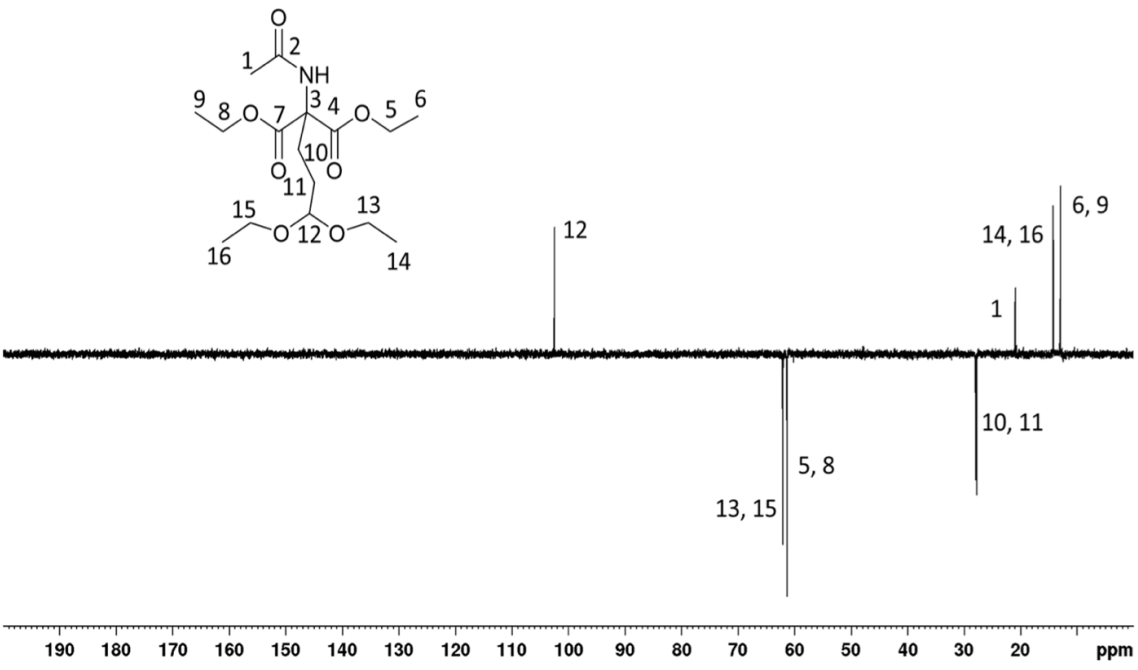

Appendix Figure 3 δ^{13}C(400 Hz) of diethyl 2-acetamido-2-(3,3-diethoxypropyl)malonate in MeOD .

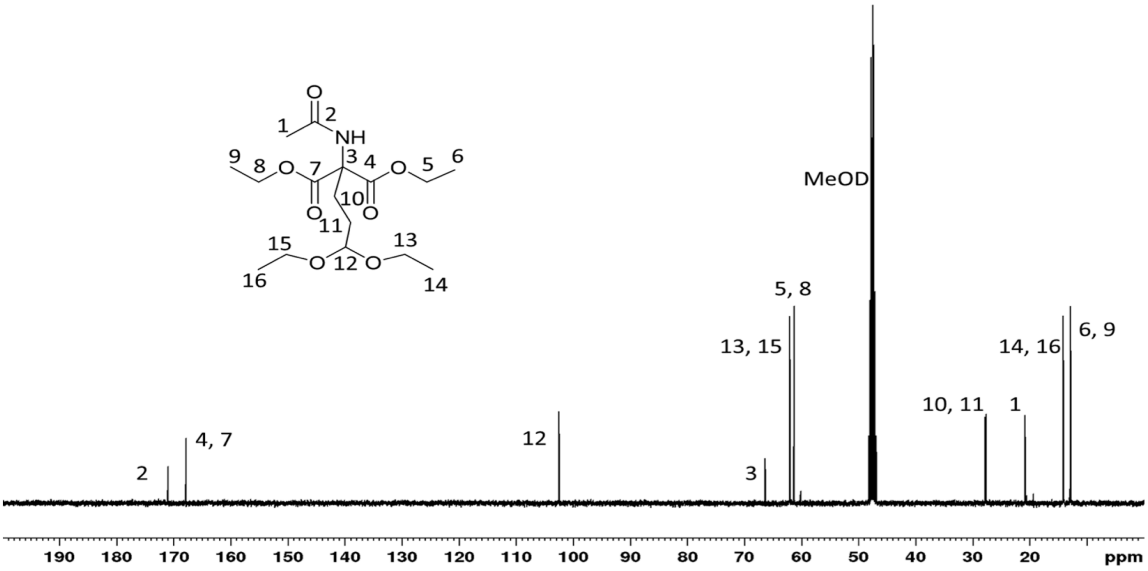

Appendix Figure 4 δDEPT135(400 Hz) of diethyl 2-acetamido-2-(3,3-diethoxypropyl) malonate in MeOD

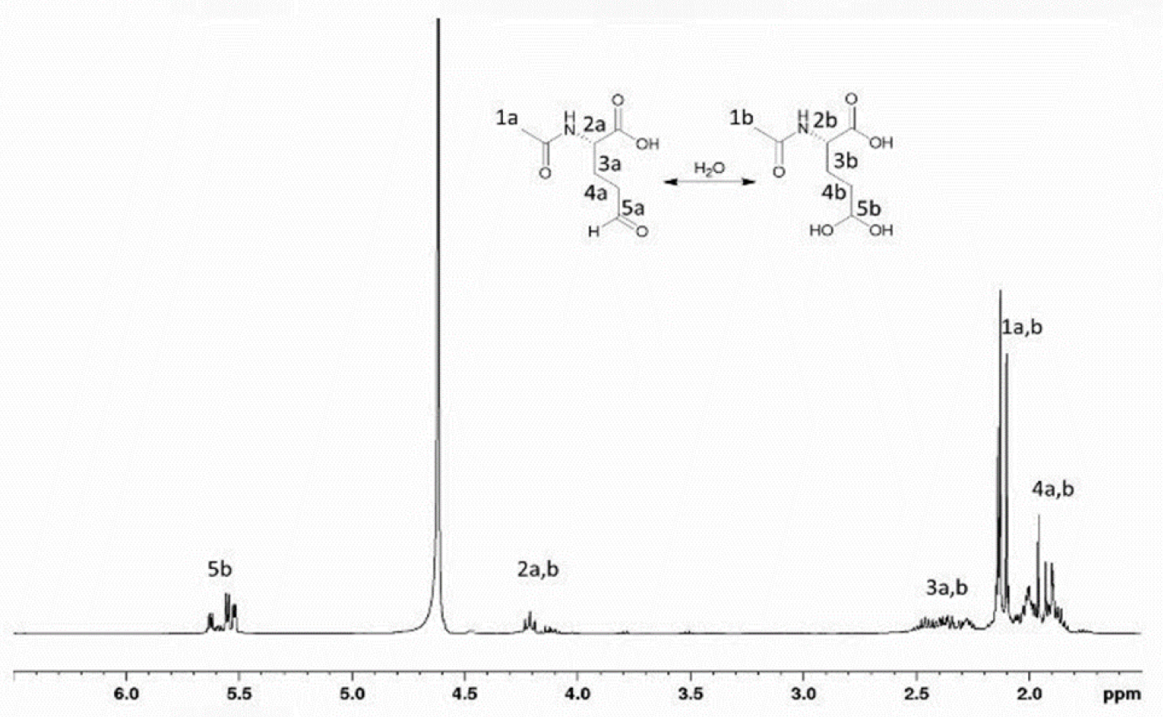

Appendix Figure 5 δ^1H (400 Hz) of 2-acetamido-5-oxopentanoic acid in D_2O

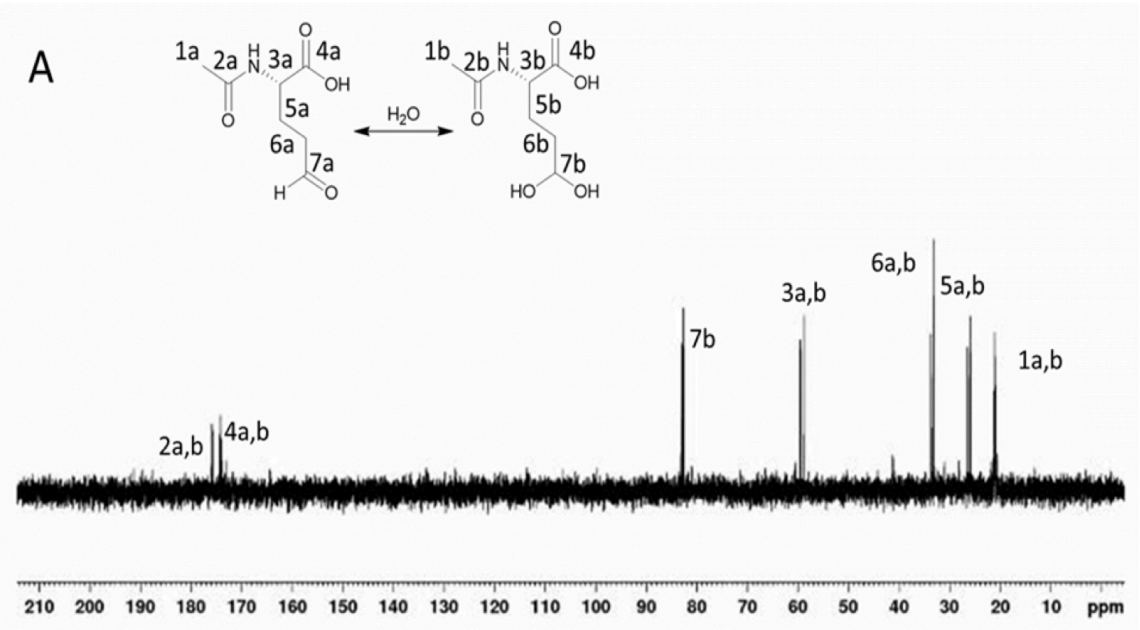

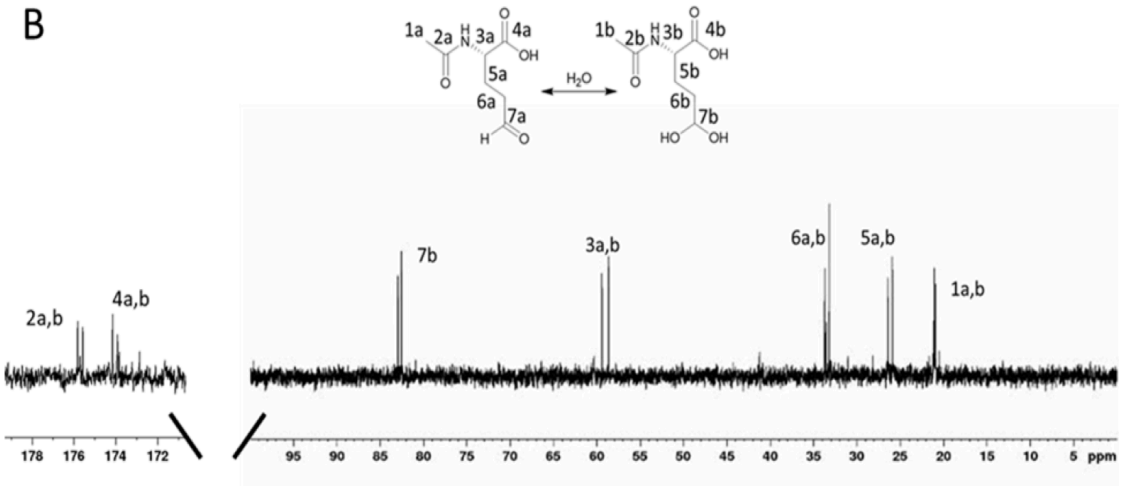

Appendix Figure 6 $\delta^{13}C$(400 Hz) of 2-acetamido-5-oxopentanoic acid in D2O 2-acetamido-5-oxopentanoic acid exists in equilibrium with its diol in D_2O. **A**) $\delta^{13}C$(400 Hz) of 2-acetamido-5-oxopentanoic acid in D2O entire spectrum. **B**) Zoom in on overlapping peaks

	F6P	**X5P**	**HP**
k_m (mM)	2.0 ± 0.4	3.0 ± 0.5	4.0 ± 0.9
k_{cat} (s^{-1})	91 ± 5.4	76 ± 3.6	6.1 ± 3.8
k_{cat} / k_m (mM^{-1} s^{-1})	54 ± 13	29 ± 6.3	14 ± 3.6

Appendix Table 1 Transketolase Kinetic Assay value with various substrate

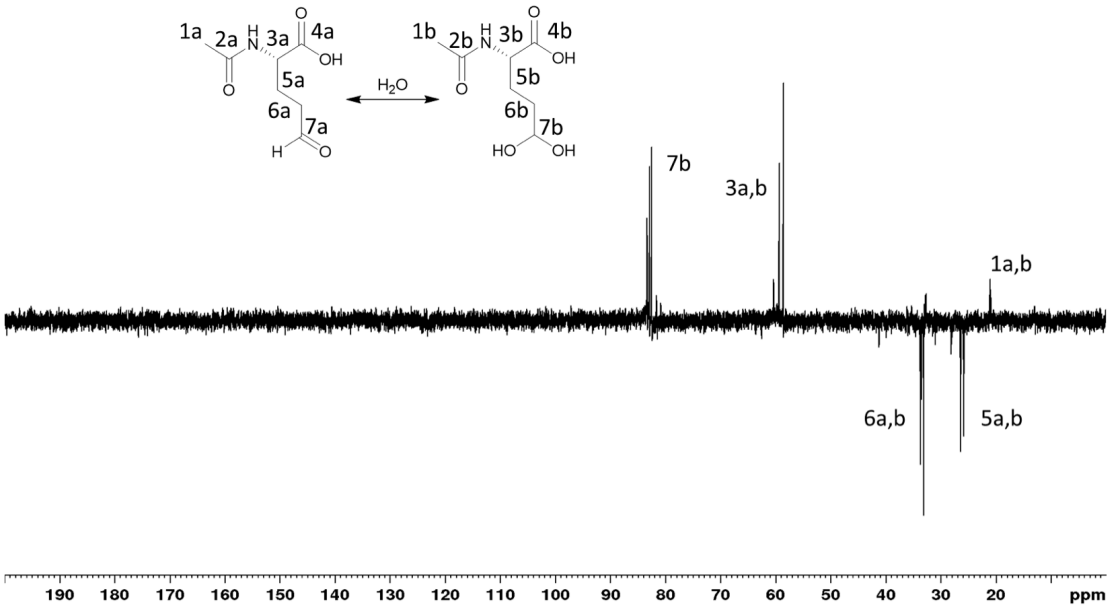

Appendix Figure 7 δDEPT135(400 Hz) 2-acetamido-5-oxopentanoic acid

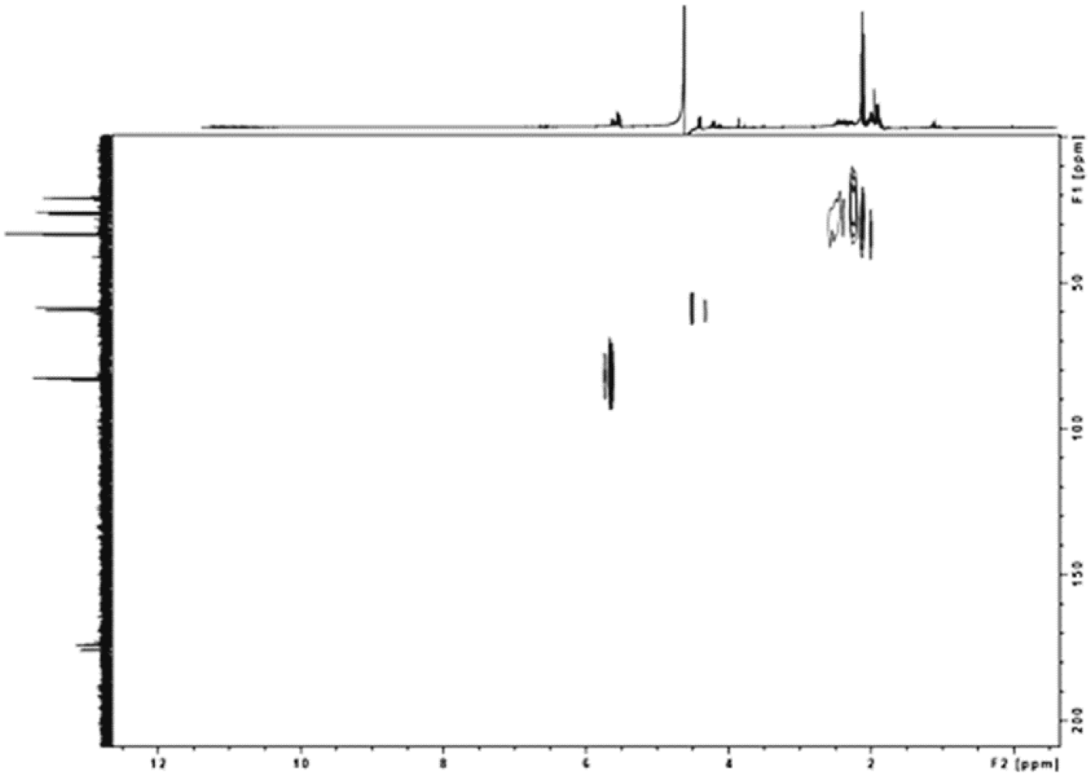

Appendix Figure 8 δHSQC (400 Hz) of 2-acetamido-5-oxopentanoic acid in D_2O 2-acetamido-5-oxopentanoic acid exists in equilibrium with its diol in D_2O.

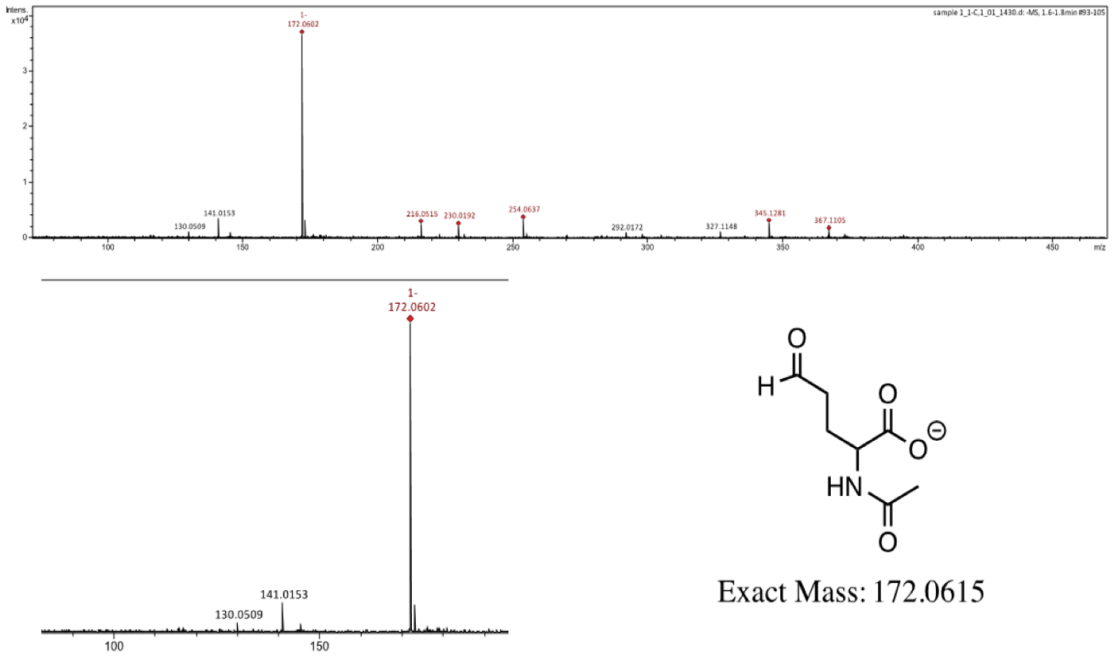

Appendix Figure 9 ESI [M-H]- of 2-acetamido-5-oxopentanoic acid

Mass error -7.56 ppm.

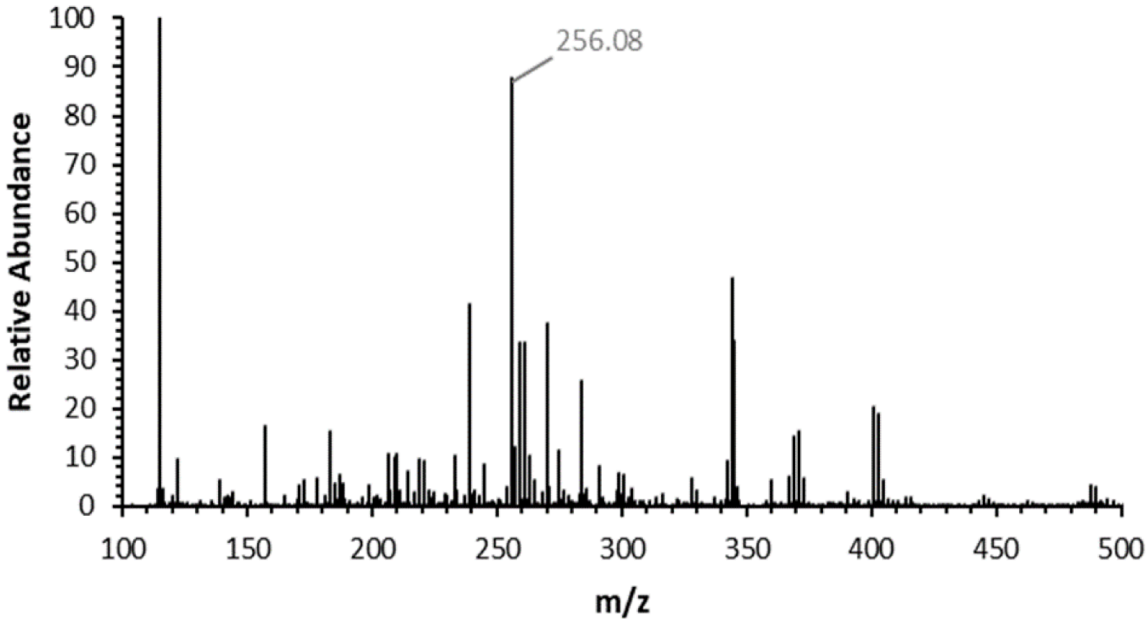

Appendix Figure 10 ESI/MS analysis of 2-acetamido-5,7-dihydroxy-6-oxoheptanoic acid obtained from the AziC5/C6 reaction

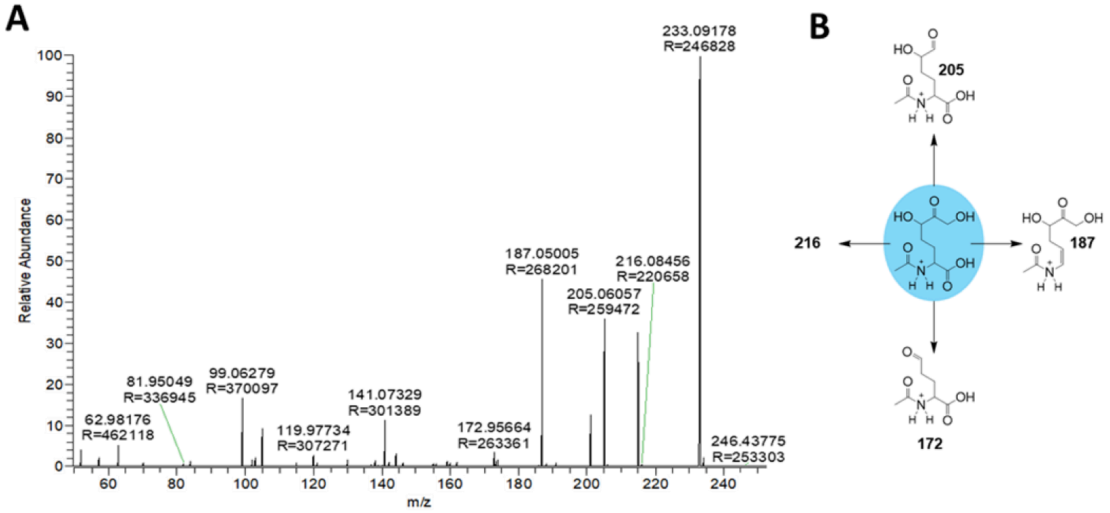

Appendix Figure 11 ESI/MS/MS analysis of 2-acetamido-5,7-dihydroxy-6-oxoheptanoic acid obtained from the AziC5/C6 reaction

Parent ion (M+Na) 256.078. 2-acetamido-5,7-dihydroxy-6-oxoheptanoic acid Expected Mass: 233.090. **A**) ESI/MS/MS of 2-acetamido-5,7-dihydroxy-6-oxoheptanoic acid. **B**) Fragmentation of 2-acetamido-5,7-dihydroxy-6-oxoheptanoic acid

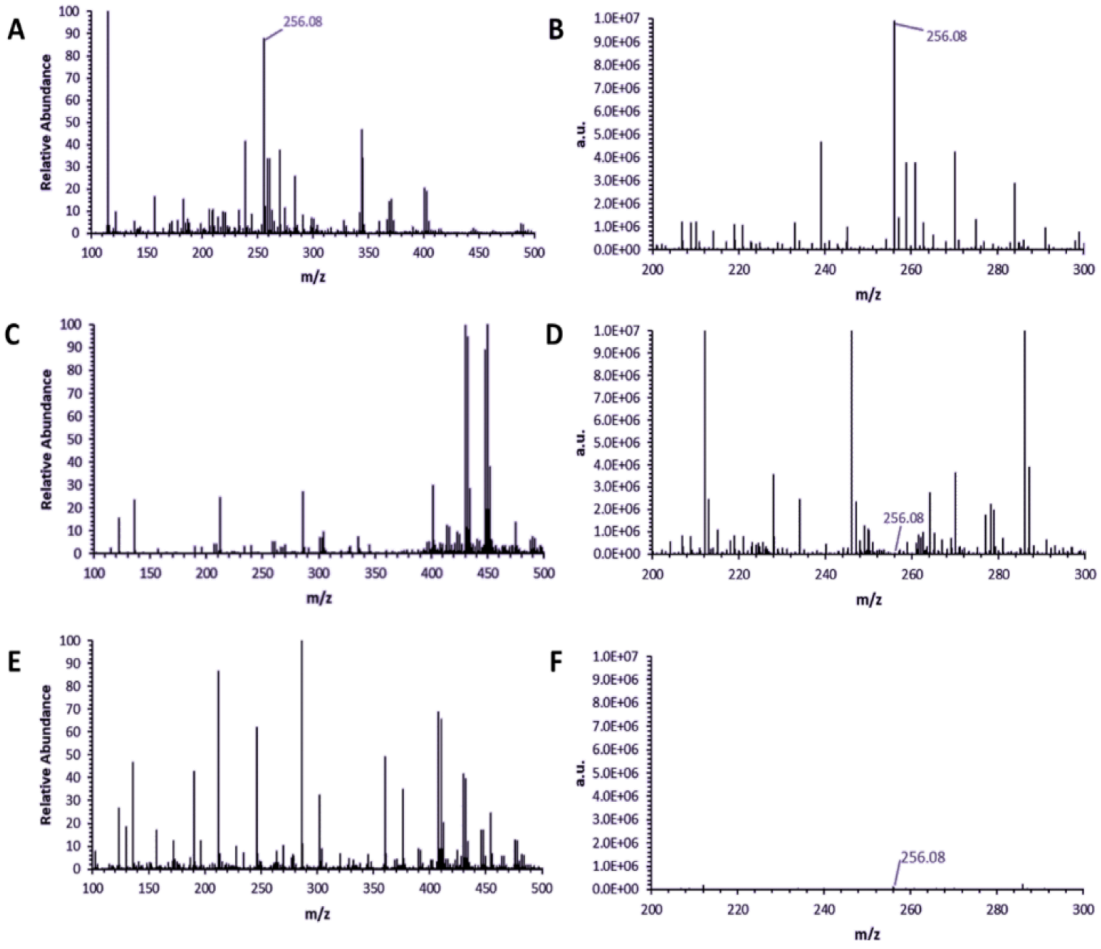

Appendix Figure 12 ESI/MS analysis of controls lacking one transketolase subunit

A. AziC5/C6 reaction with 2-acetamido-5-oxopentanoic acid showing product (M + Na = 256.08). **B**. Zoom in on AziC5/C6 reaction with 2-acetamido-5-oxopentanoic acid showing product. Y-axis in absolute intensity. **C**. Control lacking AziC5 subunit. **D**. Zoom in on control lacking AziC5 subunit. Y-axis in absolute intensity. **E**. Control lacking AziC6 subunit. **F**. Zoom in on control lacking AziC6 subunit. Y-axis in absolute intensity. Minimal product formation is observed in the controls, likely catalyzed by TPP in solution. Product Mass 233.09 (M + Na = 256.08)

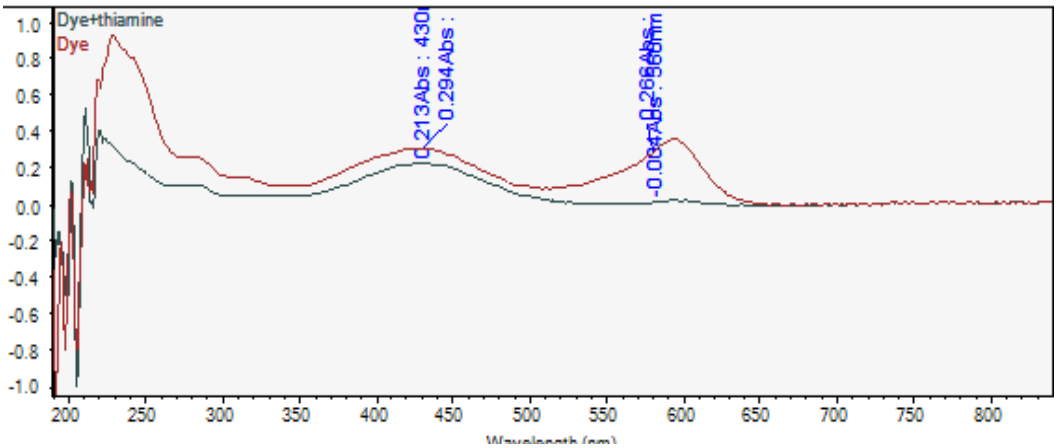

Appendix Figure 13 Bromothymol blue detection of TPP.

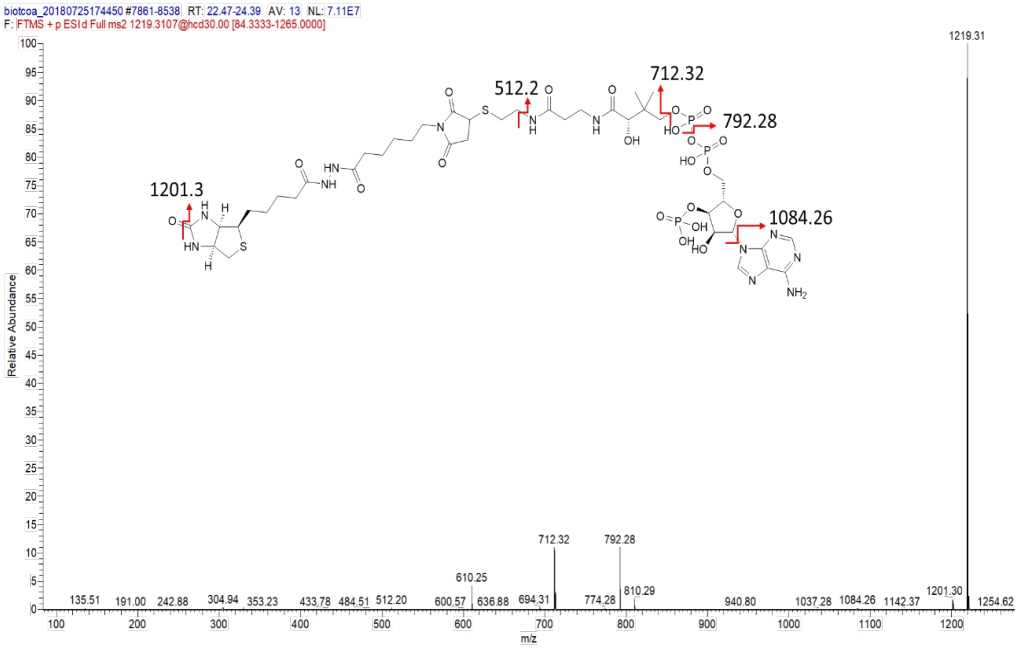

Appendix Figure 14 Biotin-Coenzyme A MS/MS
Expected product m/z [M+H] + calcd. for C41H66N12O21P3S2; 1219.311. Found [M+H] + 1219.311.

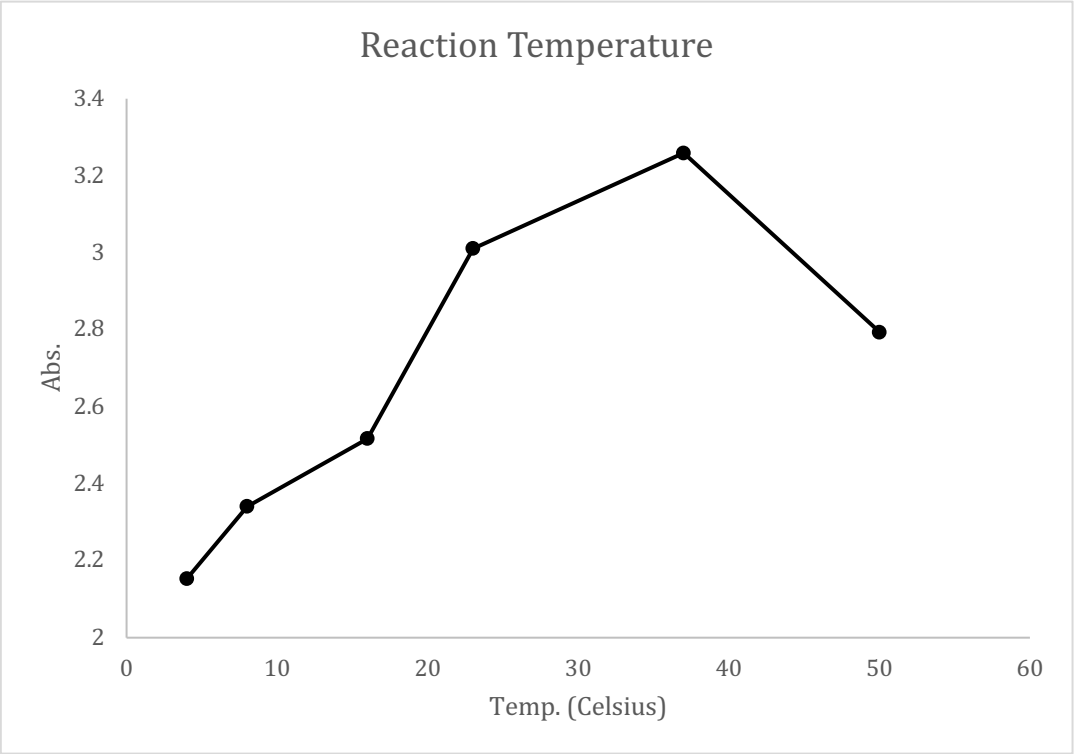

Appendix Figure 15 ELISA assay measuring temperature effects on PPTase activity

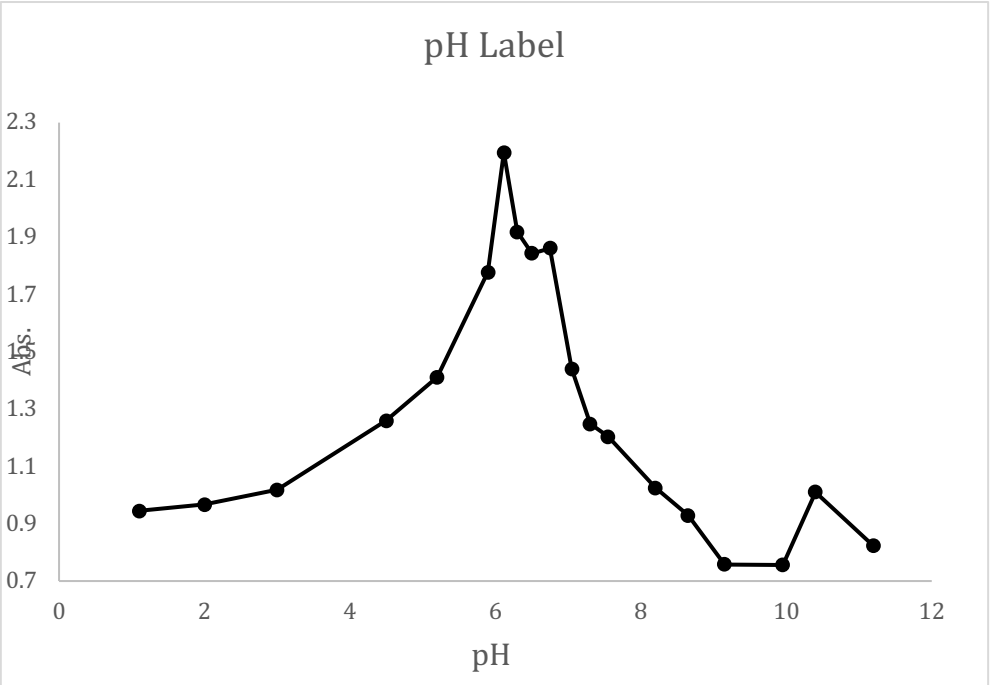

Appendix Figure 16 ELISA assay measuring pH effects on PPTase activity

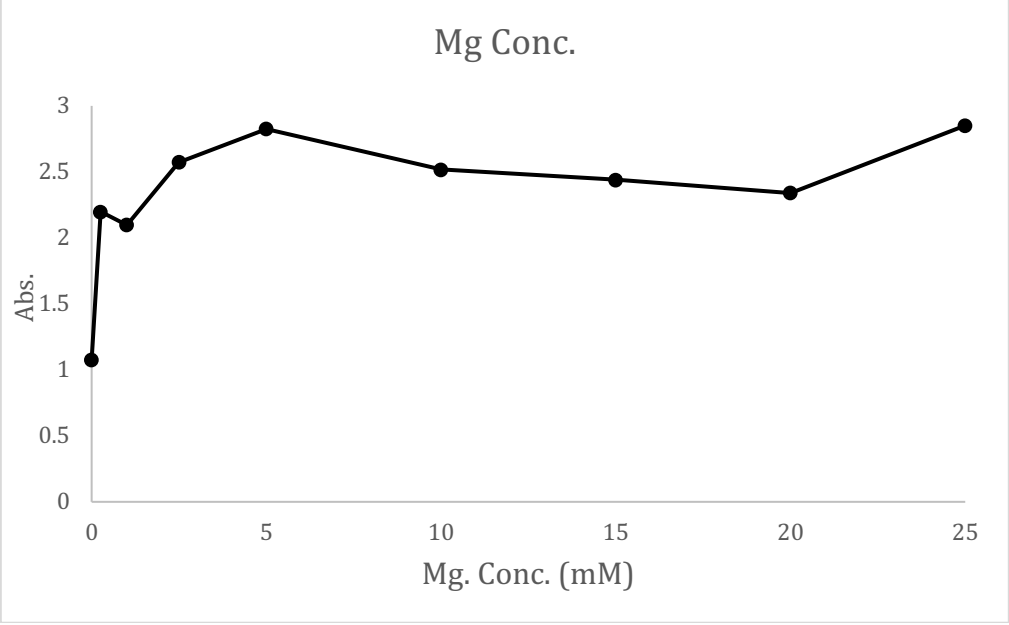

Appendix Figure 17 ELISA assay measuring Mg concentration effects on PPTase activity

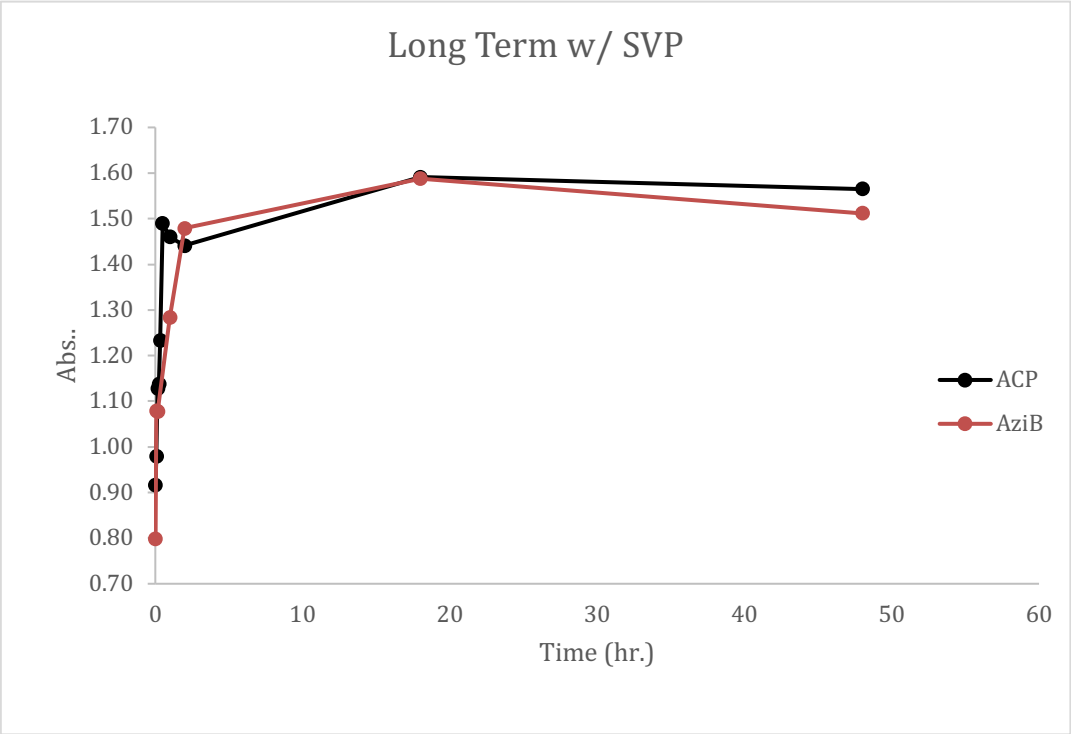

Appendix Figure 18 ELISA assay measuring PPTase activity over long periods of time

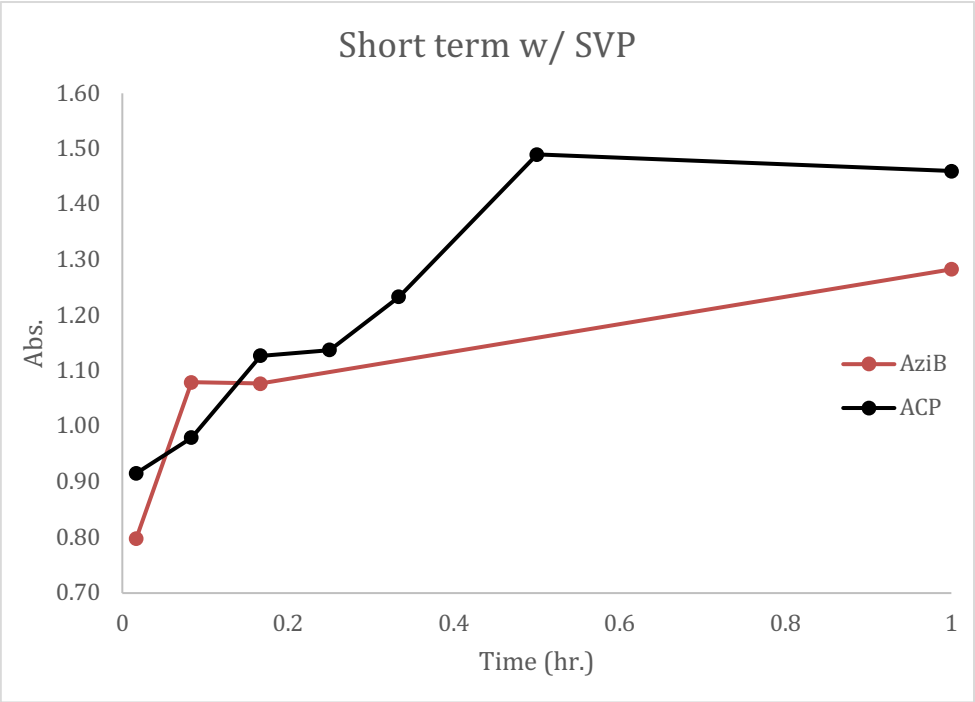

Appendix Figure 19 ELISA assay measuring PPTase activity over short periods of time

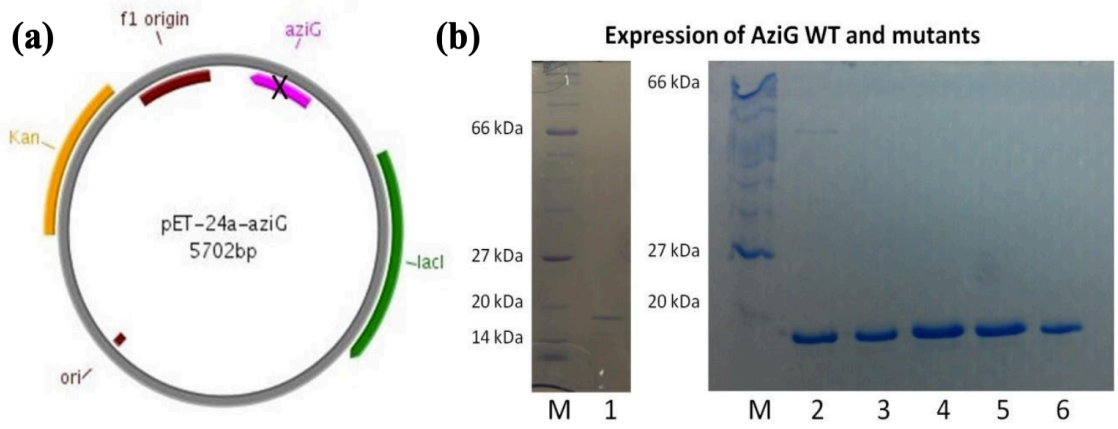

Appendix Figure 20 Expression plasmid of AziG (and its mutants) and SDS-PAGE analysis of overexpression and purification
(a): aziG was cloned into pET-24a and was mutated by site-directed mutagenesis. (b): SDS- PAGE analysis after overexpression and purification of AziG WT and mutants (M: protein marker, 1: WT, 2: H44A, 3: H48A, 4: E57A, 5: S58A, 6: S61A).

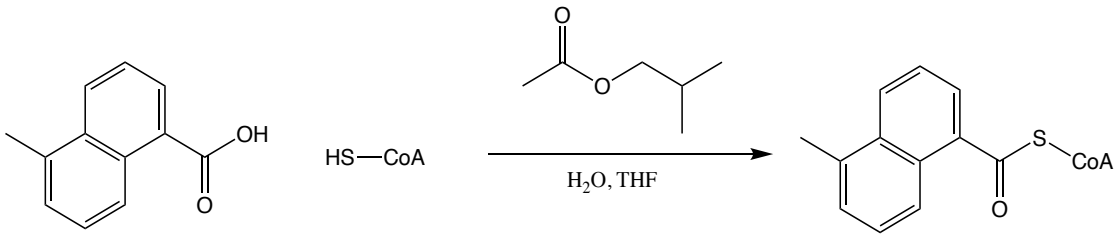

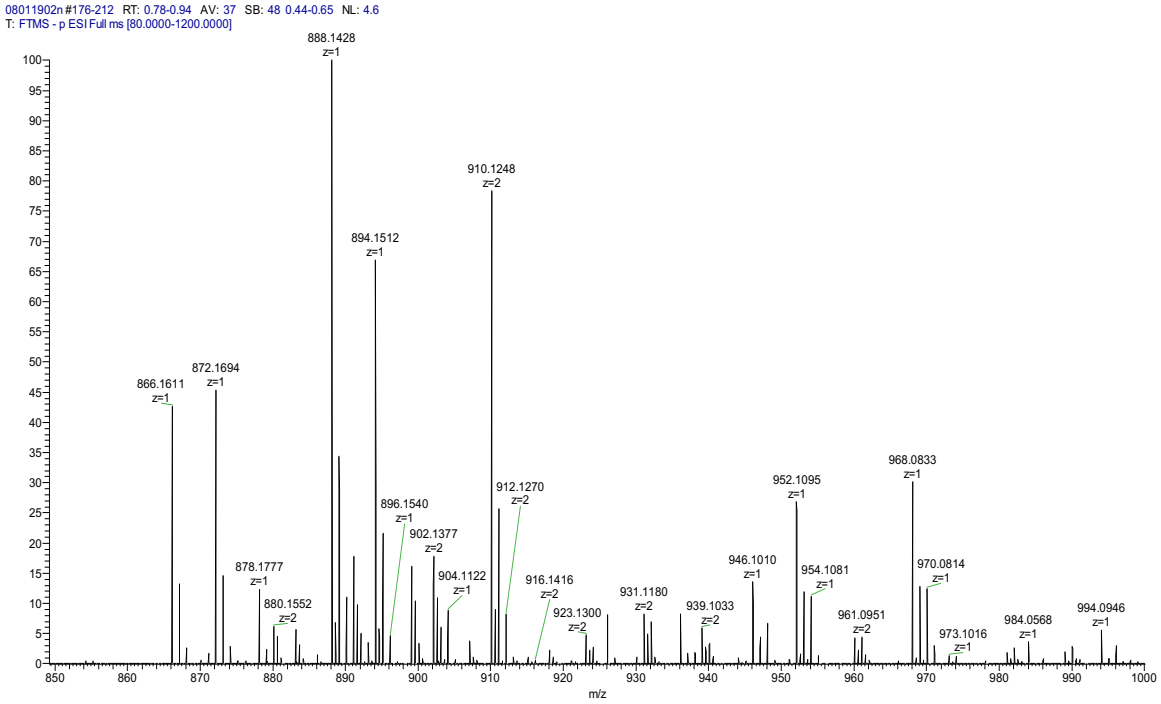

Appendix Figure 21 ESI/MS analysis of 5-methyl-naphthyl-CoA analog

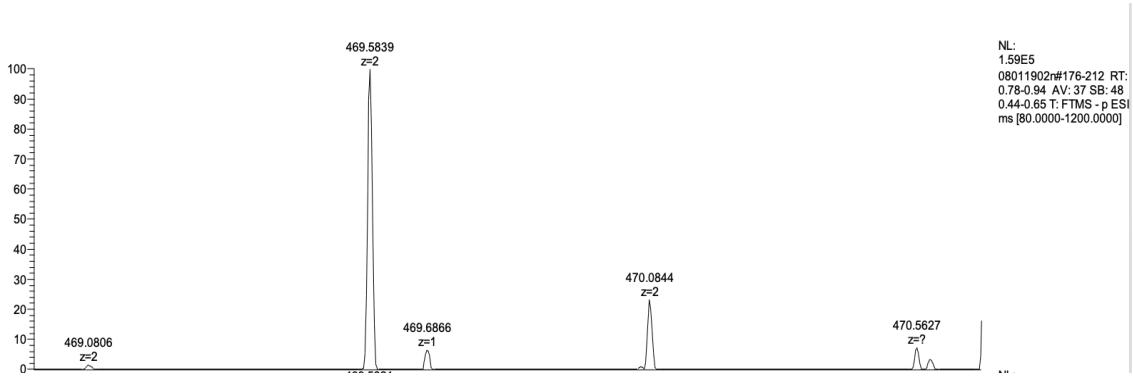

Appendix Figure 22 MS/MS analysis of 5-methyl-naphthyl-CoA analog

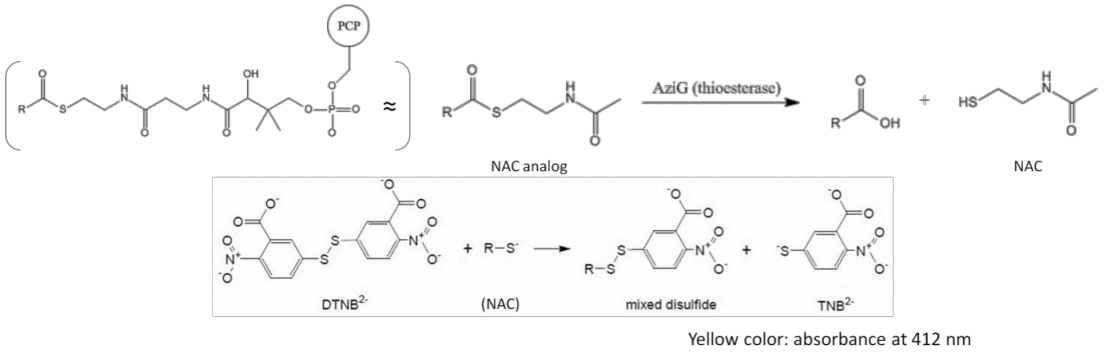

Appendix Scheme 1 AziG kinetic experiment utilizing Ellman's reagent

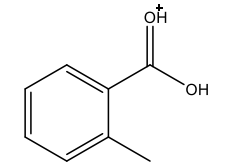

Chemical Formula: $C_8H_9O_2^+$
Exact Mass: 137.0597

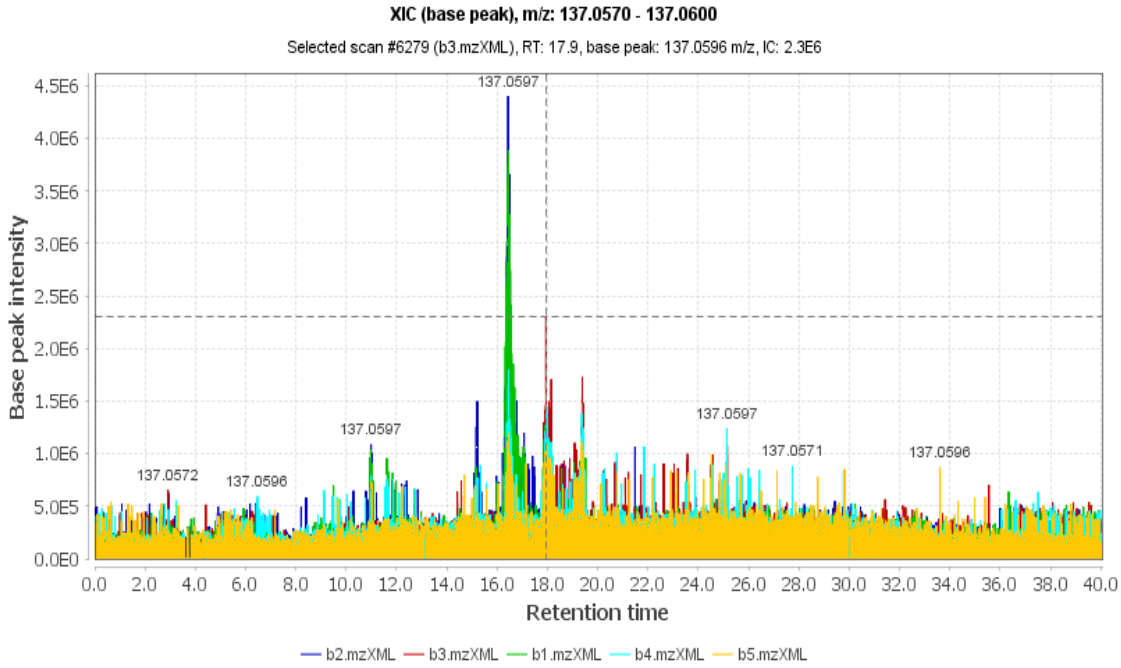

Appendix Figure 23 LC/MS analysis of PKS intermediates 1

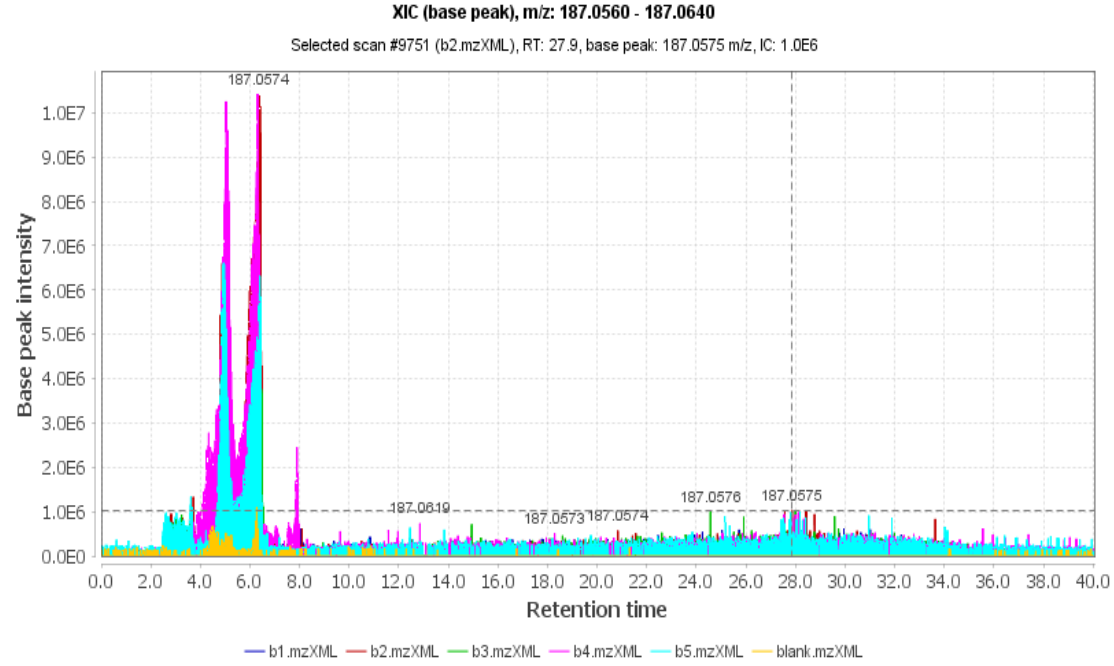

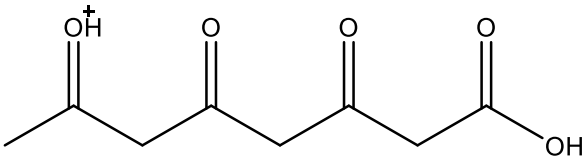

Chemical Formula: $C_8H_{11}O_5^+$

Exact Mass: 187.0601

Appendix Figure 24 LC/MS analysis of PKS intermediates 2

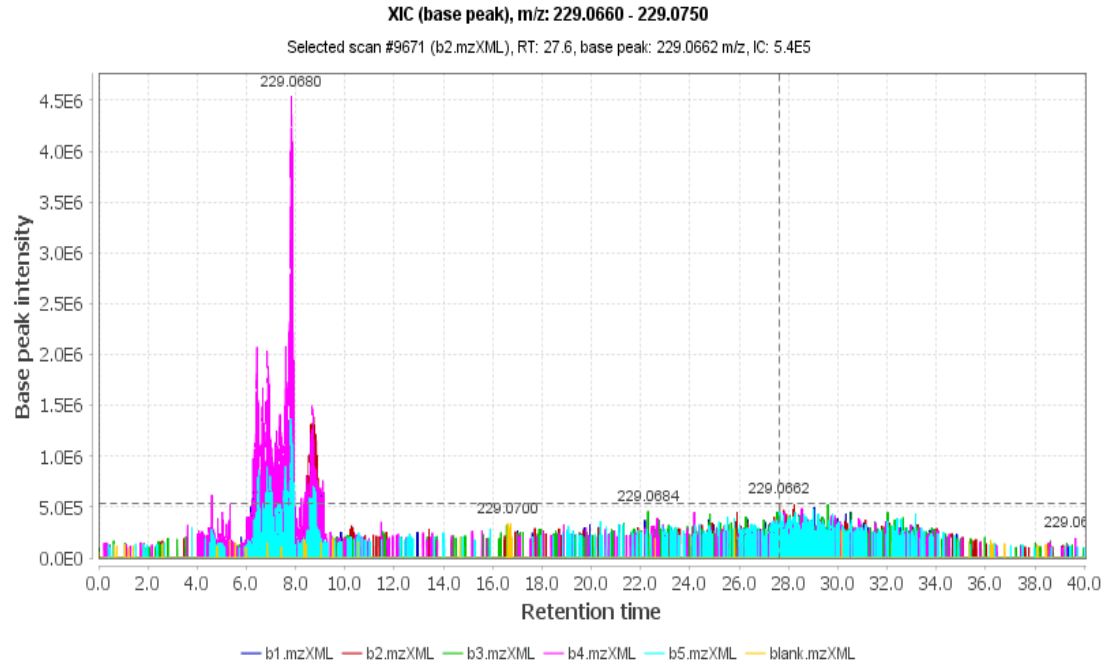

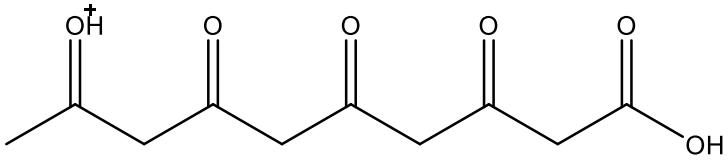

Chemical Formula: $C_{10}H_{13}O_6^+$

Exact Mass: 229.0707

Appendix Figure 25 LC/MS analysis of PKS intermediates 3

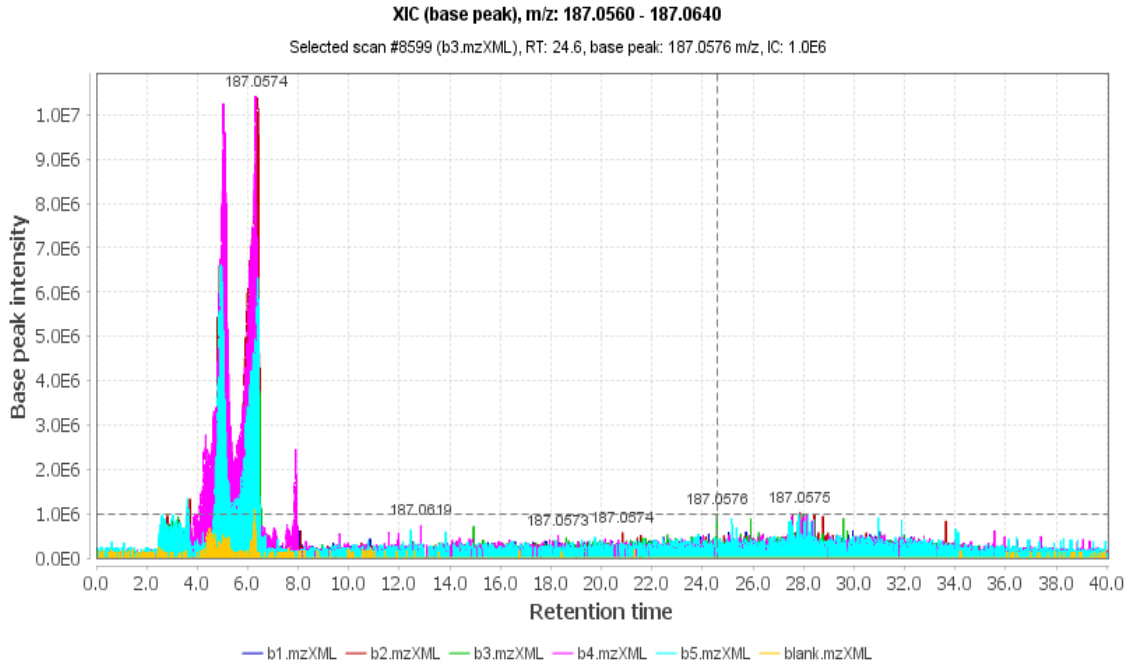

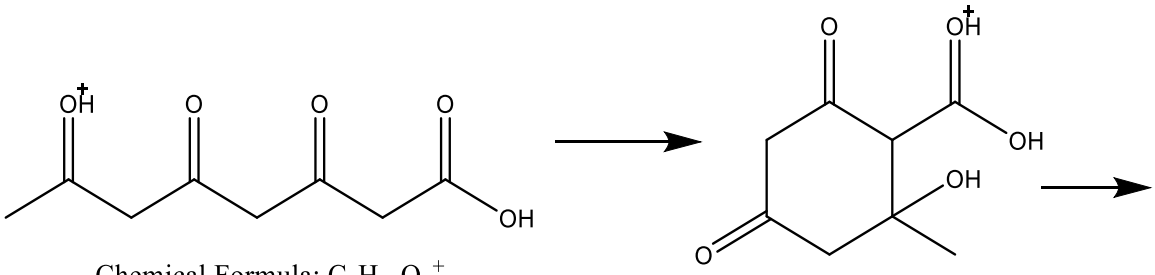

Chemical Formula: $C_8H_{11}O_5^+$
Exact Mass: 187.0601

Chemical Formula: $C_8H_{11}O_5^+$
Exact Mass: 187.0601

Appendix Figure 26 LC/MS analysis of PKS intermediates 4

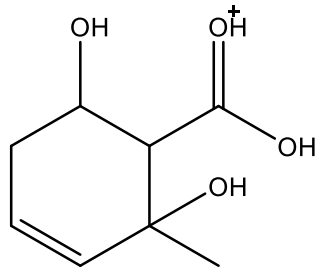

Chemical Formula: $C_8H_{13}O_4^+$

Exact Mass: 173.0808

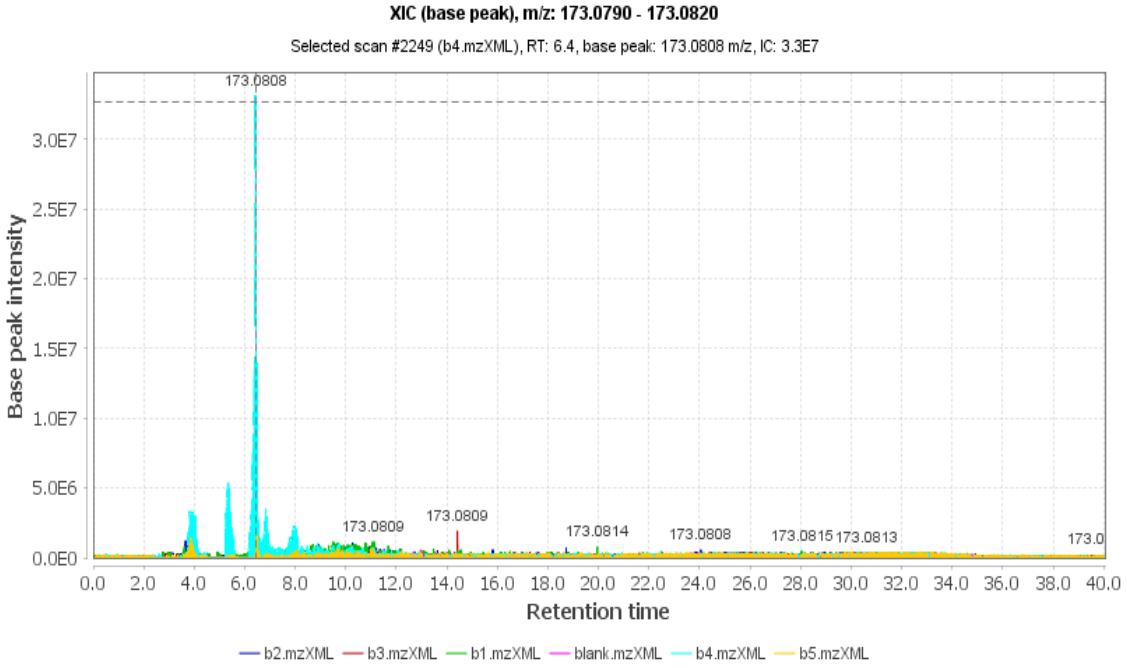

Appendix Figure 27 LC/MS analysis of PKS intermediates 5

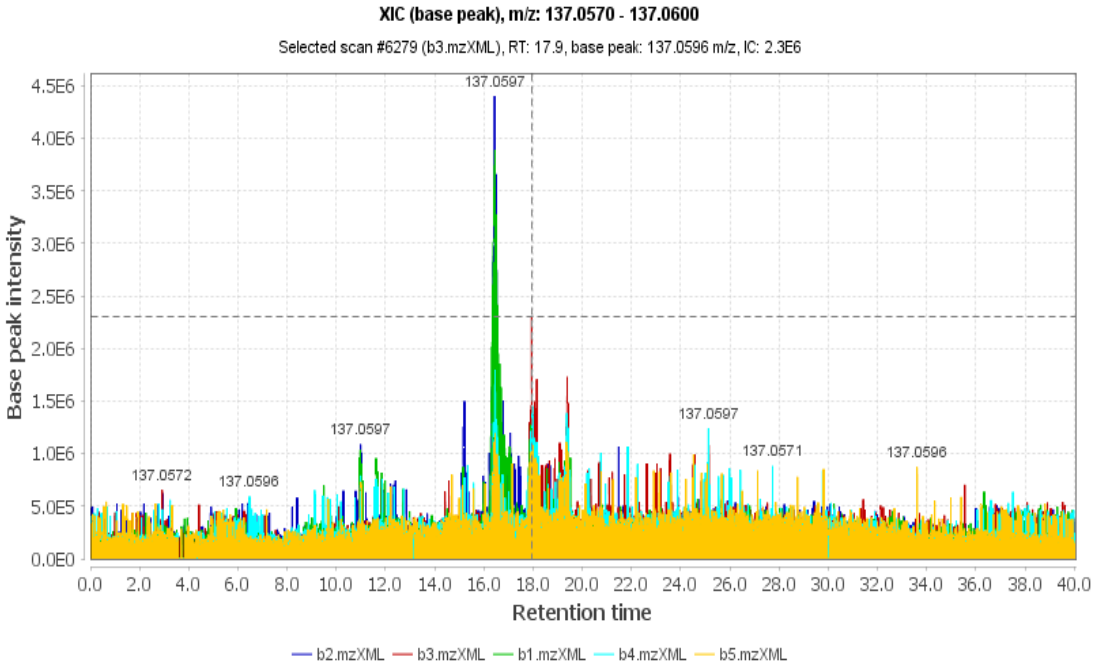

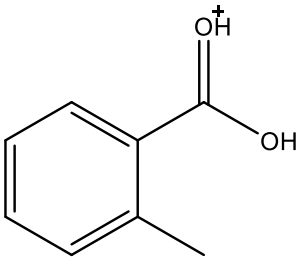

Chemical Formula: $C_8H_9O_2^+$

Exact Mass: 137.0597

Appendix Figure 28 LC/MS analysis of PKS intermediates 6

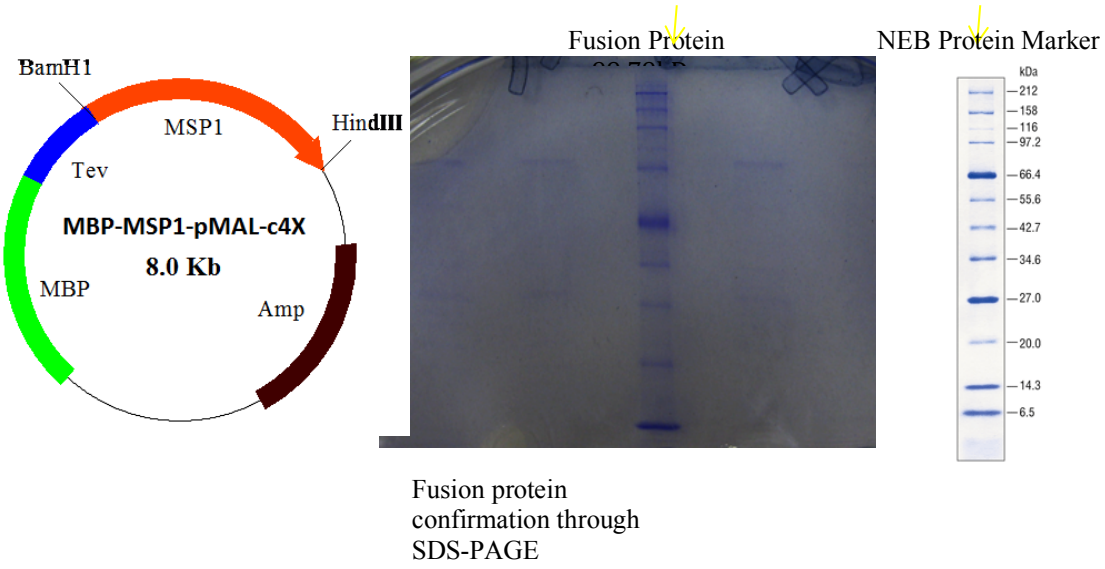

Appendix Figure 29 Expression plasmid of AziG (and its mutants) and SDS-PAGE analysis of overexpression and purification
(a): *aziG* was cloned into pET-24a and was mutated by site-directed mutagenesis. (b): SDS- PAGE analysis after overexpression and purification of AziG WT and mutants (M: protein marker, 1: WT, 2: H44A, 3: H48A, 4: E57A, 5: S58A, 6: S61A).

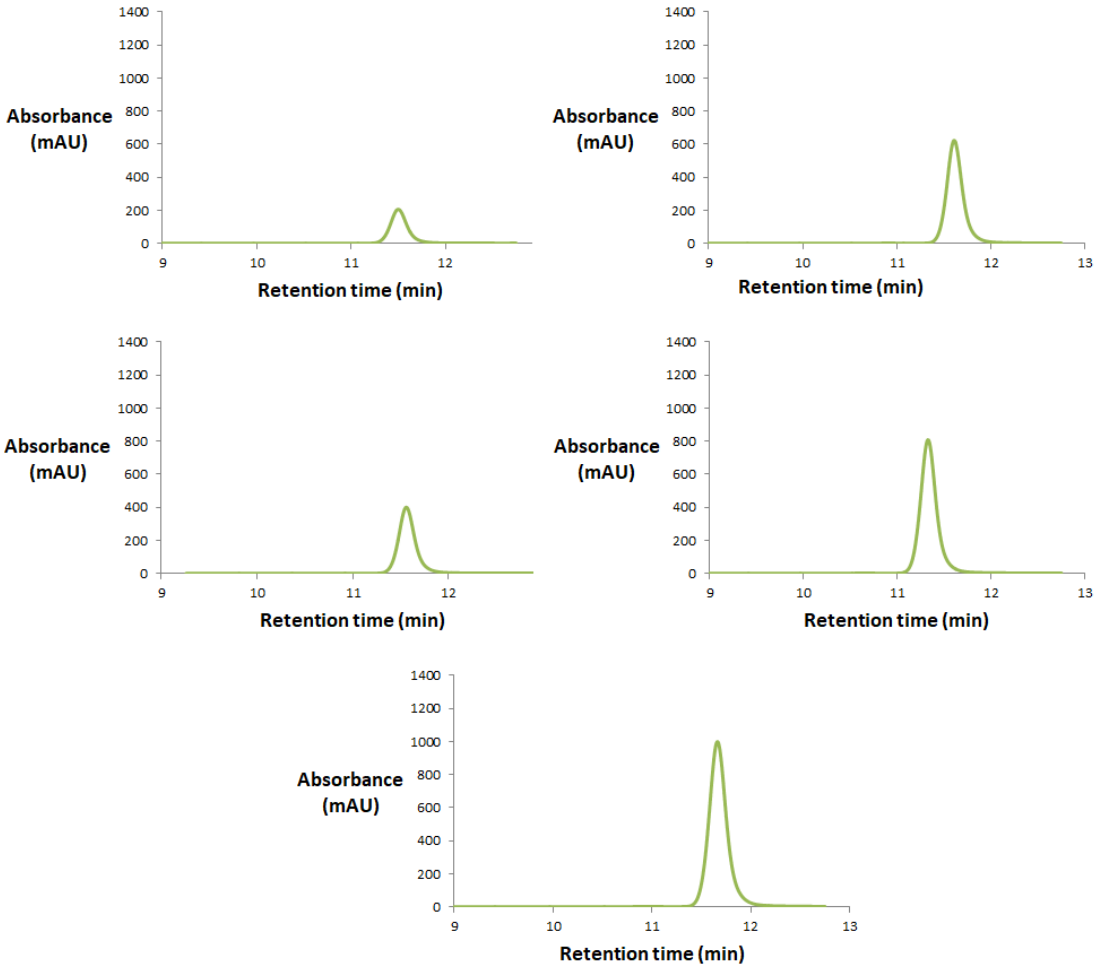

Appendix Figure 30: Analysis of synthetic 2-acetyl-5-methylfuran to generate a standard curve. The following volumes of a 86 nM solution was injected: A] 2 µL B] 4 µL C] 6 µL D] 8 µL E] 10 µL

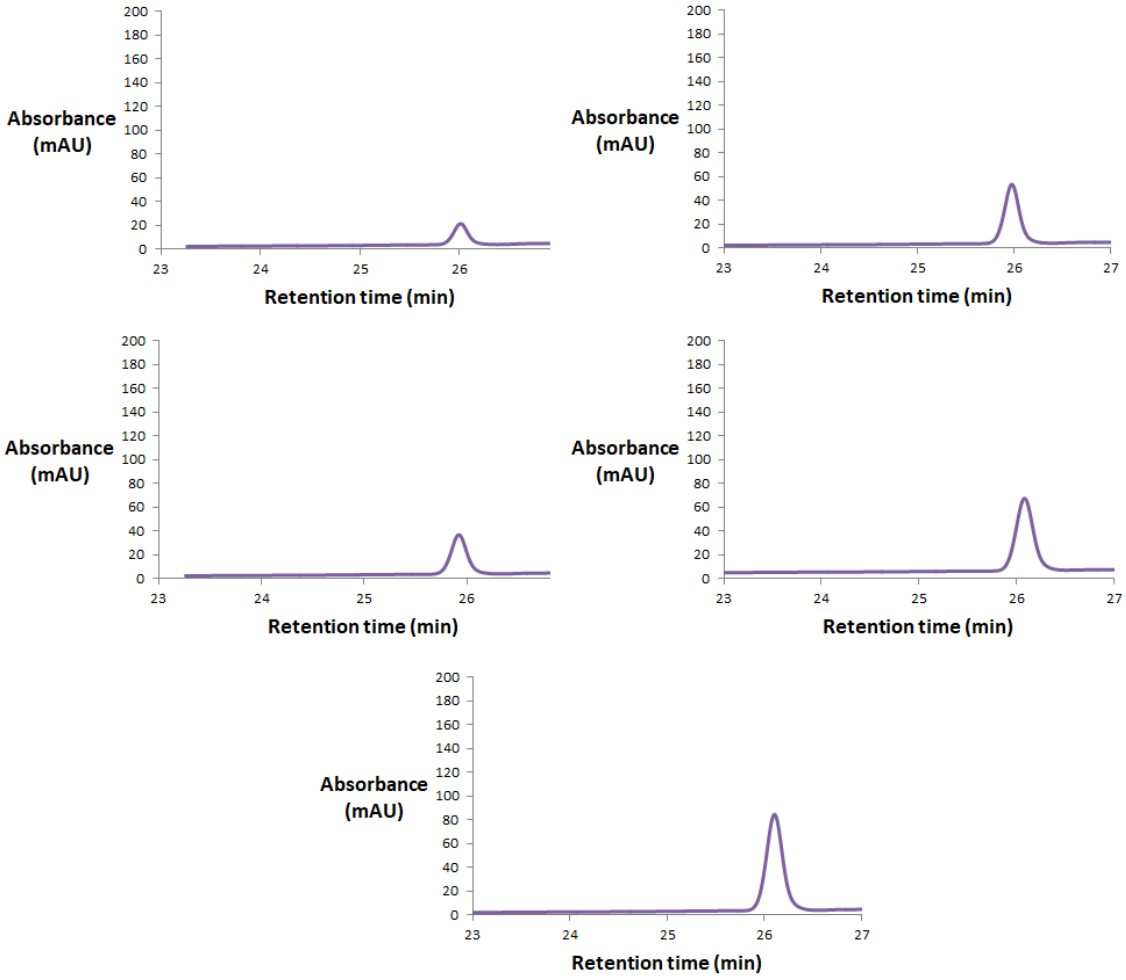

Appendix Figure 31: Analysis of synthetic acetophenone to generate a standard curve. The following volumes of a 88 nM solution was injected: A] 2 µL B] 4 µL C] 6 µL D] 8 µL E] 10 µL

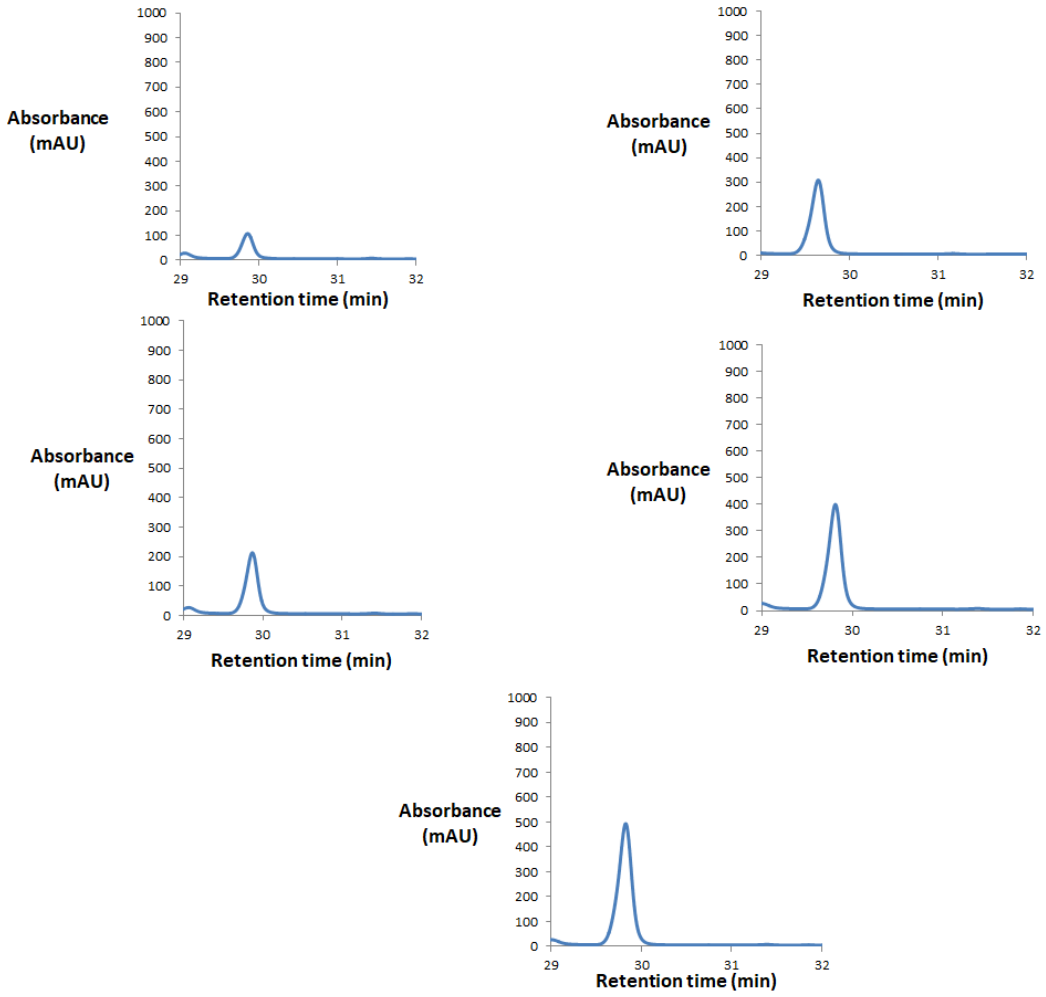

Appendix Figure 32: Analysis of synthetic 4-acetylbiphenyl to generate a standard curve. The following volumes of a 24.5 µM solution was injected: A] 2 µL B] 4 µL C] 6 µL D] 8 µL E] 10 µL

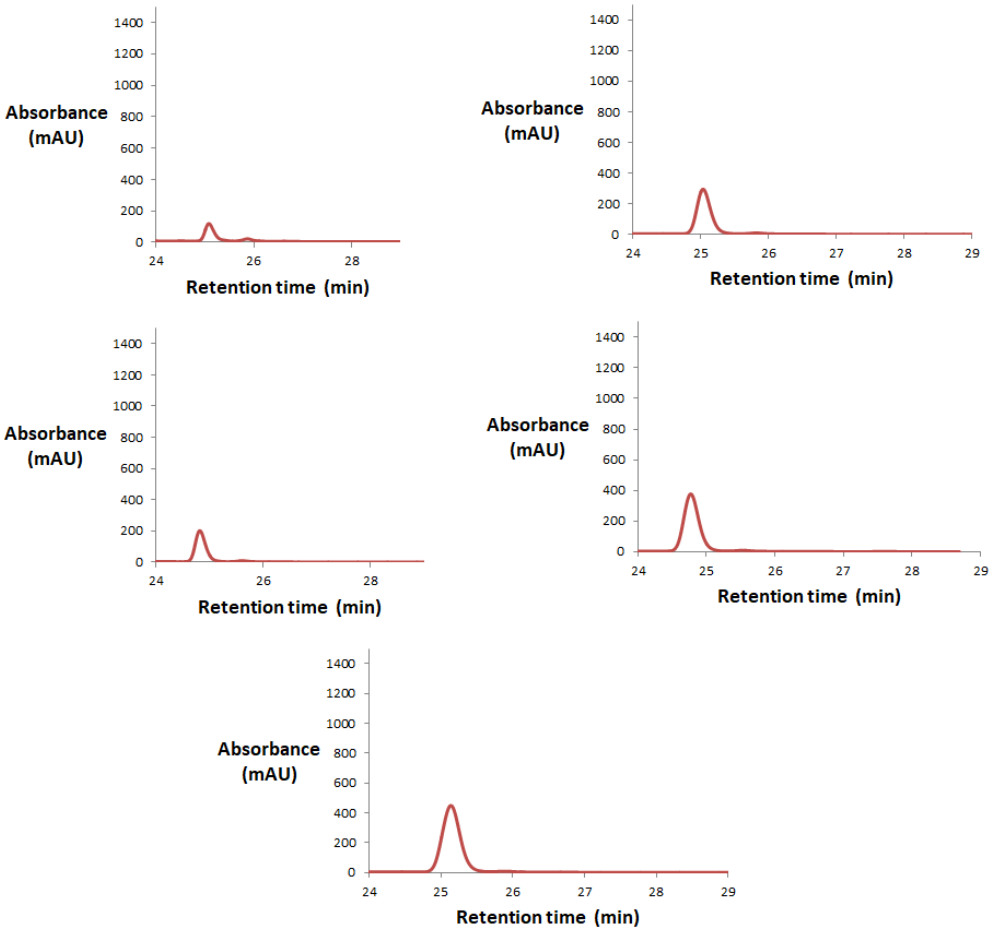

Appendix Figure 33: Analysis of synthetic 2-acetylfluorene to generate a standard curve. The following volumes of a 23 µM solution was injected: A] 2 µL B] 4 µL C] 6 µL D] 8 µL E] 10 µL

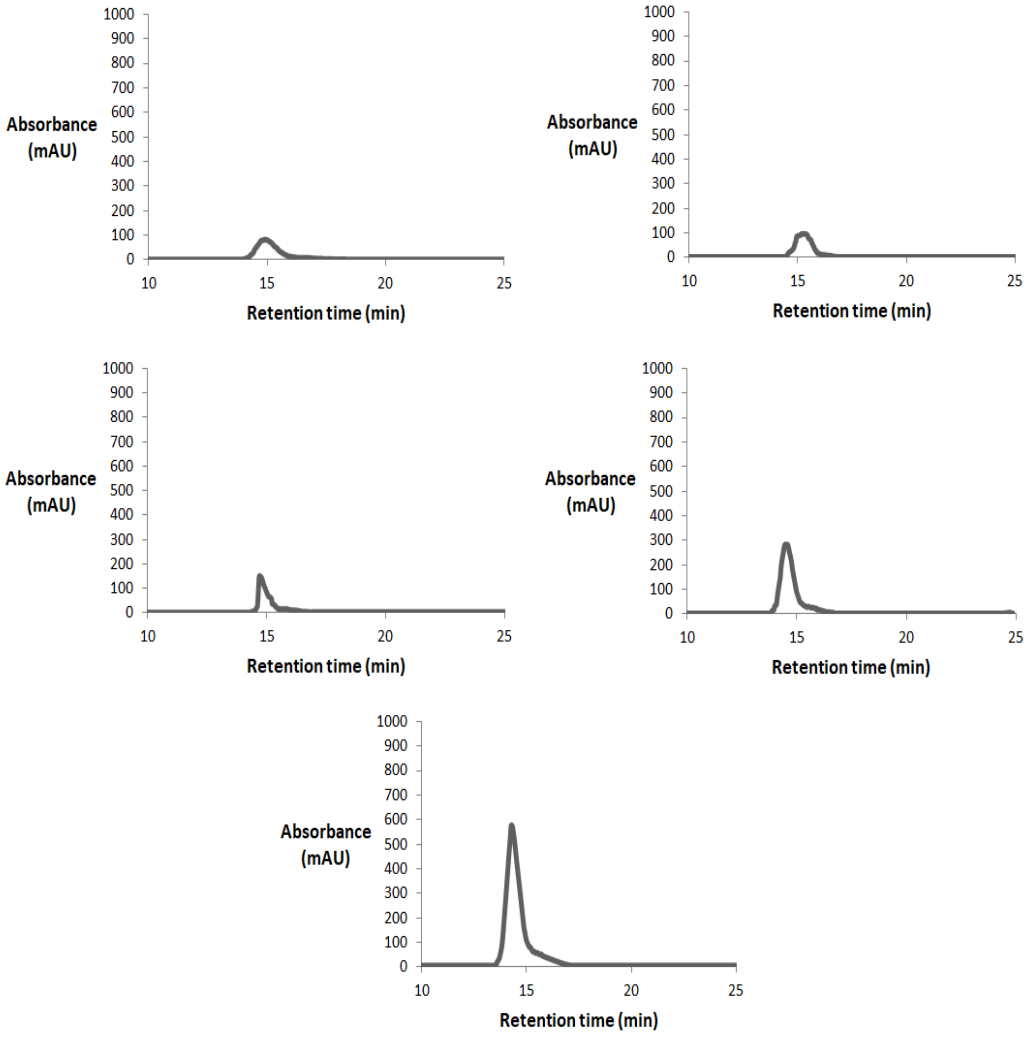

Appendix Figure 34: Analysis of synthetic acetonaphthone to generate a standard curve. The following amounts of acetonaphthone was injected: A] 2 µg B] 4 µg C] 6 µg D] 12 µg E] 18 µg

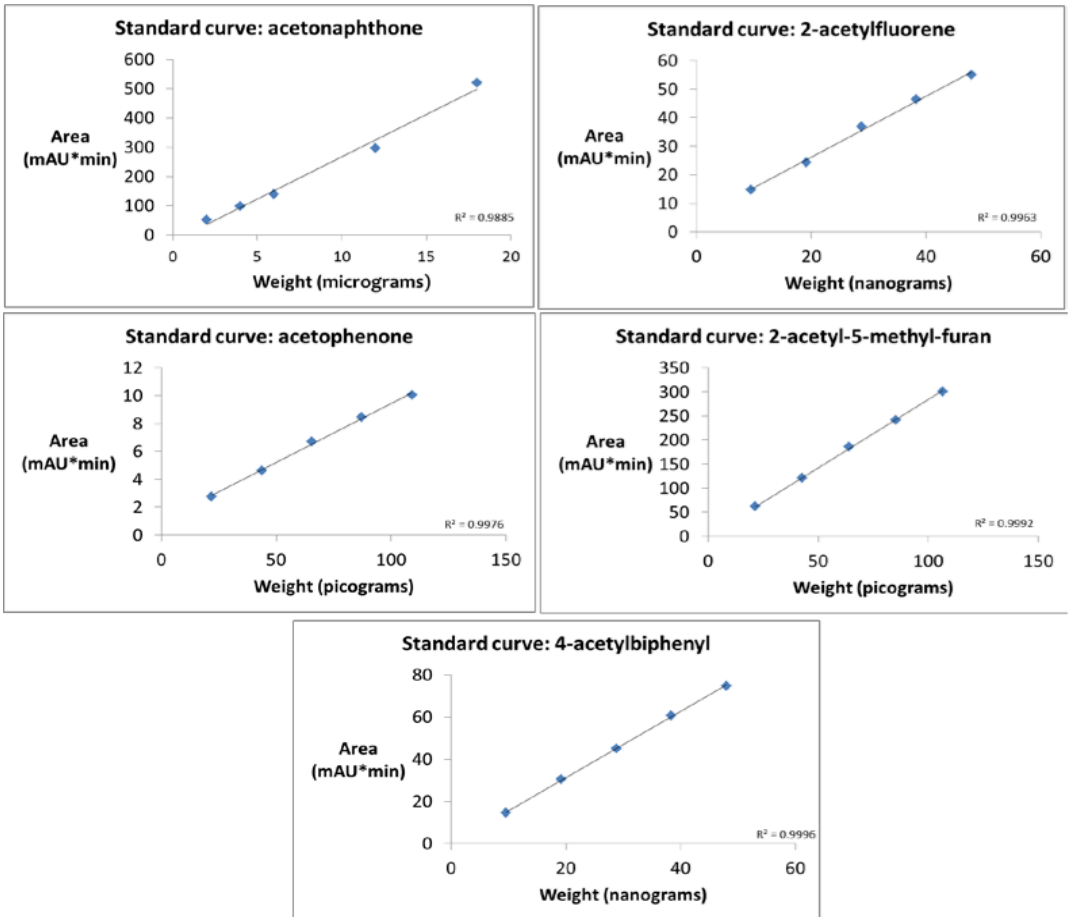

Appendix Figure 35: Standardization curves for concentrations of aldehydes

nMoles PPTase	Svp	Sfp	FAS	NFAS
0	0.009 ± 0.008	0.001 ± 0.017	0.022 ± 0.013	0.085 ± 0.007
0.26	0.144 ± 0.013	0.150 ± 0.009	0.077 ± 0.036	0.167 ± 0.055
1.3	0.293 ± 0.021	0.297 ± 0.006	0.169 ± 0.003	0.108 ± 0.105
2.6	0.255 ± 0.021	0.378 ± 0.008	0.138 ± 0.034	0.209 ± 0.20
5.2	0.363 ± 0.065	0.230 ± 0.055	0.228 ± 0.115	0.121 ± 0.056
6.5	0.921 ± 0.064	0.982 ± 0.038	0.834 ± 0.059	0.496 ± 0.059
13	0.995 ± 0.028	0.776 ± 0.023	0.680 ± 0.035	0.482 ± 0.035

Appendix Table 2 The absorbance values from the ELISA with ACP domain and four different pptases

nMoles PPTase	Svp	Sfp	FAS	NFAS
0	0.085 ± 0.001	0.329 ± 0.022	0.148 ± 0.046	0.001 ± 0.022
1.3	0.257 ± 0.030	0.524 ± 0.098	0.272 ± 0.086	0.130 ± 0.16
2.6	0.338 ± 0.020	0.450 ± 0.114	0.231 ± 0.076	0.331 ± 0.123
5.2	0.493 ± 0.031	0.575 ± 0.036	0.464 ± 0.046	0.473 ± 0.05
6.5	0.841 ± 0.065	0.719 ± 0.006	0.694 ± 0.009	0.413 ± 0.101

Appendix Table 3 The absorbance values from the ELISA with AziB and the four different pptases

E-mail: Bpfoley910@gmail.com